Sea disposal of Alum Shale – a way forward?

Experiments and modelling

Anne Line Hexeberg Henriksen

Master thesis in Geoscience
Environmental geology
60 credits

Department of Geosciences
Faculty of Mathematics and Natural sciences

UNIVERSITY OF OSLO

August 2023

Sea disposal of Alum Shale – a way forward?

Experiments and modelling

Anne Line Hexeberg Henriksen

2023

Sea disposal of Alum Shale – a way forward? Experiments and modelling

Anne Line Hexeberg Henriksen

http://www.duo.uio.no/

Printing: Reprosentralen, Universitetet i Oslo

Abstract

In the Oslo region, alum shale is often encountered during construction work. Alum shale is an organic-rich sulphide-bearing rock, which can produce acidic runoff enriched in harmful elements (e.g., heavy metals) when it is crushed and exposed to atmospheric conditions. This phenomenon is known as acid rock drainage (ARD) and can severely affect the downstream environment. Excavated rocks that are predicted to produce ARD must be delivered to an approved landfill or treatment facility by law. Landfills allowed to receive acid-producing rocks in Norway are limited in capacity, and alternative ways to dispose of acid-producing rocks are needed.

The most crucial factor in the safe disposal of acid-producing rocks is to prevent access to oxygen. Some Norwegian fjords have natural anoxic bottom conditions, and sea disposal of alum shale could, therefore, be an alternative and more cost-effective way to dispose of such rocks. Low-oxygen conditions are thought to decelerate the weathering process, and the natural buffer capacity of seawater is believed to neutralize any possibly produced acid. However, complexation with salts in seawater can lead to more leaching of heavy metals and harmful elements. The aim of this study was to assess the potential for sea disposal of alum shale from a geochemical perspective. To do that, batch experiments were conducted using weathered and unweathered alum shale in contact with fresh- and seawater under oxic, low-oxygen and anoxic conditions. pH, conductivity, redox potential, dissolved oxygen, alkalinity, trace elements, and major cat- and anions were measured over time. Rates retrieved from the batch experiments were used to assess the long-term consequences of sea disposal by geochemical modelling, using PHREEQC.

The alkalinity of seawater was not sufficient to neutralize acid produced from weathered alum shale at a 1:10 shale-to-water ratio. Further investigations are required to understand how weathered alum shale would react under anoxic conditions. The experiments and geochemical modelling revealed that unweathered alum shale leached higher concentrations of trace metals in seawater compared to freshwater. Precipitation of some trace metals (Ni, Zn, Co, and Cd) occurred under anoxic conditions in both fresh- and seawater treatments, suggesting that restricted access to oxygen plays a more significant role in immobilizing trace metals than the initial water composition. Considering the geochemical aspects, sea disposal of unweathered alum shale in a fjord with limited access to oxygen has the potential to serve as a long-term storage facility, by preventing ARD production and immobilizing trace metals.

Acknowledgements

A special thanks goes to my main supervisor, Frøydis Meen Wærsted, for her excellent guidance, regular meetings, organizational support, discussions, and corrections throughout the process of this master thesis. I am also grateful to my co-supervisors, Helge Hellevang and Jens Jahren, for their feedback and open-door policy, allowing me to seek their assistance whenever needed.

I would also like to thank Mufak Said Naoroz for conducting IC, TOC/TIC and grain size analyses and for his guidance in the lab. Thanks to Ibrahim Omar Khaled for his help with XRD analyses and Siri Simonsen for her help with SEM analyses.

Thanks to NOAH AS, by Sverre Frimann Koren, for analysing metals in my leachate samples as a part of eartresQue Centre for Research-Based Innovation (https://www.nmbu.no/en/research/projects/earthresque). I would also like to thank NIVA for their provision of seawater.

Thanks to all my fellow students for their companionship throughout these five years, with a special thanks to Maiken Eriksen for the friendship we built. Thanks to Mats Rouven Ippach for inspiring academic discussions and motivational words. And lastly, I would like to thank my parents for their patience and support.

Contents

1. Introduction

The exposure of crushed alum shale to atmospheric conditions can produce acid rock drainage (ARD) (Pabst et al., 2017). This is a well-known global problem for mine wastes containing residual sulphide minerals, usually referred to as acid mine drainage (AMD) (Egiebor and Oni, 2007). ARD and AMD are characterized by low pH (<4), elevated levels of heavy metals and sulphates, and high electrical conductivity (Sørmo et al., 2015).

Alum shale is a Scandinavian black shale that constitutes a large part of the bedrock in the Oslo region (Owen et al., 1990). The shale is enriched in sulphides, organic carbon, heavy metals and naturally occurring radionuclides (Bjørlykke, 1974). The high uranium content (around 150 ppm) produces radon gas when it decays and constitute a health risk by elevated concentrations in indoor air and prolonged exposure (Field et al., 2000). Additionally, the leaching of harmful elements, like heavy metals and radionuclides, can negatively affect the downstream environment and severely threaten living organisms. In addition to health and environmental challenges, this rock is associated with construction engineering problems like swelling and corrosion (Bastiansen et al., 1957).

Due to environmental concerns, treatment and disposal of excavated acid-producing rocks, including alum shale, are regulated by the Norwegian law (Lovdata, 2004). The existing landfills for acid-producing rocks in Norway have limited capacity, and there are high costs associated with adequately disposing such rocks. This thesis is a part of the Norwegian Geotechnical Institute's (NGI) project "Under Oslo" which investigates sustainable and cost-effective solutions for construction work under the surface (https://www.ngi.no/Prosjekter/Under-Oslo). As the population grows, more building projects are planned in the coming years, and alternative methods to dispose of alum shales are needed.

The critical point of proper disposal of alum shale is to prevent access to oxygen. Sea disposal in deep fjords with natural anoxic conditions could be an alternative way to dispose of acid-producing rocks. The low level of oxygen is thought to prevent weathering of the shale, and the natural buffer capacity of seawater is thought to stabilize the pH around the deposited masses (Sørmo et al., 2015). However, saltwater can corrode minerals such as pyrite and cause more leachates of metals to the marine environment (Skei and Sørby, 2019). Additionally, the high

salt content might lead to the complexation of heavy metals so that the metals remain in the water phase (Wærsted et al., 2023a).

Aim of study

The aim of this study was to investigate the consequences of sea disposal of alum shale from a geochemical perspective. Some primary research questions/objectives were formulated to examine the potential for sea disposal:

- Is the alkalinity of seawater sufficient to neutralize weathered shale?
- Is complexation with salts in seawater increasing leaching of metals from alum shale?
- How is leachate from alum shale affected when conditions such as dissolved oxygen concentrations, ionic activity, and alkalinity vary?
- Perform geochemical modelling to estimate the long-term consequences of sea disposal of alum shale.

Lab experiments and modelling were performed to answer these research questions. Batch experiments with unweathered and weathered alum shale in contact with sea-and freshwater under oxic, low-oxygen and anoxic/reducing conditions were prepared and analysed over time. The rates retrieved from the batch experiments were used for geochemical modelling using PHREEQC.

2. Background

The Alum Shale Formation is a part of the Cambro-Ordovician succession, where the succession is thoroughly described by Owen (1990) and Bjørlykke (1974). The thickness of the Alum shale Formation varies from 20 to 100 meters, with a thickness of approximately 50 meters in the Oslo region (Bastiansen et al., 1957; Nakrem and Worsley, 2013). The formation is found in the southern part of Norway and in the western and southern parts of Sweden (Owen et al., 1990). Figure 1 shows the bedrock in the Oslo region and where the Cambro-Ordovician succession is found.

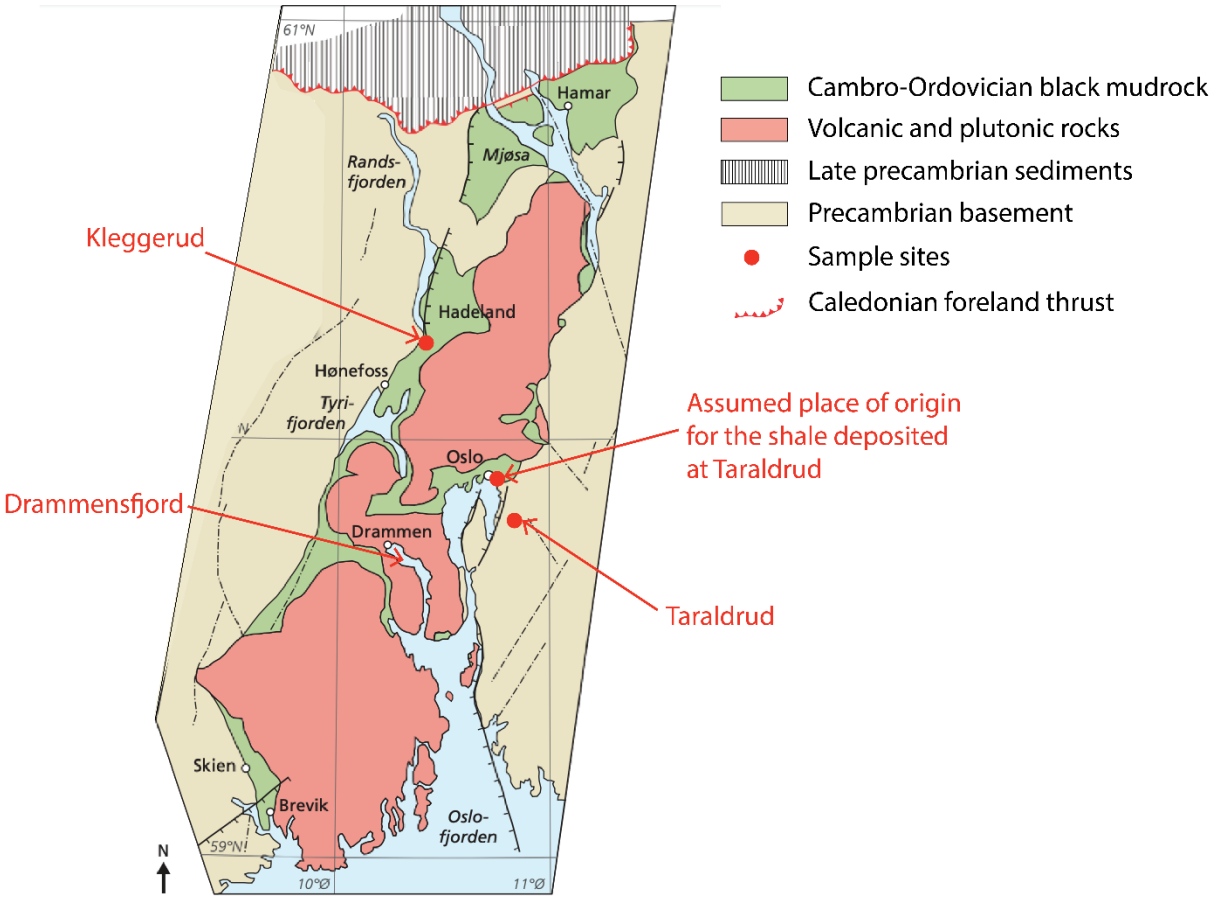

Figure 1: Map showing the bedrock in the Oslo region and where the Cambro-Ordovician succession is found (green color). The location of the alum shale from Kleggerud and the assumed location for the shale deposited at Taraldrud are marked with red dots. Modified from Nakrem and Worsley (2013).

The stratigraphic units are divided into formations, which again are divided into horizons based on their geochemical composition (Figure 2). The Alum Shale Formation constitutes horizon 2-3a (Nakrem and Worsley, 2013; Pabst et al., 2017) and is known for its ARD potential when it is crushed and exposed to air and water. Other black mudrocks within Cambro-Ordovician succession exist, but the alum shale differs and can be recognized by a black streak when it is scratched with a knife. The streak test itself is not sufficient to distinguish the different formations, and additional geochemical characterization is needed (Pabst et al., 2017).

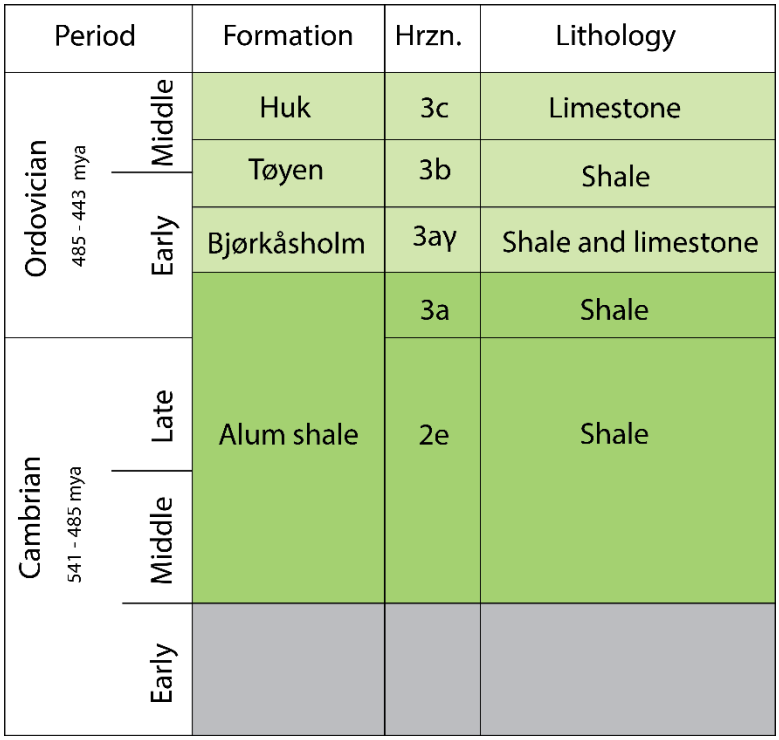

Figure 2: Stratigraphic chart of the sediments deposited from early Cambrian to middle Ordovician in the Oslo region. Modified from Nakrem and Worsley (2013).

The costs of treating black mudrocks depend on their potential environmental consequences. When encountering black mudrocks during construction work, their ability to generate ARD may vary, depending on the specific type of mudrock. Therefore, it is necessary to identify and characterize which type of mudrock that is encountered. Pabst et al. (2017) have developed an efficient characterization tool to identify the different horizons of the Cambro-Ordovician black mudrocks in Norway. The method requires whole-rock analysis of the rock, where heavy metals and other elements, are plotted in triangular plots. The plots include the chemical composition of known horizons from the Cambro-Ordovician succession for comparison and are used to estimate which horizon the shale of interest belongs to.

The main mineralogical constituents of the Alum Shale Formation are clay minerals (e.g. illite), quartz and feldspars (Bjørlykke, 1974). The shale has a high total organic carbon (TOC) content, commonly around 10%, but locally values can reach as high as 20% (Andersson et al., 1985). The sulphur content (as e.g. sulphides) can reach values around 3 % in the shale deposited in Middle Cambrian to around 10-12 % in the Upper Cambrian (Bjørlykke, 1974). Alum Shale generally has a low content of total inorganic carbon (TIC) (e.g. calcite), usually ranging from 1 to 2 % (Andersson et al., 1985). The shale is also enriched in heavy metals (e.g. Cu, V, Ni, Mo) and radionuclides (e.g. U up to ~0.02%) (Nakrem and Worsley, 2013).

Alum shale as a resource

Alum shale in Sweden has been used as raw material to produce alum [$KAl(SO_4)_2 \cdot 12\ H_2O$], pigments, oil and gas (Falk et al., 2006). It has also been used to extract elements such as uranium, sulphur, and nitrogen, while the alum shale in Norway has not been exploited for economic reasons. The economic potential for shale oil is not present in the alum shale found in Norway as opposite to Sweden. There are mainly two hypotheses for the absence of exploitable hydrocarbons in the Norwegian alum shale. One is that the organic material trapped in the shale in the Oslo region matured and migrated to the surface during the Caledonian folding in Silur (~400 mya) (Bjørlykke, 2010). The burial of the shale in Sweden was not as deep as in Norway and therefore the shale still has the potential to be exploited for shale oil. Another hypothesis is that hydrocarbons were expelled from the Norwegian alum shale due to high temperatures caused by the volcanic activity in the Oslo region under the Permian rifting (~300 mya) (Bastiansen et al., 1957).

2.1 Formation of alum shale

The sediments forming the Alum Shale Formation was deposited from the Middle Cambrian to the Early Ordovician (~500 mya) as the global sea level rose and intruded over a flat landscape (Nakrem and Worsley, 2013). Fine particles (<10 µm) were deposited with a slow deposition rate (~1 mm/1000 years) in shallow, oxygen-poor and stagnant water (Bjørlykke, 1974). The high supply of organic matter, probably of algal origin (Schovsbo, 2002), and low water circulation caused anoxic conditions as the oxygen was depleted under the degradation of organic matter. When oxygen is unavailable, dissolved sulphate (SO_4^{2-}) can act as an electron acceptor and sulphate is reduced to hydrogen sulphide (Berner et al., 1985). Hydrogen sulphide can further react with metals in the sediment to produce insoluble sulphides. In this way, iron sulphides, like pyrite (FeS_2) was formed and is the most common sulphide mineral in the alum shales (Sørmo et al., 2015). Other elements can also precipitate to form sulphide minerals or be incorporated in iron sulphides as impurities (Bierens de Haan, 1991). Additionally, heavy metals can be sorbed to clay minerals and organic carbon due to large reactive surfaces (Parviainen and Loukola-Ruskeeniemi, 2019) and enrich the shale in high levels of various metals/elements.

2.2 Weathering of alum shale

Alum shale was formed under anoxic conditions on the seafloor, but today it occurs on the surface due to different geological processes. The shale is not stable under atmospheric conditions and will therefore start to weather. This is a natural and relatively slow process. The problem arises when the shale is excavated and crushed. A larger surface area is exposed to oxygen and water, and the weathering reactions are accelerated. Oxidation of sulphides is the main cause of ARD. Equation 1 shows the overall reaction of pyrite oxidation (Appelo and Postma, 2005). The surplus of H^+ shows that acid is produced.

$$FeS_2(s) + \frac{15}{4}O_2(aq) + \frac{7}{2}H_2O \rightarrow Fe(OH)_3(s) + 2SO_4^{2-} + 4H^+ \qquad \textit{Equation 1}$$

The initial step of this reaction is the oxidation of pyrite (Equation 2) (Appelo and Postma, 2005). Subsequently, ferrous iron is oxidized to ferric iron (Equation 3). Ferric iron will further react with water and precipitate as iron(oxy)hydroxides under neutral pH conditions (Equation 4). However, the solubility of iron(oxy)hydroxides increases with low pH. If pH drops below

~ 4, Fe^{3+} will be soluble (reversing Equation 4) and poorly crystalline iron(oxy)hydroxides can dissolve. The ferric iron can be used as an electron acceptor to oxidize more pyrite (Equation 5). Oxidation of pyrite by ferric iron is a fast process and the acid-producing processes are accelerated.

$$FeS_2(s) + \frac{7}{2}O_2(aq) + H_2O \rightleftharpoons Fe^{2+} + 2SO_4^{2-} + 2H^+ \qquad \textit{Equation 2}$$

$$Fe^{2+} + \frac{1}{4}O_2(aq) + H^+ \rightleftharpoons Fe^{3+} + \frac{1}{2}H_2O \qquad \textit{Equation 3}$$

$$Fe^{3+} + 3H_2O \rightleftharpoons Fe(OH)_3(s) + 3H^+ \qquad \textit{Equation 4}$$

$$FeS_2(s) + 14Fe^{3+} + 8H_2O \rightleftharpoons 15Fe^{2+} + 2SO_4^{2-} + 16H^+ \qquad \textit{Equation 5}$$

2.3 Kinetics of pyrite oxidation

Reaction rates of minerals are dependent on the reactive surface area, the activity of solutes affecting the rate (reactant, inhibition or catalysis) and temperature (Appelo and Postma, 2005). Solutes affecting pyrite oxidation are mainly oxygen, but under acidic conditions (pH < 4), ferric iron is the main oxidant. The specific rate of pyrite oxidation in water by O_2 and Fe^{3+} is described by Williamson and Rimstidt (1994) and can be seen in Equation *6* and Equation 7.

$$r = 10^{-8.19}[O_2]^{0.5}[H^+]^{-0.11} \qquad \textit{Equation 6}$$

$$r = 10^{-6.07}[Fe^{3+}]^{0.93}[Fe^{2+}]^{-0.40} \qquad \textit{Equation 7}$$

The rate of pyrite oxidation by Fe^{3+} in the absence of oxygen can be seen in Equation 8.

$$r = 10^{-8.58}[Fe^{3+}]^{0.3}[Fe^{2+}]^{-0.47}[H^+]^{-0.32} \qquad \textit{Equation 8}$$

The rates of pyrite oxidation observed in lab experiments often deviate from those observed in the field (Appelo and Postma, 2005). As seen in Equation 2 to Equation 5, pyrite oxidation involves several reactions. The oxidation rate of ferrous iron to ferric iron (Equation 3) is pH dependent, where the process is slow at low pH and gets faster with increasing pH. Therefore,

when pyrite oxidation occurs and pH drops, the oxidation of ferrous to ferric iron becomes rate-limiting in an inorganic system. On the other hand, the chemical oxidation of pyrite by ferric iron is a fast process, but ferric iron is not available in solution when the pH is > 4. Iron-oxidizing bacteria (e.g. *Thiobacillus ferrooxidans*) can catalyse the oxidation of ferrous to ferric iron in an acidic system (Wakao et al., 1982), and explain the discrepancy between the observable rates of pyrite oxidation in the laboratory vs field. Additionally, precipitation of iron(oxy)hydroxides can armour the pyrite from further oxidation under neutral to alkaline pH conditions and slow down the rate of pyrite oxidation as less reactive surface area is available (Huminicki and Rimstidt, 2009).

2.4 Neutralizing potential

The net ARD potential of a rock depends on the ratio between acid producing minerals and neutralizing minerals (Pabst et al., 2017). As seen in Equation 1 sulphides, like pyrite, produce acid when it is oxidized. On the other hand, carbonates, like calcite, buffers the produced acid (Equation 9).

$$CaCO_3 + 2H^+ \rightleftharpoons Ca^{2+} + CO_2 + H_2O \qquad \text{Equation 9}$$

If sulphides are available in the rock after the neutralizing minerals are exhausted, a drop in pH will occur with further oxidation of sulphides. A method where AP (acid potential) is plotted against NP (neutralizing potential) can be used to estimate a rock's potential to produce ARD (Pabst et al., 2017). AP represents the theoretical amount of acid that can be produced from all sulphides in the rock when it is oxidized. NP is the theoretical total buffer capacity of all the neutralizing minerals in the rock, where carbonates are the most important ones. Other minerals (e.g., quartz, mica, and feldspars) are also acid-neutralizing. However, the reaction rates are way slower than for carbonates and are often neglected when assessing the potential of ARD (Khaidar Ali et al., 2020).

If NP:AP < 1, the rock is considered to be acid-producing (Wærsted et al., 2022). If NP:AP is between 1-3, it is uncertain if the rock will give acid drainage. These uncertainties come from the assumptions that all sulphides and carbonates behave like pyrite and calcite and that all the sulphur comes from sulphides (Pabst et al., 2017). All the sulphides and carbonates might not be available for reaction and these assumptions can result in an overestimation of both NP and

AP. Furthermore, the rock is not considered acid-producing if NP:AP > 3 (Wærsted et al., 2022).

2.5 Complexation

2.5.1 Surface complexation

When oxidation of pyrite occurs, iron(oxy)hydroxides will precipitate under neutral pH conditions (Equation 4). Like clay minerals and organic material, iron(oxy)hydroxides can sorb elements to their surface (Appelo and Postma, 2005). The pH affects the sorption capacity, as H^+ will compete with other cations for the binding sites on the sorption surface. If the pH is low, H^+ ions will outcompete other metals and release previously sorbed metals into the solution. Different elements behave differently in terms of sorption under different pH conditions (Figure 3), but the general trend is that more metals will be desorbed when the pH decreases. Additionally, iron(oxy)hydroxides will dissolve at low pH (< ~4) releasing metals into solution.

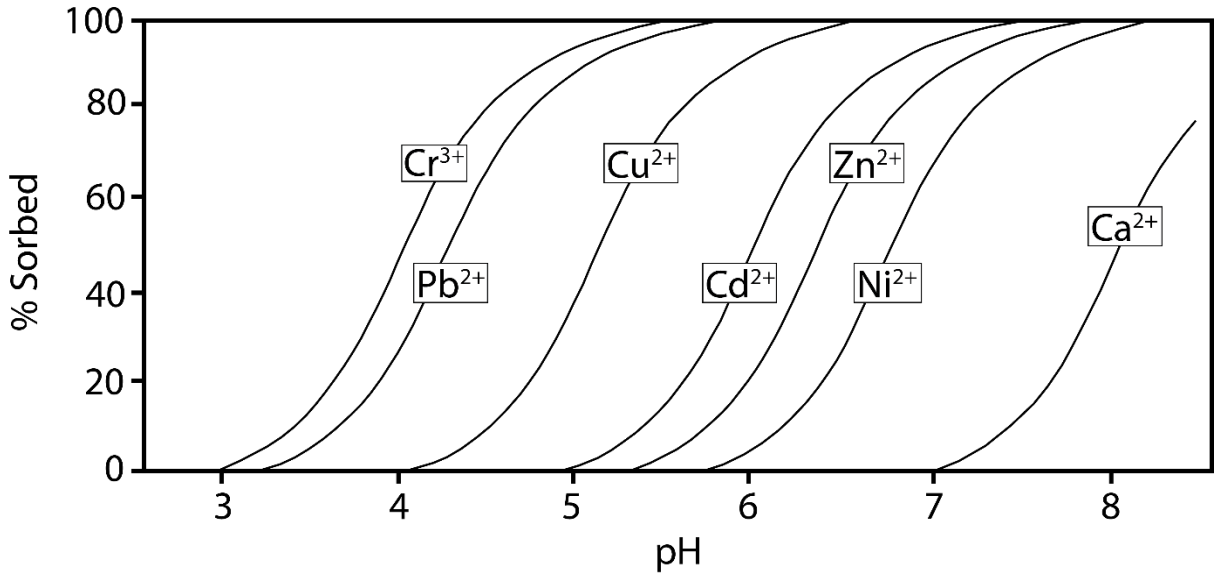

Figure 3: Adsorption of some metals on the surface of iron(oxy)hydroxides (ferrihydrite) as a function of pH. Modified from Appelo and Postma (2005).

2.5.2 Complexation in natural waters

When metals are present in a solution, they are surrounded by one or more ligands forming a complex ion (Zumdahl and DeCoste, 2017). Typical ligands are H_2O, Cl^-, NH_3, SO_4^{2-}, carbonates and small organic molecules (VanLoon, 2011). Ligands are recognized by having a lone electron pair that can form covalent bonds with the metal ion or be held in position by electrostatic forces.

All metals dissolved in pure water are present as "aquo" complexes, i.e., surrounded by water molecules as ligands (VanLoon, 2011). In natural waters, other dissolved substances that can act as ligands are often present. The water molecules can be displaced and form new, more stable complexes. Species distribution of metal complexes is a major factor in determining the mobility of the metal. It depends on the metal's nature itself and available ligands in the solution. Speciation of metal complexes can affect the solubility, sorption and precipitation of metals. The total concentration of ligands is often higher than the concentration of the metal ions. In seawater, chlorine is an obvious ligand that can affect the mobility of metals.

2.6 Secondary sulphate minerals

Acid drainage formed by the oxidation of sulphides contains elevated concentrations of sulphates, iron and other metals (Hammarstrom et al., 2005). Under acidic conditions, iron is more prone to form soluble secondary minerals, such as jarosite, than iron-oxides. Secondary iron-sulphate can then precipitate on weathered rocks and can be seen as a yellow-brownish coating on the surface (Figure 4b). Other heavy metals, including uranium can be incorporated in these secondary sulphate minerals (Lahrouch et al., 2022; Sørmo et al., 2015). These secondary sulphate minerals are soluble and produce acidic runoff immediately after they are dissolved. Seasonal peaks in the release of acid drainage can occur if a pile of crushed sulphide-bearing rocks are disposed of under atmospheric conditions (Hammarstrom et al., 2005): Sulphate-and metal enriched water can be produced from oxidation of sulphides by pore water and oxygen in the air during dry periods and secondary sulphate minerals can precipitate. When

the same rock is exposed to water, through rainfall or snow melting, a flush of acidic water with high concentration of heavy metals and secondary sulphates can occur.

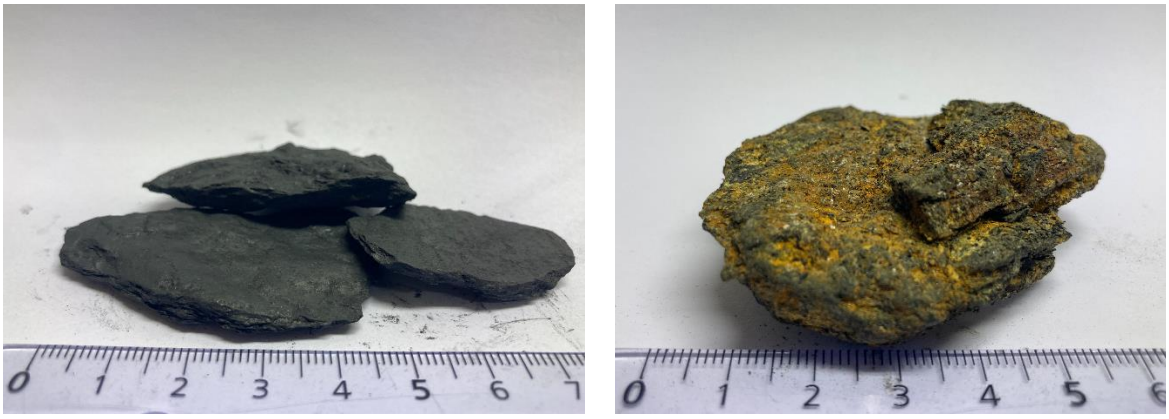

(a) (b)

Figure 4: Figure (a) shows unweathered alum shale from Kleggerud with its characteristic black colour. Figure (b) shows weathered alum shale deposited at Taraldrud with secondary sulphate minerals on the surface.

2.7 Disposal of alum shale

There are examples of unfortunate disposal of alum shale before special treatment of excavated alum shale was required by law, resulting in acid drainage and harmful elements leaching into the downstream environment. In 2004, it was decided in Norway's legislation that: "§ 2-3a: Rocks that form acid, or other substances that can cause pollution in contact with water and/or air are considered a contamination if nothing else is documented" (Lovdata, 2004). This legislation is valid for excavated masses, and states that, "§ 2-5: Contaminated masses must be delivered to an approved landfill or treatment facility with a permit under the Pollution Act". Some types of alum shales are classified by the Norwegian Radiation Protection Agency (NRPA) as radioactive waste. Rock masses with > 1 Bq/g (~80 ppm U) are classified as radioactive waste by the NRPA, and require special disposal (Wærsted et al., 2022). Acid producing black shales can leach radionuclides above the limits for release and must be delivered to a disposal site with permit from NPRA even if they are below the limit.

Limiting access to oxygen is crucial to ensure the safe disposal of acid-producing rocks. Today at least three approved landfills in Norway can receive alum shale (NOAH Langøya, Borge pukkverk massedeponi, Heggvin Alun).

2.7.1 Legacy sites for disposal of alum shale

Taraldrud, Norway

In Ski commune, large masses (~50,000 m^3) of alum shale, probably from the centre of Oslo (Figure 1), were disposed of next to E6 in the 1980s and 1990s (Børresen et al., 2022). In 2006, contamination from the disposed alum shale was detected. The nearby streams received acidic runoff with high concentrations of heavy metals, including uranium. Consequently, dead vegetation in the vicinity was observed (Figure 5). Geochemical characterization done in recent times implies that the shale mainly originated from horizons 2-3a and had the potential to produce ARD (Sørmo et al., 2017).

Precipitation ponds were installed in 2009 to reduce the spreading of contaminants. The clean-up work is still in the planning phase, and a plan for measures to reduce the contamination risk has been sent to the relevant authorities and is still under evaluation (Børresen et al., 2022).

Figure 5: Dead vegetation in the vicinity of the disposed alum shale at Taraldrud. Photo: BIOFORSK (https://taraldrud.info/alunskiferdeponi/).

Kvarntorp, Sweden

In 1942-1966, alum shale was excavated from open pits to extract oil in Kvarntorp, Sweden (Sjöberg and Karlsson, 2015). The oil was extracted from the shale by pyrolysis. Still glowing residual masses and unprocessed shale was placed back in waste piles or returned as fill material in an open pit. The pile of masses is currently 100 meters high and cover an area of 450 000 m^2 (Åhlgren et al., 2021) (Figure 6). The glowing residuals, in combination with free access to oxygen, caused pyrite and kerogen oxidation to proceed unhindered, and the pile was ignited. These oxidation reactions are exothermic and still ongoing today, and parts of the pile are still burning. Recently, temperatures of 700 °C have been observed 15 meters below the surface (Sjöberg and Karlsson, 2015). As a result, the groundwater in the pile's vicinity has elevated concentrations of elements such as molybdenum, nickel and uranium (Åhlgren et al., 2021). The leaching of harmful elements is expected to increase when the pile stops burning as more water can infiltrate without evaporation.

Figure 6: Kvarnstorp, Sweden: Burning pile of residual masses from oil extraction of alum shale. The photo is probably from the mid-1970s. (Photo: Pål-Nils Nilsson).

Jaren-Røykenvik

Heat generation resulting from exothermic reactions during the weathering process of alum shale has also been observed in Norway. Back in the late 19th century, when constructing a new railway (Jaren-Røykenvik), alum shale was used as a filler material (Løken, 2007). The railway remained free of snow for multiple winters, due to the heat generated by the exothermic reactions taking place during the weathering of the shale. The exothermic reactions occurring during weathering of alum shale pose a concern of self-ignition when alum shale is stored in huge piles with free access to oxygen.

2.7.2 Disposal of alum shale today

Disposal of alum shale in landfills - NOAH Langøya

NOAH Langøya is one of the approved landfills in Norway for the disposal of alum shale. The landfill is located in a former limestone quarry (Figure 7). The limestone has a low permeability and neutralizing potential, which makes it suitable for the disposal of acid-producing rocks (Sørmo et al., 2015). Limited access to oxygen is the most crucial factor in ensuring safe disposal of sulphide-bearing rocks. Therefore, disposal of alum shale in landfills is done in air-tight cells. The shale within the cells is stored in alternating layers of masses with alkaline properties to regulate the pH (NOAH, 2022).

Figure 7: The former limestone quarry at Langøya, where NOAH's landfill for hazardous waste is located (Photo: NOAH, 2014).

Local disposal of alum shale - RV4 Hadeland, Gran, Norway

Local disposal, closer to the construction site, has been carried out for alum shale from Hadeland (Gran) in 2014/2015 (Fjermestad et al., 2018). Alum shale was blasted out while constructing a tunnel for the new R4 road. A marsh nearby the construction site was exchanged with alum shale for local disposal under theoretically reducing conditions to prevent the sulphides from oxidizing. The alum shale was disposed of under the water table and covered, but leaching of uranium and heavy metals has already been observed (Engebretsen et al., 2020). The disposal site is monitored, and the long-term consequences of the disposal are still uncertain.

2.7.3 Sea disposal

Sub-aquatic disposal of mine tailings has been practised for approximately 30 years in Norway and Canada, amongst others (Skei and Sørby, 2019). The idea is to use water as an oxygen barrier and decelerate the weathering processes as water serves as an effective oxygen barrier, due to its significantly slower oxygen diffusion rate compared to air (approximately 10,000 times slower) (Sylvette Awoh et al., 2020). The main difference between mine tailings and alum shale is the grain size. Mine tailings are crushed to fine fractions (~100 µm) to extract as much metals as possible, while alum shale is excavated due to removal and contains larger fractions. The main problem associated with sea disposal of mine tailings reported from existing sites is suspension of fine material (Skei and Sørby, 2019).

Sub-aquatic disposal has been banned in most countries due to its potential negative impact on the marine environment (Sylvette Awoh et al., 2020). However, the geomorphology of some Norwegian fjords could make them suitable for sea disposal, as natural anoxic conditions can develop over time. The fjords are close to the shore with relatively deep waters and are often separated from the outer sea by a sill. The fjords are also suitable due to their flat bottom topography caused by high sedimentation and little tide activity, giving stagnant bottom water (Skei and Sørby, 2019). However, to protect the marine environment and ecosystems, a thorough risk assessment should be carried out to properly assess the consequences of sea disposal of alum shale. Nevertheless, sea disposal offers advantages compared to landfills as it avoids utilizing valuable land areas for waste disposal sites. In addition, landfills come with logistical challenges, demanding a construction that ensures safe long-term storage, leading to continuous monitoring and potentially high costs.

Drammensfjord

An example of a fjord that could be suitable for sea disposal is the Drammensfjord, due to its potential to naturally develop anoxic bottom conditions. The Drammensfjord is located near the occurrence of the Alum Shale Formation and other black mudrocks within the Cambro-Ordovician succession (Figure 1). The fjord is about 20 km long, less than 3 km wide, and is separated from the outer Oslofjord by a sill in Svelvik (Alve, 1995). The water depth is gradually increasing from around 10 meters by the outlet of the River Drammen in the north to approximately 124 meters in front of the sill in the south. The River Drammen flows into the fjord and freshwater is partially mixed with the marine fjord water, creating a stratigraphic water profile due to differences in density (Figure 8). Brackish surface water flows from north to south, acting as a lid over the deeper saline bottom water and preventing vertical mixing. The oxygen in the bottom water can be depleted under the degradation of organic matter (from primary production on the surface), and natural anoxic conditions can occur. The deep saline water is renewed every 3 to 5 years and has minor annual variations in temperature (ranging from 6.2 to 8.0 °C) and salinity (ranging from 30 to 31.5 ‰). The sill has been dredged several times to make a deeper passage for cargo shipping, and the current water depth by the sill is approximately 13 meters (Bechmann et al., 2017).

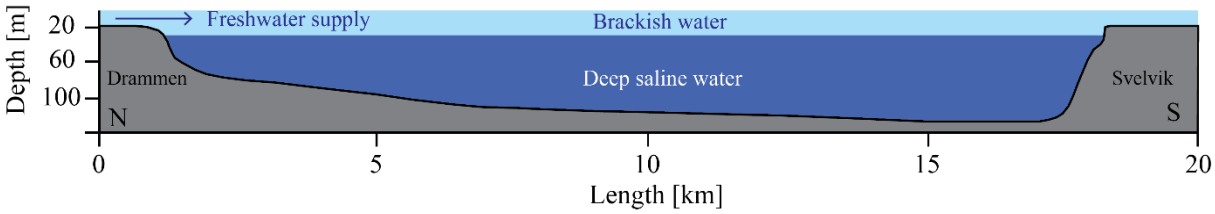

Figure 8: Conceptual cross-section of the Drammensfjord showing the morphology and the stratigraphic water profile. Modified from Alve (1990).

3. Method

3.1 Materials

3.1.1 Unweathered alum shale from Kleggerud

Unweathered shale used in the experiments was collected in august 2020 from an alum shale blast during the construction of new E16 between Eggemoen and Olum (Wærsted et al., 2023a). The approximate location of where the shale was sampled can be seen in Figure 1. The blasted alum shale is characterized as horizons 2 and 3a and was intruded by magmatic sills (Figure 9). 7-9 tons of the shale was sent to NGI for further experiments four days after the blasting.

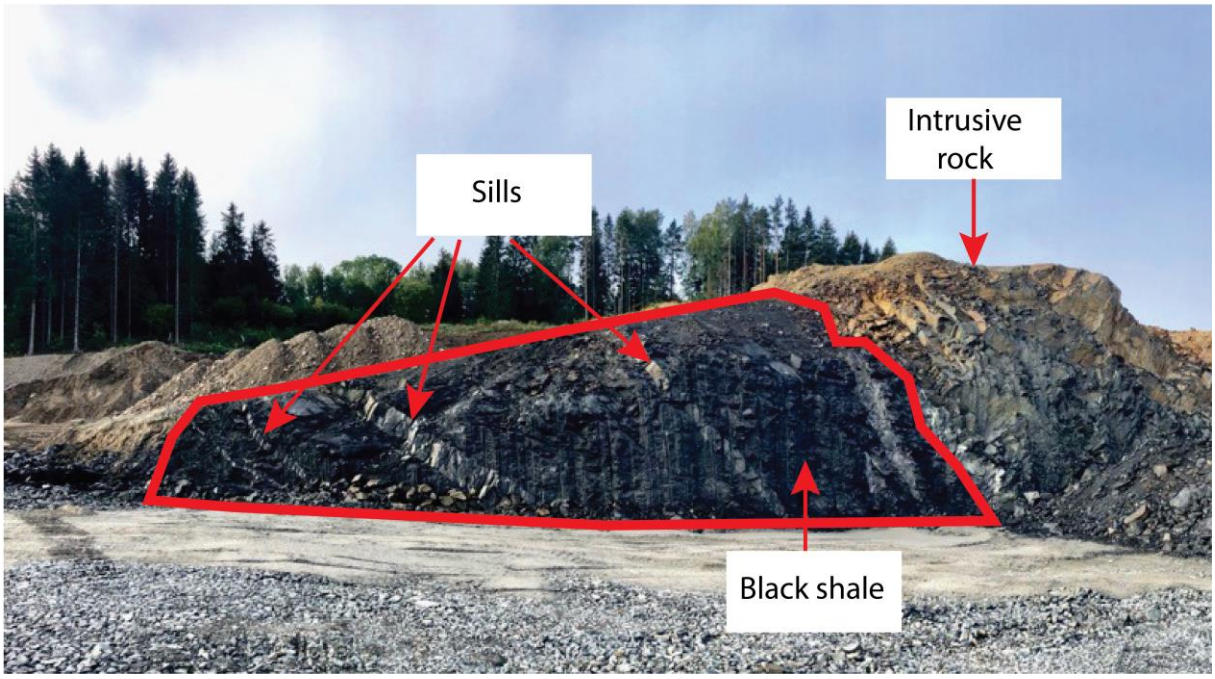

Figure 9: Sample site for the unweathered alum shale at Kleggerud. The road cut shows alum shale intruded by sills. Photo: Andreas Harstad, Skanska AS.

3.1.2 Weathered alum shale from Taraldrud

Weathered shale sampled by NGI in 2016 and 2021 from Taraldrud was used in Experiment 1 (Sørmo et al., 2017). 16 shafts were excavated and sampled for geochemical analyses. Samples from shaft 5 (390 g), 9 (150 g) and 16 (408 g), described by Sørmo et al. (2017) were mixed and used in the experiment. The assumed origin of the disposed of alum shale (Oslo City Centre) and where it was disposed of can be seen in Figure 1. To be sure that the fraction represented weathered shale, pieces less than ~8 cm were picked for the experiment. This fraction was chosen based on the concern that the bigger rocks (> 8 cm) had a core where the weathering reactions was not yet occurring. With further crushing, the big rocks could not be representable for weathered shale. Fractions less than 2 mm before crushing were also left out due to the concern that most of the possible weathering reactions had already occurred.

3.1.3 Preparation of samples for experiments

The shale was crushed manually with a hammer and sieved to a fraction less than 2 mm before it was transferred to a box. The shale was homogenized in the box by shaking followed by stirring the crushed shale with a spoon.

3.2 Rock characterization

The mineralogical and chemical composition of the unweathered (Kleggerud) and weathered (Taraldrud) starting material used in Experiment 1 and 2 were analysed with Scanning Electron Microscope (SEM), X-ray diffraction (XRD) and whole rock analysis. Additionally, analyses of the grain size distribution and total inorganic- and organic carbon (TIC and TOC) were conducted.

3.2.1 Scanning Electron Microscope (SEM)

The different mineral phases and morphology of the bulk material used in the experiments were qualitatively identified by scanning electron microscopy (SEM). Salahalldin Akhavan made thin sections of the crushed debris of unweathered and weathered shale at the Department of Geosciences at the University of Oslo. The two thin sections were later analysed using a Hitachi TM4000 Plus Tabletop Scanning Electron Microscope (Department of Geosciences).

The instrument scans the sample with a beam of electrons and detects radiation signals caused by the interaction between the sample and the electrons (Klein and Dutrow, 2008). Signals detected are secondary electrons (SE) and backscattered electrons (BSE). SE has the lowest energy and is reflected from the sample's surface, giving information about the surface topography. BSE has more energy and provides information from deeper parts of the sample. BSE is a function of the mean atomic weight and gives different compositions as contrasts in an image. The instrument is also equipped with an Energy-Dispersive X-ray detector (EDS) that measures the energy of X-rays produced by interactions with the electrons. X-rays' energy is characteristic of each element and provides information about the chemical composition as X-ray spectra. The spectra produced are compared to spectra of known minerals and are used to interpret which mineral phases are observed in the BSE images. One outcrop (representing the majority of the matrix of the shales) from the unweathered and weathered shale were chosen for mapping, i.e., specific elemental composition across a larger area. This was done using a Hitachi SU5000 FE-SEM by the Department of Geosciences at the University of Oslo.

3.2.2 X-ray diffraction (XRD)

Semi-quantitative analysis with X-ray powder diffraction (XRD) was used to identify the mineral phases and relative amounts in the bulk material. In XRD, a beam of X-rays is directed at the sample, and the diffracted X-rays are detected (Klein et al., 2008). X-rays are diffracted by the arranged three-dimensional structure in the crystal lattice of a mineral (Figure 10). The diffracted rays can cause constructive interference if Bragg's equation, given by $n\lambda = 2d \sin \theta$ is satisfied (Bragg and Bragg, 1913). Here n is an integer, λ is the wavelength, d is the d-spacing in the crystal lattice, and θ is the incidence angle of the X-rays. Bragg's law states that constructive interference, or diffraction maxima, will only occur at specific angles of incidence (θ). By alternating λ and θ, the d-spacing for all lattice planes can be found from diffraction maxima. The d-spacing for different minerals is already known and makes it possible to determine the mineralogical composition of a sample by identifying the diffraction maxima at specific values of λ and θ.

XRD analyses were performed on the starting materials (unweathered and weathered shale) and the samples treated with water under different conditions for 7 and 9 months. XRD was performed at the Geological Department of the University of Oslo with a Bruker D8 Advance

using Cu-Kα radiation. The diffractograms retrieved from the XRD were further analysed in the XRD software Profex (Doebelin and Kleeberg, 2015).

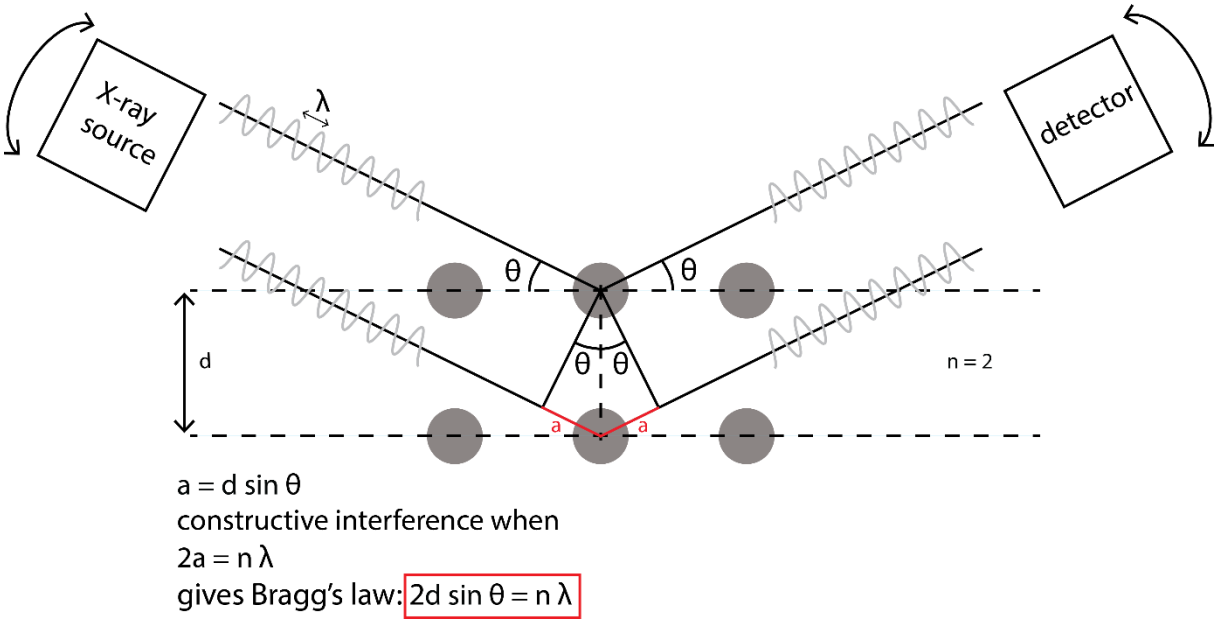

Figure 10: Conceptual sketch showing how X-rays are diffracted in a lattice of a mineral and how Bragg's law is used to find the d-spacing of the equally spaced planes. Modified from (Klein et al., 2008).

Sample preparation

The sample was milled and homogenized in two steps. The sample was first dry milled to a grain size < 0.5 mm before it was further wet milled to a fraction smaller than approximately 5-10 µm (micronized). To micronize the sample, 2.5 - 3.0 g sample material and 8 mL ethanol was added to a milling beaker together with agate milling stones. The beaker was placed in a McCrone Micronizing Mill for approximately 12 minutes. 8 mL ethanol was added after milling to transfer the fine sample material from the beaker to a plastic container. The samples were then placed in a heating cabinet of approximately 50 °C until the ethanol had evaporated. The dried sample material was disintegrated by a mortar and transferred to XRD sample holders. A glass plate was used to compact the sample and make an even surface with no preferential orientation of the grains.

3.2.3 Total carbon (TC)

The carbon content in the weathered and unweathered shale was analyzed with a Thermo scientific FlashSmart CHNS/O Analyzer with Micro Volume Correction (MVC). The analysis was performed at the Department of Geosciences at the University of Oslo by Mufak Said Naroz. This instrument subjects a sample to a high-pressure oxygen environment and high temperatures ~1800°C (Schumacher, 2002). This causes the sample to combust. The gas mixture caused by the combustion (N_2, CO_2, H_2O, and SO_2) is separated through a column and measured using a thermal conductivity detector. The instrument uses the measured CO_2 to calculate the total carbon (TC). Total inorganic carbon (TIC) is measured indirectly by analysing one sample treated with acid and one that is not. Combustion of the acid-treated sample gives total organic carbon (TOC), and the one that is not treated with acid gives TC. TIC can then be calculated from *Equation 10*.

$$TIC = TC - TOC \qquad \textit{Equation 10}$$

Sample preparation

Approximately 1 gram of the sample was pulverized and added to a 50 mL centrifuge tube. The exact weight was noted. 15 mL of 1 M Hydrochloric Acid (HCl) was added to the sample and left overnight to remove inorganic carbon (TIC). Then the samples were centrifuged at 3000 rpm for 10 minutes before decanting the acid supernatant. The remaining acid was removed by adding distilled water to the sample before it was centrifuged again. The supernatant was decanted, and the sample was dried at 40 degrees before it was weighed again.

Parallels of pulverized acid-treated samples and untreated samples were packed with electrolytic copper and copper oxide. The samples were placed in a tin sample crucible and installed in the reactor for combustion.

3.2.4 Whole rock analysis

The starting material of weathered and unweathered shale used in the experiments were analysed at Activation Laboratories Ltd (ActLabs) in Canada for whole rock analysis. Also, samples that had been in contact with fresh -and seawater for nine months in experiment 1 were analysed. The analyses at ActLabs were performed after Lithium Borate Fusion of the samples followed by digestion in a weak nitric acid solution. In this way, all elements are dissolved, and can be analysed with inductively coupled plasma mass spectrometry (ICP-MS) and inductively Coupled Plasma Optical Emission spectroscopy (ICP-OES).

The samples were analysed for S, Al, Fe, Mn, Mg, Ca, Na, K, Ti, P, Sc, Be, V, Cr, Co, Cd, Ga, Ge, As, Rb, Sr, Y, Zr, Nb, Mo, In, Sn, Sb, Cs, Ba, La, Ce, Pr, Nd, Sm, Eu, Gd, Tb, Dy, Ho, Er, Tm, Yb, Lu, Hf, Ta, W, Tl, Bi, Th, U and Loss of Ignition (LOI). The results obtained from the whole-rock analyses were plotted by Frøydis Meen Wærsted (NGI) in NP:AP -and Fe:S diagrams, in addition to triangular plots. The samples are compared to other black mudrocks within the Cambro-Ordovician succession in the plots to identify horizon of origin. The method is developed by Pabst et al. (2017) and was used to characterize which horizon the unweathered -and weathered shale originated from.

3.2.5 Grain size distribution

A particle Size Analyzer (Beckman Coulter LS13 320) was used to determine the grain size distribution for the unweathered and weathered shale used in experiments 1 and 2. The analysis was performed at the Department of Geosciences at the University of Oslo by Mufak Said Naroz. The instrument uses the diffraction of light from lasers to determine grain size distribution in the range of 0.4 µm - 2000 µm. Lasers are directed to the grains, and the light from the lasers is diffracted at different angles depending on the size of the grains. The diffracted light and its intensity are detected. Each particle size will give a specific diffractogram, and the intensity of the diffracted light gives the number of particles in a specific size interval. The method assumes all particles to be spherical.

3.3 Experiment 1: Oxic and low-oxygen

A batch experiment of 192 plastic bottles were set up to assess the consequences of storing alum shale in seawater and freshwater under different conditions. The experiment was started 20th of April 2022. The plastic bottles in Experiment 1 were filled with weathered and unweathered shale in contact with sea- and fresh water with associated blanks, i.e., bottles with fresh- and seawater treated the same way as the samples, only without added alum shale. The bottles were stored under different conditions and sampled over approximately 11 months (44 weeks). Half of the samples, hereafter called "oxic samples", were stored in contact with the atmosphere. The other half, hereafter called "low-oxygen samples", were stored in a box filled with water to reduce the access to oxygen. All samples were kept still at room temperature during the sampling period.

The experiment was set up and stored in the sediment lab in the Department of Geosciences at the University of Oslo. The experimental set up can be seen in Figure 11. Approximately 10 grams of shale were weighed onto a piece of paper before being transferred to plastic bottles with a volume of 100 mL. The exact weight and type of shale, type of water and storing conditions were noted on each bottle. The labelling system can be seen in Table 1. Deionized water was used for the freshwater samples, and seawater from the Oslo fjord, supplied by Norwegian Institute for Water Research (NIVA), was used for the seawater samples. The seawater was collected at NIVA's research station at Solbergstrand at a water depth of 50 meters. Due to evaporation, the samples stored under oxic conditions were refilled with deionized water during the sampling period.

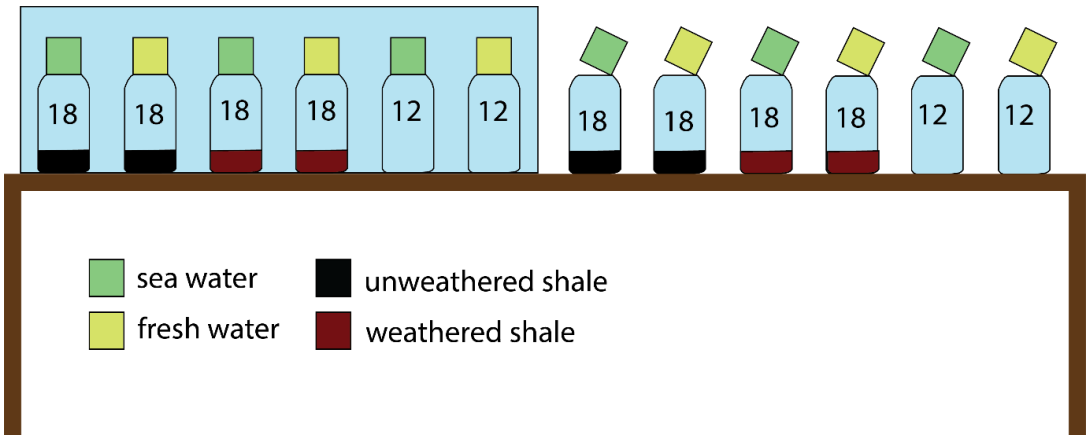

Figure 11: Experimental setup for Experiment 1 with number of samples, content in the bottles and storing conditions of the samples.

Table 1: Labelling of samples in Experiment 1.

Sample	Shale	Water	Treatment
1_FO	Unweathered	Fresh	Oxic
1_SO	Unweathered	Sea	Oxic
1_WFO	Weathered	Fresh	Oxic
1_WSO	Weathered	Sea	Oxic
1_BFO	Blank	Fresh	Oxic
1_BSO	Blank	Sea	Oxic
1_FL	Unweathered	Fresh	Low-oxygen
1_SL	Unweathered	Sea	Low-oxygen
1_WFL	Weathered	Fresh	Low-oxygen
1_WSL	Weathered	Sea	Low-oxygen
1_BFL	Blank	Fresh	Low-oxygen
1_BSL	Blank	Sea	Low-oxygen

Oxic samples were prepared under atmospheric conditions and stored with the cap laying loose on top (Figure 12a). Low-oxygen samples were also prepared under atmospheric conditions, but the caps were mounted under water of the respective sample water (fresh -or seawater) to ensure no air bubbles in the bottles. The low-oxygen samples were stored in two 30x40x11cm plastic boxes filled with water to reduce the rate of oxygen intrusion (Figure 12b). The freshwater blanks did not sink to the bottom of the water-filled box. Therefore, a glass plate was taped under the bottle to make it sink.

(a) Oxic samples stored under atmospheric conditions with the lid laying loose on top.

(b) Low-oxygen samples stored in boxes filled with water. Photo was taken before freshwater blanks got glass plates to avoid floating.

Figure 12: Storing conditions for the samples in Experiment 1.

Sampling schedule

The number of samples was decided based on sampling points and triplicates. All the water in one bottle was used for one sampling point. Each treatment was sampled one day, one week, two weeks and one month after experiment start, followed by sampling each month for the first seven months. The last four months sampling was done at two-month intervals. Triplicates for all treatments, except the blanks, were made for the sampling at one, six, and 11 months. Figure 13 shows the timeline of the sampling schedule.

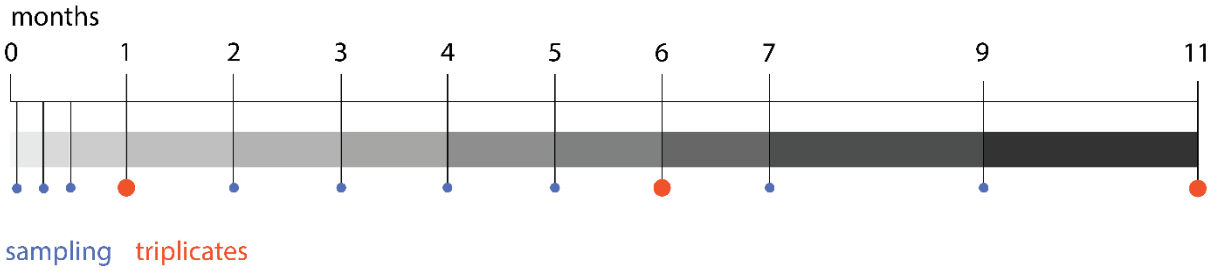

Figure 13: Timeline of the sampling schedule for Experiment 1 showing timepoints and triplicates (in red) for the sampling.

3.3.2 Experiment 1: Method Evaluation

An additional experiment was set up to examine if the plastic bottles used for the "low-oxygen samples" prevented a fast diffusion of oxygen when stored in water. Nitrogen-bubbled water with an oxygen concentration of 1.2 mg/L was filled in the same type of plastic bottles as used in Experiment 1. The bottles were filled with water in a nitrogen-flushed glove box. The bottles were stored under water for one week before the dissolved oxygen was measured again in a nitrogen-flushed glove box.

A beaker with water was also placed in the glove box during the measurements. The oxygen concentration in this water was originally 8.7 mg/L (before flushing the glove box with nitrogen). The dissolved oxygen was measured after the glove box was filled with nitrogen and after the measurements of the other bottles were done, to investigate how quickly oxygen was removed from solution under the sampling conditions.

3.4 Experiment 2: Oxic and anoxic

Due to the concern of unsatisfying high oxygen concentrations in the "low-oxygen samples", a new batch experiment using glass bottles was started 26th of October 2022 to get anoxic conditions. Only unweathered shale was used, and the experiment lasted for 16 weeks. Experiment 2 was set up the same way as described for Experiment 1. Instead of using plastic bottles, dark glass bottles of 100 mL and nitrogen-bubbled water were used. The anoxic samples cannot be directly compared with the "oxic samples" from Experiment 1 since metals tend to be sorbed to the glass surface (Matusiewicz, 2017). The glass itself can additionally contaminate the sample with trace elements. Therefore, oxic samples using glass bottles were also prepared, giving a total of 40 bottles with unweathered shale under anoxic and oxic conditions treated with seawater and freshwater, with associated blanks. The labelling system of the bottles in Experiment 2 can be seen in Table 2. The bottles were filled with nitrogen-bubbled water with an oxygen concentration of approximately 0.5 mg/L in a nitrogen-flushed glove box. Rubber stoppers and crimp caps were used to seal the anoxic glass bottles. The anoxic treatments were stored in the same way as the low-oxygen samples in Experiment 1, i.e., in a water filled box.

Experiment 2 was sampled after one week, one month, two months and four months. Triplicates of the samples, except the blanks, were sampled at the last measuring point. Figure 14a shows the conceptual set-up of the experiment, and Figure 14b shows the timeline of sampling.

Table 2: Labelling of samples in Experiment 2.

Sample	Shale	Water	Treatment
2_FO	Unweathered	Fresh	Oxic
2_SO	Unweathered	Sea	Oxic
2_BFO	Blank	Fresh	Oxic
2_BSO	Blank	Sea	Oxic
2_FA	Unweathered	Fresh	Anoxic
2_SA	Unweathered	Sea	Anoxic
2_BFA	Blank	Fresh	Anoxic
2_BSA	Blank	Sea	Anoxic

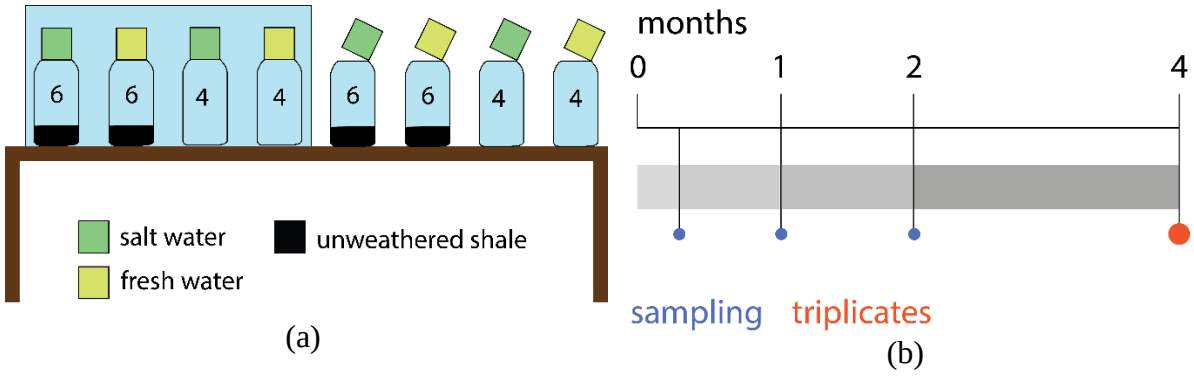

Figure 14: (a) Shows the experimental setup for Experiment 2, and (b) shows the sampling timeline with triplicates in red.

3.5 Water analyses

The oxic samples were sampled under oxic conditions, while the low-oxygen and anoxic samples were sampled in a nitrogen-flushed glove box (Figure 15). The box was flushed until desirable oxygen concentrations were reached. Due to lack of equipment to measure the oxygen concentration in the glove box, the same probe used to measure the dissolved oxygen was used in air as an indicator for when the oxygen concentration was low enough for measurements. The box was flushed for approximately 30-40 minutes until the probe showed a measure of less than 1 mg/L. After the desirable O_2 concentration was reached, the flushing was stopped, and the box was kept close during the measurements.

As the bottles had narrow bottle necks, the water leachate was transferred to a beaker with a pipette. 20 mL leachate was filtered with 0.45 µm syringe filter directly into 15 mL tubes for IC (10 mL), alkalinity (5 mL) and ICP-MS (5 mL).

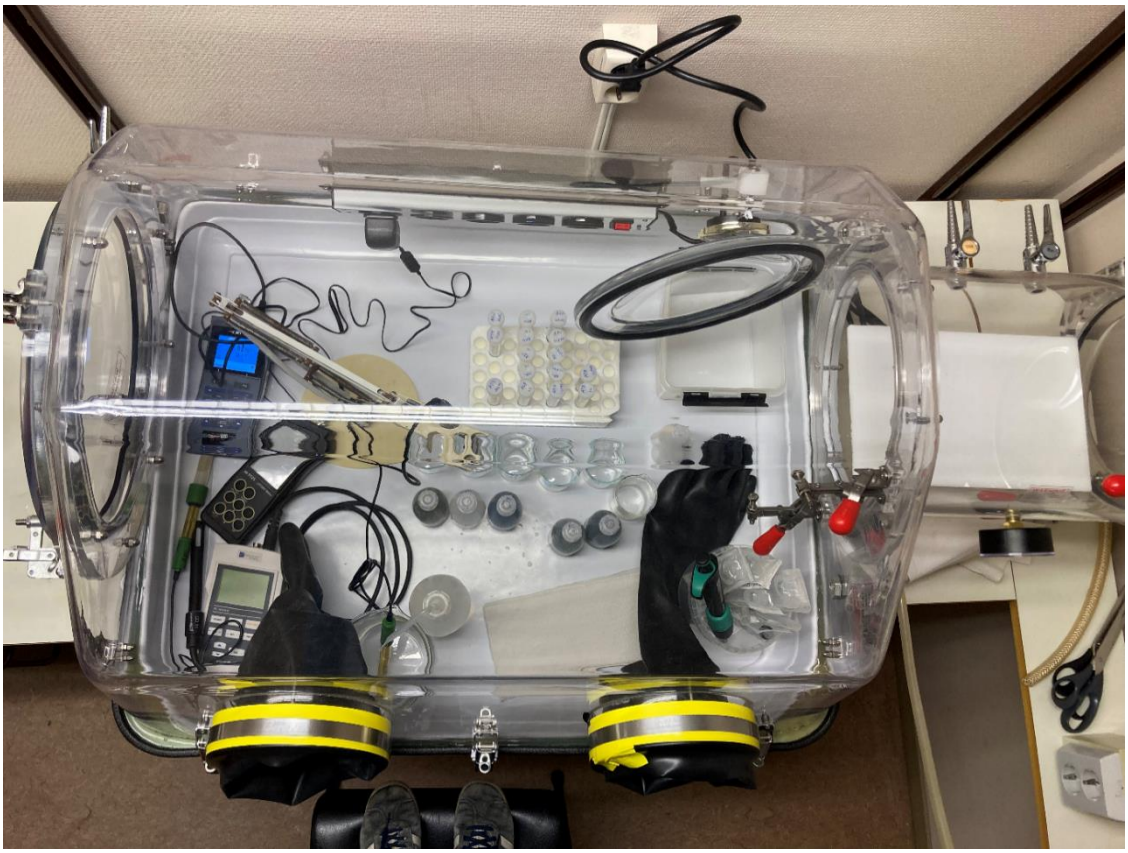

Figure 15: Sampling of low-oxygen samples in the glove box.

3.5.1 Field parameters

Field parameters, i.e., conductivity, dissolved oxygen, pH and redox potential, were measured in the remaining water of the beaker, as the probes could not fit through the bottle necks. Conductivity was measured first with a pH / conductivity meter (PC 5000 H, VWR), followed by measurements of dissolved oxygen (DO) with a Multi 3410 IDS (WTW). Then pH and redox potential were measured with a Portable pH/ORP Meter (HI9125, Hanna). Eh was calculated by adding a correction factor of 220 mV to the oxidation-reduction potential (ORP) based on the standard reduction potential for an Ag/AgCL electrode (Zumdahl and DeCoste, 2017).

3.5.2 Alkalinity

Alkalinity is a measure of the acid neutralizing capacity, which in natural water mainly is composed of the carbonate ions HCO_3^- and CO_3^{2-}(VanLoon, 2011). The alkalinity is found by titrating the sample with acid to a pH of approximately 4.5. Metrohm 702 SM Titrino Titrator was used to measure the alkalinity. Due to large differences in alkalinity between the samples, different hydrochloric acid (HCl) concentrations were used for titration: a concentration of

0.001 M HCl was used for the freshwater samples, while 0.01 M HCl was used for the seawater samples. 5 mL of the sample was transferred to a 20 mL plastic container. The auto titrator added a known volume of HCl with a known concentration to calculate the alkalinity by Equation 11.

$$Alkalinity\ \left(\frac{meq}{kgw}\right) = 1000 \cdot \frac{V_{ep} N_{HCl}}{V_{smpl}} \qquad \textit{Equation 11}$$

Where V_{ep} is the volume of acid added, N_{HCl} is the concentration of the acid and V_{smpl} is the volume of the sample (5 mL).

3.5.3 Ion chromatography (IC)

Dionex ICS-2000 Ion Chromatography System was used to measure major anions and cations from the water in experiments 1 and 2. Mufak Said Naroz analysed the samples at the Department of Geosciences at the University of Oslo. The instrument injects the sample into an eluent (Potassium hydroxide for anions and Methane sulphonic Acid for cations) which is pumped into an ion-exchange column (Borba and Rohrer, 2004; Thomas and Rohrer, 2013). Different columns are used for cations and anions and the exchange resins is changed based on which ions are analysed. The retention time in the columns varies for the different ions according to their affinity. The separated ions are transported to a device that suppresses the eluent's conductivity so the separated ions' conductivity can be detected. Different ions are identified by comparing the retention time to known standards. Their quantitative amounts are derived from peak heights or areas in chromatograms produced.

Sample preparation

The filtered (0.45 µm) leachates from the experiments had too high ion concentrations for the IC analysis and had to be diluted. Freshwater samples were diluted to 1:100, and the seawater samples were diluted to 1:1000. This was done by pipetting out 1 mL sample water and adding 9 mL of deionized water to a 15 mL centrifuge tube to get a 1:10 dilution. 1 mL of the 1:10 solution was then pipetted out, and 9 mL of deionized water was added to make a 1:100 dilution. The same procedure was repeated to make a 1:1000 dilution for the seawater samples.

3.5.4 Inductively coupled plasma mass spectrometry (ICP-MS)

Agilent 8900 ICP-MS Triple Quad was used to measure trace elements (Al, As, Ba, Cd, Co, Cr, Cu, Fe, Mn, Mo, Ni, Pb, Sb, Se, Sn, Tl, U, V, Zn) in the leachate from the experiments. The ICP-MS analyses were carried out at NOAH AS langøya, by Sverre Frimann Koren. The instrument works by injecting the sample (in liquid form) into a nebulizer, which converts the sample into aerosols when mixed with argon (Thomas, 2013). Further, the larger aerosols are removed when entering the cooled spray chamber. The fine aerosols move further into a high-temperature argon plasma torch, where the aerosols are dried and decomposed until the matrix is ionized, giving a source of positively charged ions. The charged ions are extracted from the plasma through a skimmer cone and pumped into a high vacuum region where ion optics focus the beam of ions into the mass separation device. The ions are separated based on their mass-to-charge ratio before they are sequentially converted into electrical signals by an ion detector. The instrument produces a mass spectrum, and analyte concentrations are found using ICP-MS calibration standards.

Sample preparation

The samples had to be stored for up to 11 months before the ICP-MS analyses. Therefore, nitric acid HNO_3 was added to the filtered (0.45 µm) sample water for conservation. This was done by adding 50 µL of concentrated HNO_3 to 5 mL leachate.

3.6 Modelling

PHREEQC (version 3) was used to do geochemical modelling to predict the long-term consequences of sea disposal of unweathered alum shale. PHREEQC is a hydrogeochemical modelling program based on a thermodynamic database of chemical reactions (Parkhurst and Appelo, 2013).

The chemical processes implemented in the model were

1) Oxidation of pyrite (source of acid).
2) Dissolution of calcite (providing buffer capacity) and jarosite (source of acid).
3) Precipitation of gypsum, barite, and iron(oxy)hydroxide as goethite (FeOOH), chalcopyrite ($CuFeS_2$) and sphalerite (ZnS).
4) Sorption of trace elements (or other cations) to goethite.
5) Cation exchange capacity (CEC) of the shale.
6) Partial pressure of oxygen (p_{O2}) and carbon dioxide (p_{CO2}).

A conceptual sketch summarizing the chemical processes implemented in the model can be seen in Figure 16. The model was calibrated according to experimental data (pH, sulphate, calcium, and uranium) for unweathered shale treated with freshwater under oxic conditions (1_FO). The model was further validated by changing the initial solution from deionized water to seawater and compared with experimental data for the batch treated with seawater under oxic conditions (1_SO). An extrapolation was carried out to predict how long it would take before the batch, 1__FO would produce ARD. To assess the consequences of sea disposal, Drammensfjord was chosen as a case study, and temperature and exchange time of bottom water were implemented after the conditions reported in the Drammensfjord by Alve (1995).

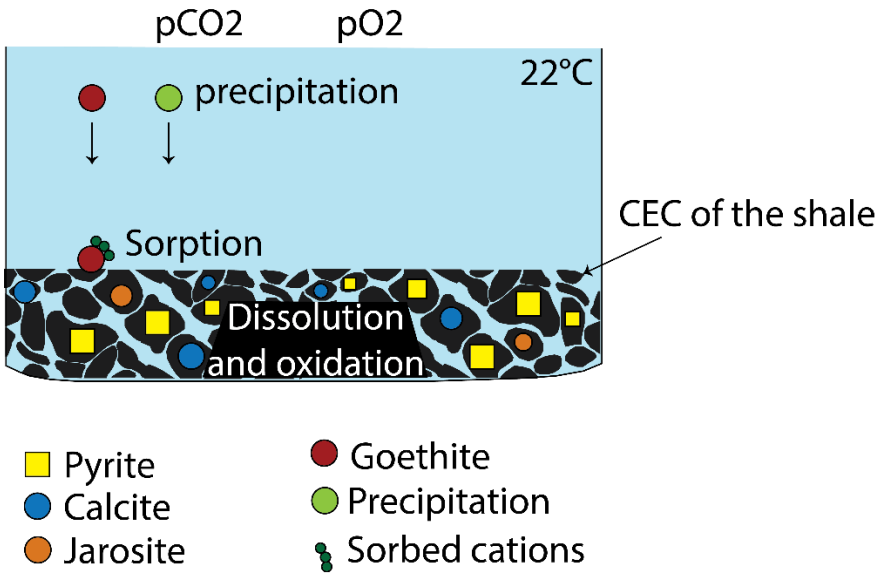

Figure 16: Conceptual sketch summarizing the chemical processes implemented in the model: 1) Pyrite oxidation, 2) Dissolution of calcite and jarosite, 3) Precipitation of gypsum, barite, goethite, chalcopyrite and sphalerite 4) Sorption of cations to goethite 5) Cation exchange capacity (CEC) of the shale, 6) partial pressure of oxygen and carbon dioxide.

3.6.1 Implementations in PHREEQC

The database used in the model was Lawrence Livermore National Laboratory (llnl.dat) as this database included thermodynamic data of uranium. The model was simulated in a system with 1 L of water. Therefore, the batch experiment was multiplied by 10, and the amount of shale used for the calculations was 100 g. Calculations of input parameters for the model can be seen in Table A 1 (Appendix) and the code for the calibration, validation and Drammensfjord model can be accessed through the following link: https://github.com/alhenrik/PHREEQC.git.

Phases

The number of moles of different minerals implemented in the model was based on XRD and whole rock analysis. Precipitation of iron(oxy)hydroxides (as goethite), gypsum, barite, chalcopyrite and sphalerite were implemented in the model by setting the target saturation index to zero which forces the defined phases into equilibrium and will simulate precipitation if Saturation index (SI) exceeds 0. SI can be defined under the PHREEQC command EQUILIBRIUM PHASES and is equal to the logarithm of the ion activity product (Q) divided by the equilibrium constant (K) (SI = log(Q/K)). The system was initially set in equilibrium with the atmospheric pressure of O_2 (21 %) and CO_2 (400 ppm) by setting the saturation index

to the logarithm of the partial pressure. The amount of uranium was retrieved from whole-rock analysis and implemented as uraninite. Schovsbo (2002) postulated that U(VI) was trapped in the alum shale by scavenging to particles and organic matter in the water column (in addition to diffusion) and was later reduced and precipitated as U(IV) phases (as uraninite) in the sediment. Pyrite, calcite, feldspar, and uraninite was implemented in the model under the PHREEQC command KINETICS.

Rates

A default rate of pyrite oxidation is available in the database; however, this rate-equation does not take Fe^{3+} into consideration as an oxidizing agent in the absence of oxygen. Another rate-equation (Equation *6* to Equation *8*) of pyrite oxidation modified from example 9.9 in Appelo and Postma (2005) was implemented in the model. This rate equation includes both oxygen and ferric iron as electron acceptors and is compiled from Williamson and Rimstidt (1994). Rate for uraninite was lacking from the database, and was compiled from Palandri and Kharaka (2004) and implemented in the model under the PHREEQC command RATES.

Trace elements

Amounts of barium (Ba) and manganese (Mn) were based on whole rock analysis, while amounts of copper (Cu) and zink (Zn), were based on results obtained from Wærsted et al. (2023a), which have characterized the same batch of unweathered shale from Kleggerud. Cu, Zn, Ba and Mn were implemented in the model as impurities in pyrite (FeS_2) substituting iron. These trace metals were chosen to be included in the model because thermodynamic data for sorption on iron(oxy)hydroxides was available in the database and because they are relevant for environmental toxicity.

Surface complexation: Ion- exchange and sorption

To model ion exchange, the PHREEQC command EXCHANGE was used. This requires the definition of cation exchange capacity (CEC). CEC was calculated from the empirically derived formula Equation 12 (Appelo and Postma, 2005). To estimate the elemental composition of the exchangeable cations in the shale, another solution (SOLUTION 2) with major cat- and anions measured in 1_FO (unweathered shale in freshwater, oxic treatment) after one month was implemented. This solution was equilibrated with exchange sites available defined by CEC. PHREEQC calculates the composition of the exchangeable assemblage on the exchanger when

it is in equilibrium with SOLUTION 2 without changing the composition of the initial solution (SOLUTION 1).

$$CEC = 7\ (\%clay) + 35\ (\%organic\ C) \qquad \textit{Equation 12}$$

To model sorption of trace elements on precipitated goethite, the command SURFACE was used. This requires implementation of sites per mol available for sorption and specific surface area of goethite. This was retrieved from Table 7.5 from Appelo and Postma (2005). Further, sorption of uranyl was implemented under the PHREEQC command SURFACE_SPECIES as it was lacking in the database. This requires thermodynamic data for the sorption species of uranyl and were retrieved from the PHREEQC database Tipping_Hurley.dat.

Calibration and validation

The model was calibrated using the batch with deionized water in contact with unweathered shale (1_FO). In this model, porewater calculations were performed using PHREEQC, by implementing a shale-to-water ratio of 1:10. To be able to calibrate the model based on the results obtained from Experiment 1, an assumption of perfect mixing between the porewater and the water above the shale was made. The model was calibrated by changing the reactive surface area of pyrite, calcite and uraninite until it fitted the pH and the measured concentrations of sulphate, calcium, and uranium over the sampling period. The pressure of oxygen was also adjusted (set lower) until it fitted the dissolved oxygen concentrations measured in the experiment, as it deviated when partial pressure was set to 0.21. A rapid increase in sulphate was measured in 1_FO the first 14 days, followed by a slower linear increase in the sulphate concentrations during the rest of the sampling period. This first rapid increase was assumed to come from dissolution of secondary sulphate minerals, and jarosite was implemented in the model. The amount of jarosite was adjusted until it fitted the first rapid increase measured in Experiment 1. The model was validated by changing the initial solution from freshwater to seawater and comparing the measured and modelled concentrations.

Sea disposal of alum shale (Drammensfjord)

To simulate sea disposal of alum shale, with Drammensfjord as a case study, the model was adjusted. These adjustments involved the implementation of water transport mechanisms and the modification of the temperature from 22 to 7 degrees Celsius. A conceptual sketch of the modified transport model can be seen in Figure 17. The residence time of the stagnant bottom water was defined as either 3 or 5 years under the command TRANSPORT. This was based on the periodic renewal of the anoxic bottom water with freshly oxygenated surface water occurring every 3 to 5 years (Alve, 1995). The oxygenated surface water was set in equilibrium with the atmospheric pressure of O_2 and CO_2. It is important to note that the bottom water, in contrast to the oxygenated surface water, was not set in equilibrium with the atmosphere. Consequently, the only source of oxygen and carbon dioxide for the bottom water originated from the surface water, giving a limited oxygen supply to the bottom water.

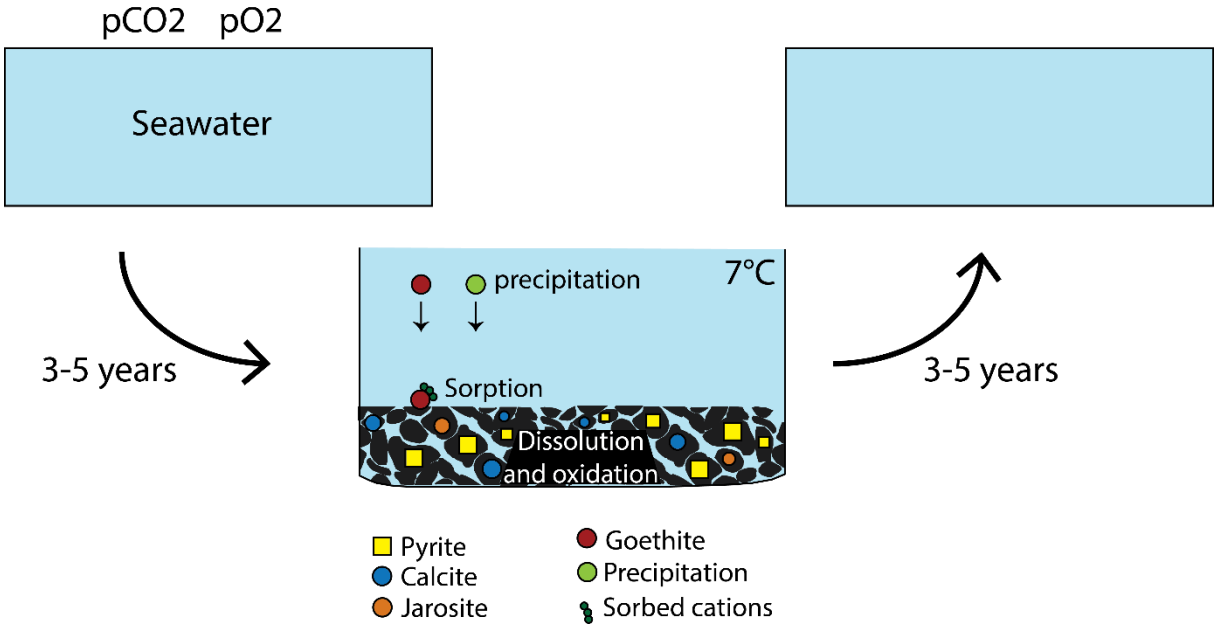

Figure 17: Conceptual sketch of the transport mechanism implemented in the model to simulate sea disposal of alum shale in the Drammensfjord.

3.7 Statistics

Significant differences between treatments in the experiments and the standard deviation of the triplicates were calculated in Excel using the commands T.TEST and STDEV. Relative standard deviation (RSD%) was calculated for the last measuring point in Experiments 1 and 2 by dividing the standard deviation by the mean in Excel. Further, to see how well the modelled data fitted the observed data, R-squared was calculated using the command RSQ in Excel.

4. Results

4.1 Rock characterization

4.1.1 Scanning electron microscopy (SEM)

Scanning electron microscopy was performed on the starting material for the experiments, i.e., unweathered shale from Kleggerud and weathered shale from Taraldrud. Figure 18 depicts a BSE outcrop of the unweathered shale, showing some of the most common mineral phases and the corresponding EDS spectra generated during the analyses.

The identification of minerals was accomplished by comparing the spectra and relative atomic percentages of elements (measured on the thin section with EDS) with those of known minerals. Pyrite and pyrrhotite had similar spectra but could be distinguished based on their relative atomic percentages. A relative atomic ratio of Fe:S close to 1:2 was identified as pyrite, whereas a Fe:S ratio closer to 1:1 was identified as pyrrhotite.

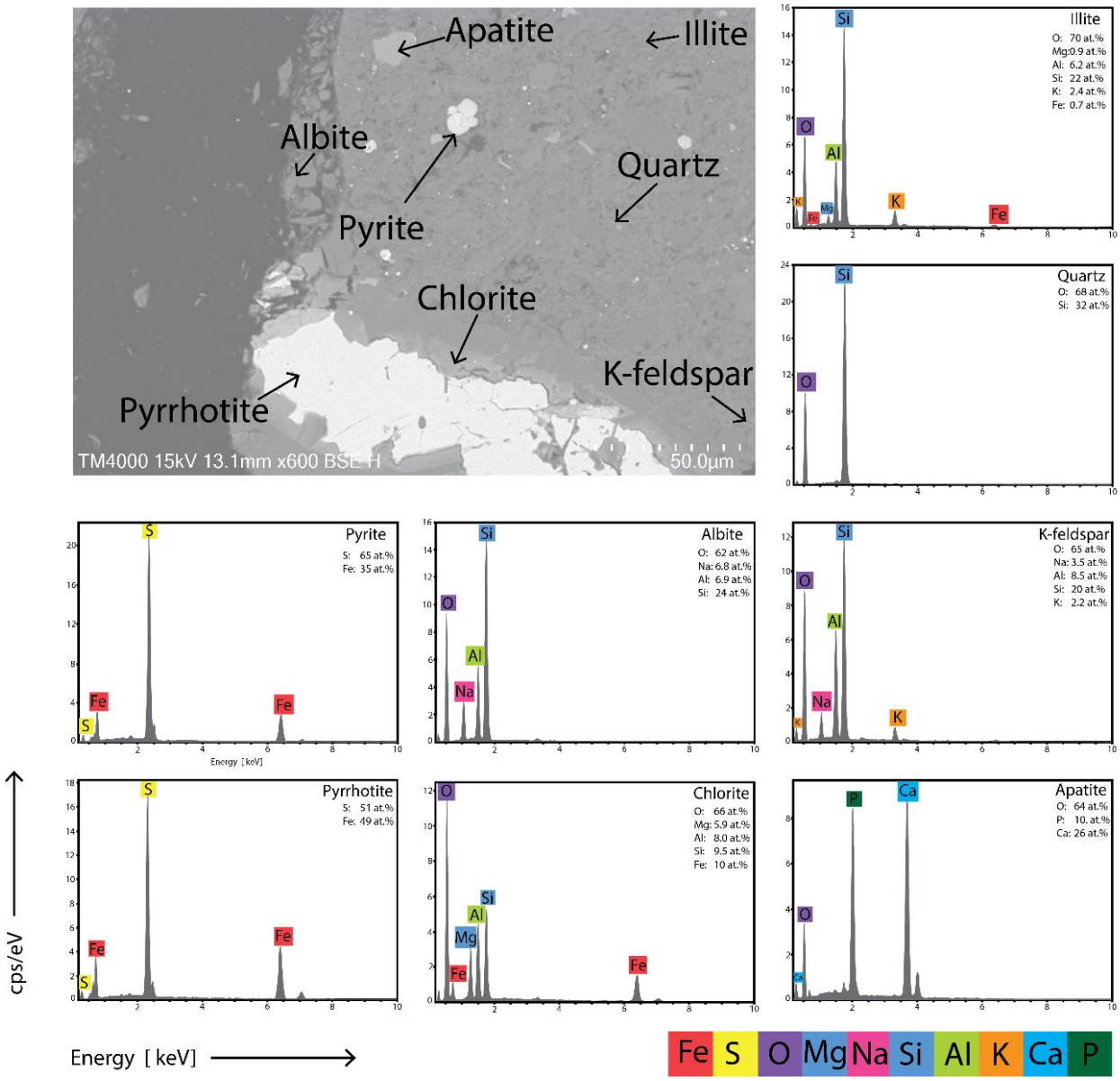

Figure 18: BSE image of unweathered shale showing some of the most common mineral phases and the corresponding EDS spectra generated during the analyses.

Unweathered shale from Kleggerud

An overview of the mineral phases observed in SEM analyses, and identified using EDS, in the unweathered shale is shown in Figure 19. Most of the outcrops of the unweathered shale had a fine-grained matrix composed mainly of quartz [SiO_2] and Na,K-feldspars [($NaAlSi_3O_8$), ($KAlSi_3O_8$)]. Some micas, such as muscovite [$KAl_2(AlSi_3O_{10})(OH)_2$] and biotite [$K(Mg, Fe)_3AlSi_3O_{10}(F, OH)_2$] and clay minerals, such as illite [$(K,H_3O)(Al,Mg,Fe)_2(Si,Al)_4O_{10}[(OH)_2,(H_2O)]$], were also observed in the matrix. Sulphides,

like pyrite [FeS_2], mainly occurred as small (~1-20 µm) spheroidal aggregates (Figure 19.1), known as framboidal pyrite. Larger pyrrhotite [$Fe_{1-x}S$] and non-framboidal pyrite minerals with a less distinct structure than framboidal pyrite were also observed (Figure 19.12). Some carbonates, like calcite [$CaCO_3$] and dolomite [$CaMg(CO_3)_2$], were seen and occurred mostly together with non-framboidal pyrite and pyrrhotite (e.g. Figure 19.12). Other sulphides like chalcopyrite [$CuFeS_2$], pentlandite [Ni_9S_8] (Figure 19.11) and sphalerite [ZnS] (Figure 19.9) were observed, but in smaller amounts than what was observed for the pure iron sulphides. Zircon [ZrSiO4] were also observed in small amounts (Figure 19.7).

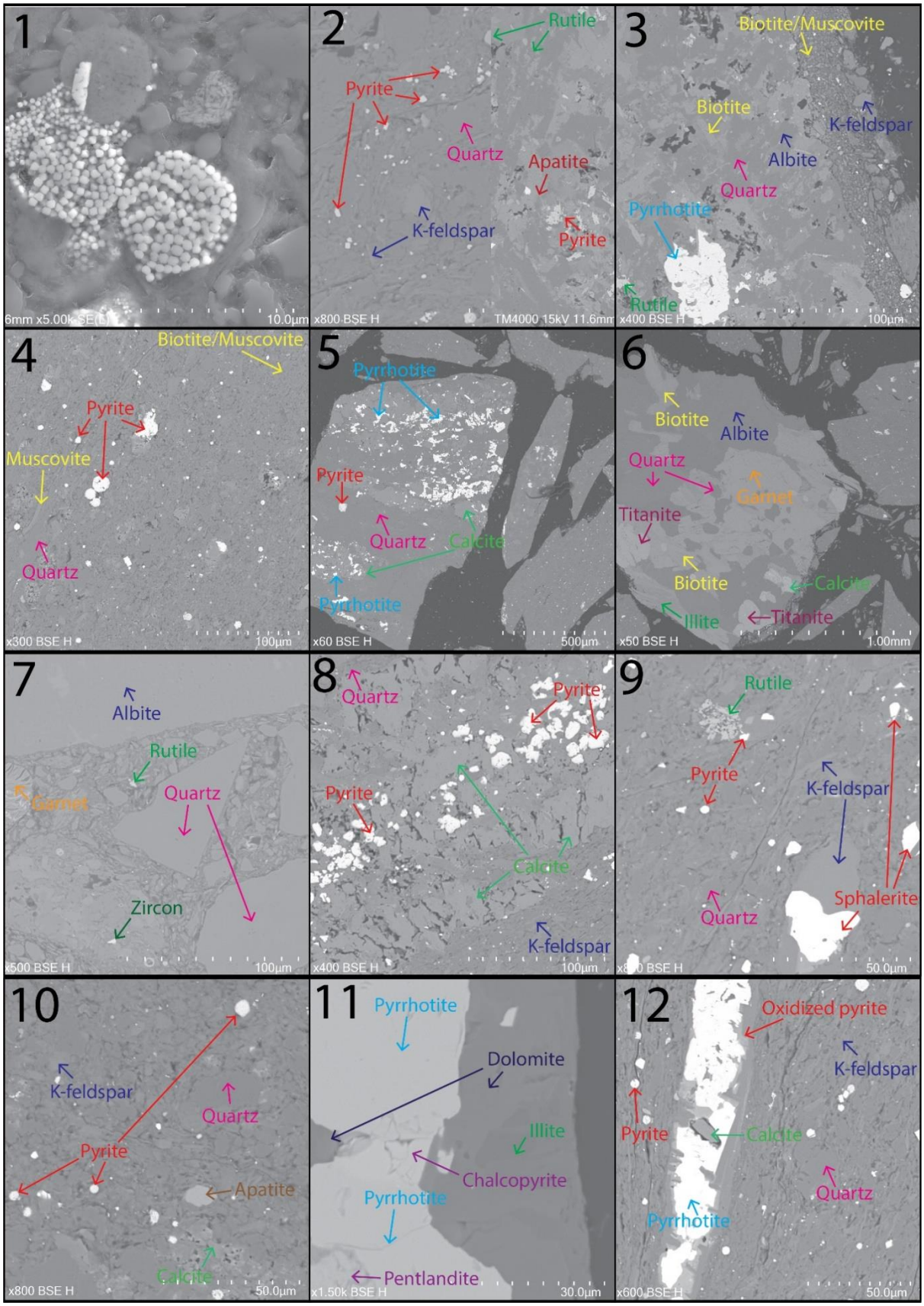

Figure 19: Overview of the minerals observed in SEM and identified with EDS for the unweathered shale. Outcrop 1 is a secondary electron (SE) image of framboidal pyrite, while outcrop 2-12 are backscattered electron (BSE) images showing different mineralogical compositions as contrasts. Note different scales for the different outcrops.

One outcrop (representing the majority of the unweathered shale matrix) was analysed using SEM mapping. The specific elemental composition is shown in Figure 20. The main constituents of the matrix were found to be quartz, micas, and clays (e.g., illite), which contain Si, K, Al and Fe when Fe didn't occur in the same area as S. Areas with quartz were identified by the presence of Si without K and Al, while regions with both K, Al and Si indicated the presence of feldspars and muscovite. Areas with K, Al, Si and Fe represent illite or biotite. Apatite [$Ca_5(PO_4)_3(OH,F,Cl)$] was identified in areas with P and Ca, while calcite was associated with regions containing Ca lacking P. Iron-sulphides were observed in the lighter areas in the BSE image, containing Fe and S. The occurrence of uranium appeared in all phases, but with lower intensity in the areas identified as quartz.

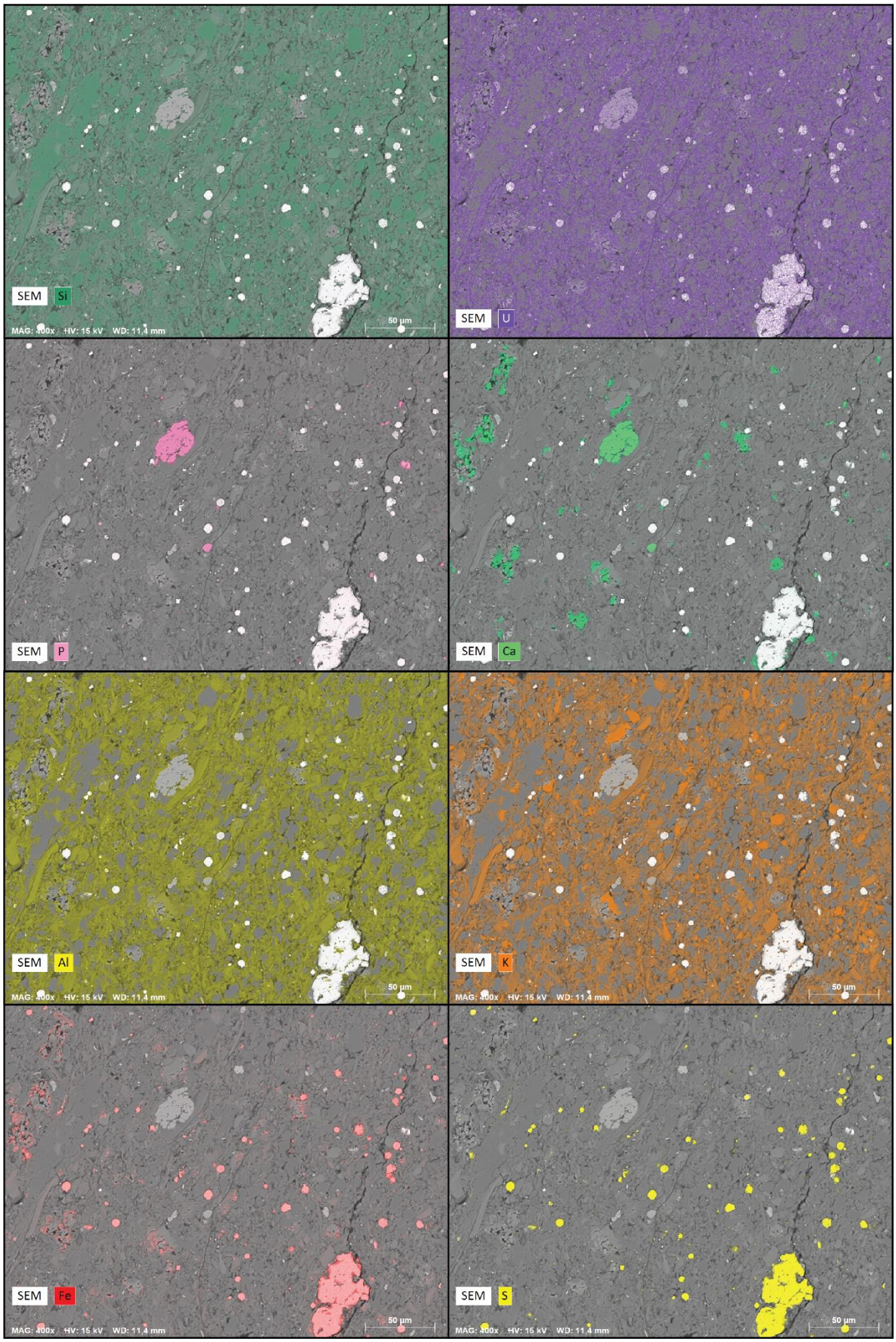

Figure 20: Specific elemental composition of the matrix of the unweathered shale showing selected elements (Si, U, P, Ca, Al, K, Fe and S). Scale of BSE image 50 µm.

Weathered shale from Taraldrud

The outcrops of the weathered shale also show a fine-grained matrix composed mainly of quartz and feldspars. Micas, such as biotite, muscovite and phengite [$K(AlMg)_2(OH)_2(SiAl)_4O_{10}$], were observed in the matrix but in smaller amounts than what was seen for the unweathered shale (Figure 21). Pyrite was observed in one outcrop (Figure 21.8) in the vicinity of a void with the approximately same size and shape as the pyrite. No other sulphides were found, but iron-oxides with an indistinct shape were observed and can be seen in Figure 21.5. No carbonates, like calcite, were found in the weathered shale. "Unknown sulphate" minerals were found, with a spectrum having the highest peak for oxygen, followed by iron and sulphur, then approximately equal peaks for phosphorus and aluminium, and a low silicon and calcium peak (Figure 22). Such minerals occurred mainly as a crust on rock fragments or in cracks, as seen in Figure 21.1 and Figure 21.10. Minor amounts of the "unknown sulphate" also occurred in the matrix (Figure 21.2). Additionally, more voids were observed for the weathered shale than the unweathered. The voids in Figure 21.9 show elongated hexagonal voids in the vicinity of the "unknown sulphate".

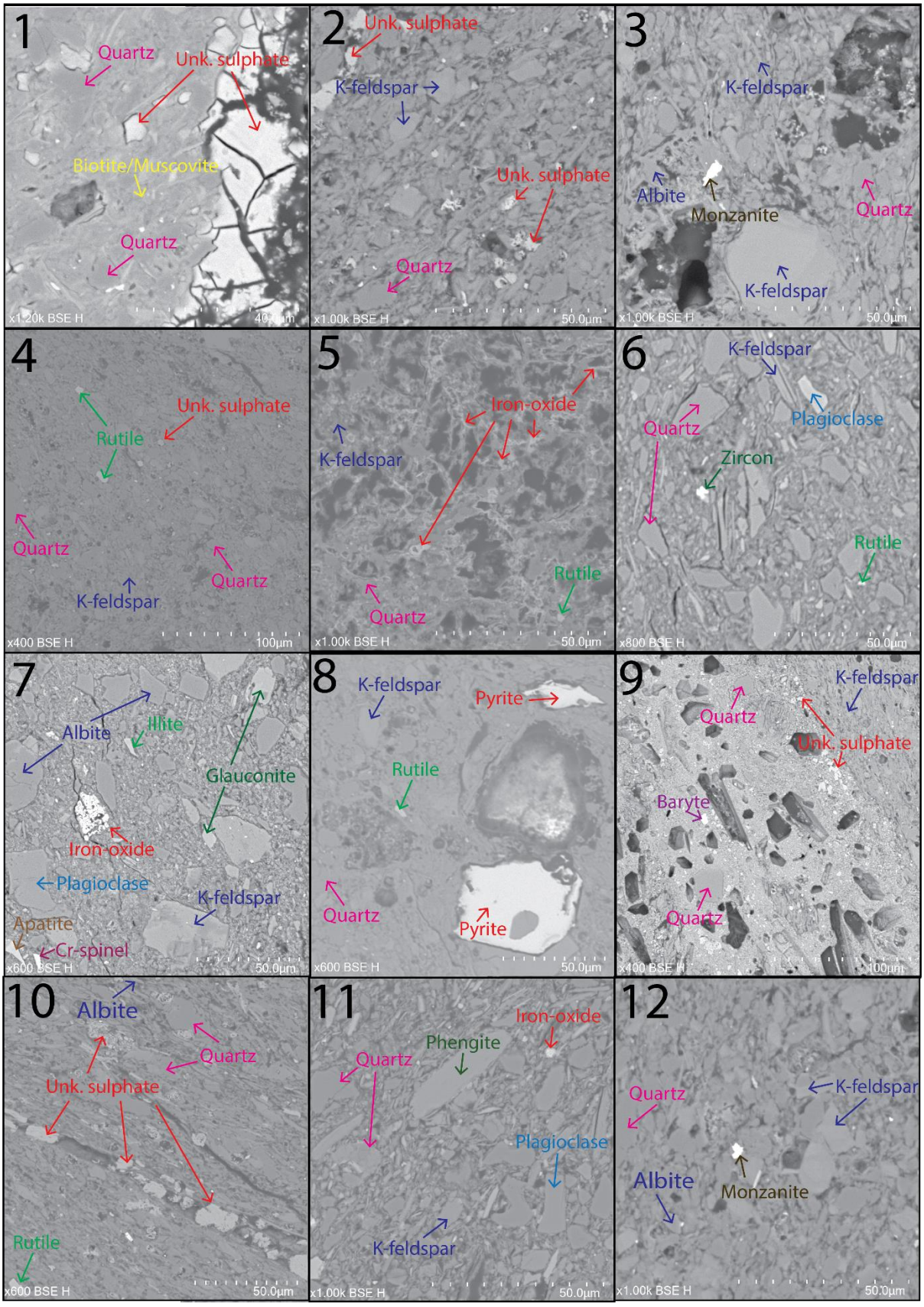

Figure 21: Overview of the minerals observed in SEM for the weathered shale. Outcrop 1-12 are backscattered electron images (BSE) showing different mineralogical compositions as contrasts. Note different scales for the different outcrops.

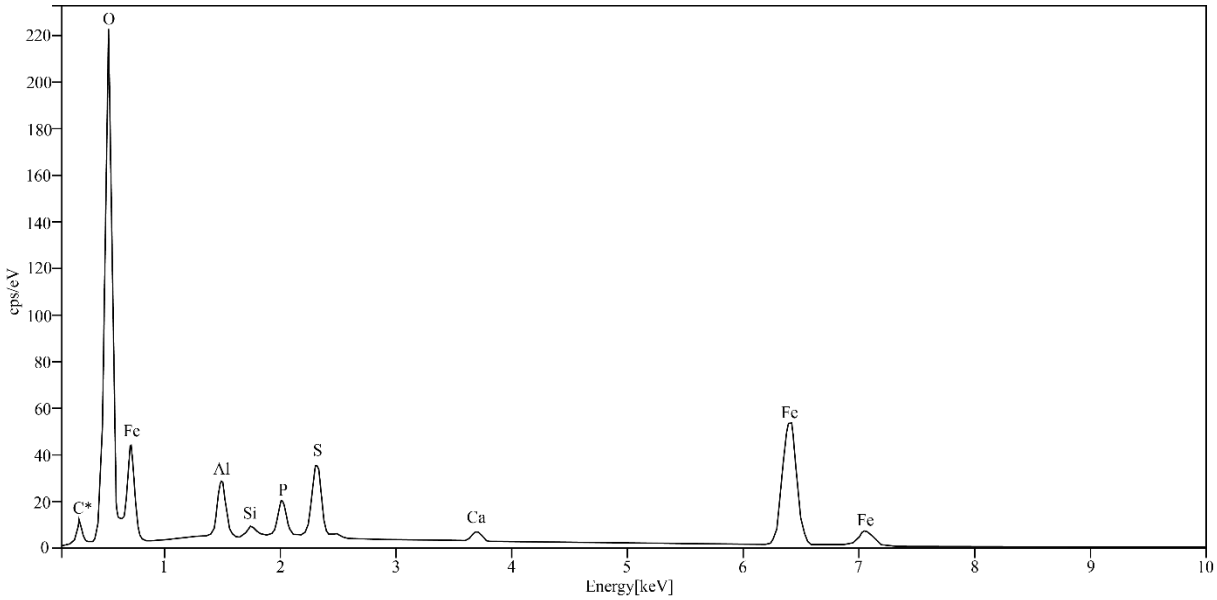

Figure 22: Spectre of the chemical composition of the "unknown sulphate" found in the weathered shale.

One outcrop (representing the majority of the weathered shale matrix) was analysed using SEM mapping and is shown in Figure 23. The matrix of Outcrop 4 mainly consists of quartz, feldspar, and micas, characterized by the presence of Si, K, and Al. SEM mapping showed the occurrence of U, Ca, and P throughout the entire BSE image. U and Ca had lower intensities in regions where quartz was observed. Conversely, P was detected in all mineral phases with approximately equal intensities. Compared to the unweathered shale, Fe and S appeared to be more dispersed and spread out in the matrix rather than concentrated in distinct areas.

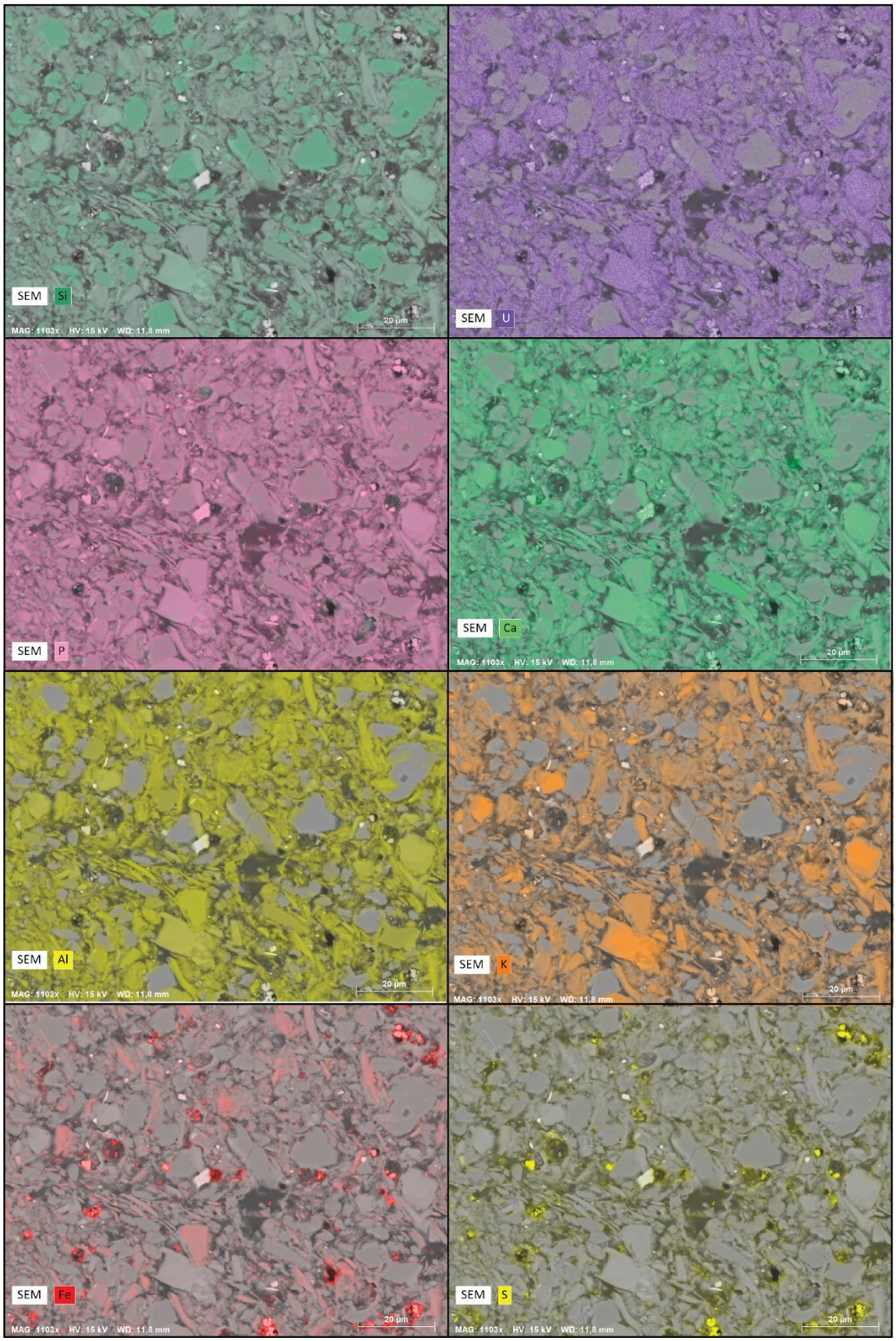

Figure 23: Specific elemental composition of the matrix of the weathered shale showing selected elements (Si, U, P, Ca, Al, K, Fe and S). Scale of BSE image 20 µm.

4.1.2 X-ray diffraction (XRD)

Starting material

The relative amount of different minerals measured in the XRD analyses for the starting material and the samples stored under different conditions for 7 and 9 months can be seen in Table A 2 and Table A 3 (Appendix). The XRD results for both the unweathered (U1, U2) and weathered (W1, W2) shale before it was treated with water show that both samples are mainly composed of mica, quartz, feldspars, and clay (illite and kaolinite) (Figure 24). Small amounts of pyrite (~3 wt. %), pyrrhotite (~1 wt. %) and calcite (~0-1 wt. %) are present in the unweathered shale but are close to absent in the weathered shale. Secondary sulphate minerals were present in both weathered and unweathered shale, but in lesser amounts in the unweathered shale (~1.2 wt.%). In the weathered shale, jarosite [$KFe_3(SO_4)_2(OH)_6$] was the most abundant secondary sulphate mineral followed by schwermanite [$Fe_8O_8(OH)_6(SO_4)\cdot nH_2O$] and rozenite [$Fe(SO_4)\cdot 4H_2O$]. Gypsum [$CaSO_4\cdot 2H_2O$] and anhydrite [$CaSO_4$] are present in the weathered shale but not in the unweathered shale.

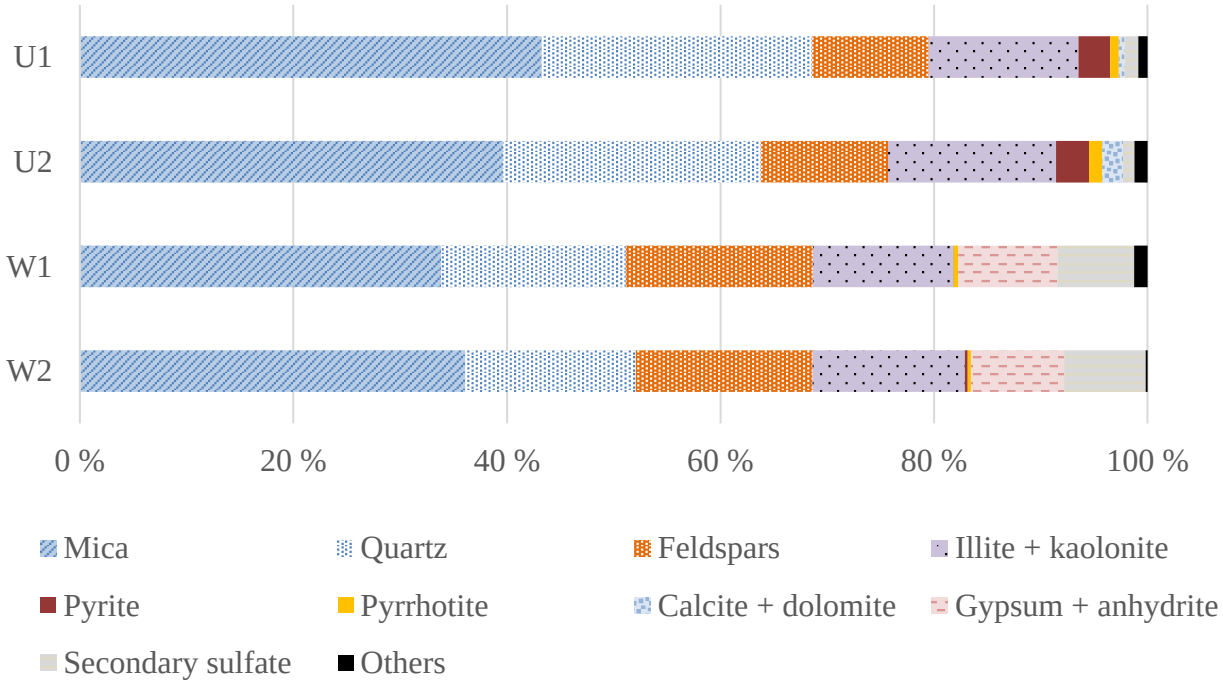

Figure 24: Relative amounts of minerals present in the starting materials of unweathered (U1 and U2) and weathered shale (W1 and W2). "Others" refer to the sum of minerals that were present in small amounts.

Experiment 1: Change in mineralogical composition after 7 and 9 months

The mineralogical composition of the unweathered and weathered shale was relatively constant during treatment with fresh – and seawater for 7 and 9 months (Figure 25 and Figure 26). However, a significant higher relative amount of feldspar (p-value = 0.0013) and a smaller relative amount of clay minerals (illite and kaolinite) (p-value = 0.0017) were observed for the seawater treatments compared to the starting material and freshwater treatments. This was observed for both weathered and unweathered shale but was more pronounced for the weathered shale. Further, a less relative amount of secondary sulphate minerals was seen in all treatments of weathered shale with an average decrease of around 2 wt. %.

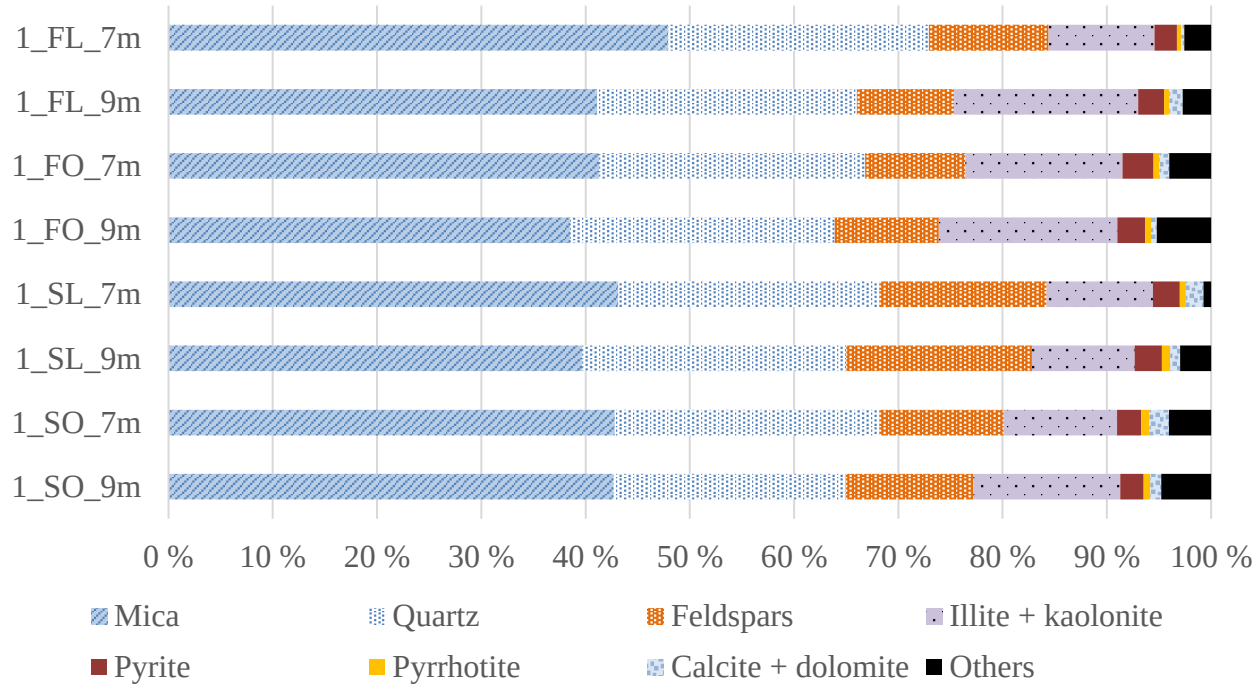

Figure 25: XRD results for the unweathered shale treated with water for 7 and 9 months in Experiment 1. "Others" refer to the sum of minerals that were present in small amounts. F: Freshwater, S: Seawater, O: Oxic, L: Low-oxygen.

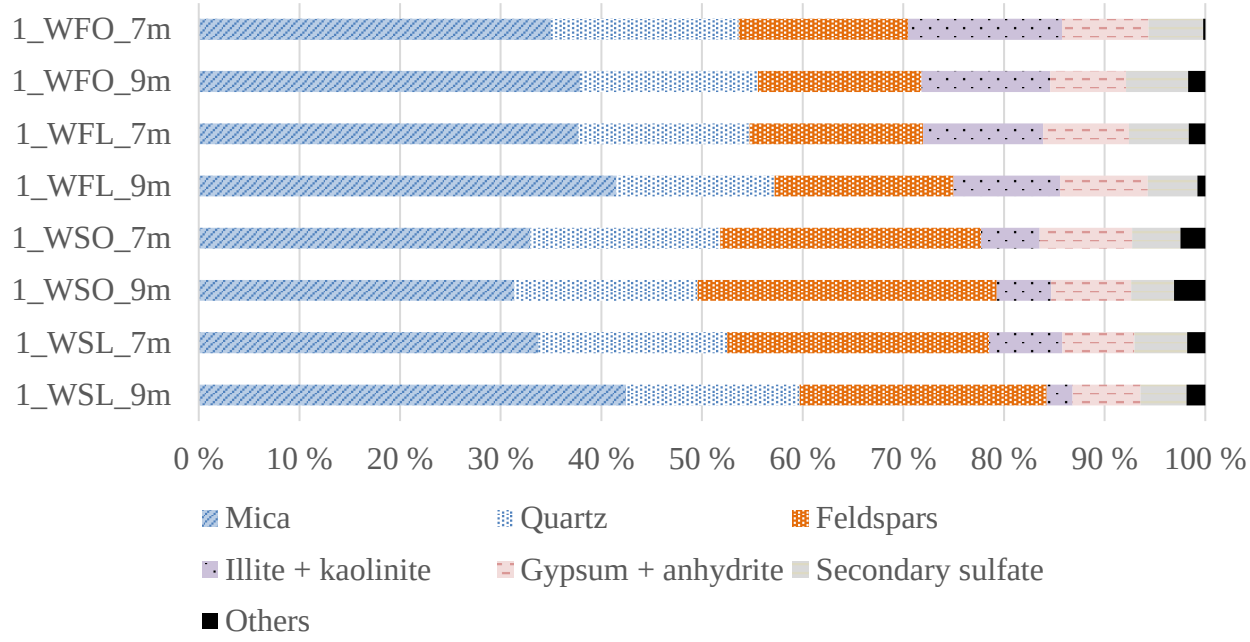

Figure 26: XRD results for the weathered shale treated with water for 7 and 9 months in Experiment 1. "Others" refer to the sum of minerals that were present in small amounts. W: Weathered shale, F: Freshwater, S: Seawater, O: Oxic, L: Low-oxygen.

4.1.3 Total carbon (TC)

The results for Total Carbon (TC), Total Organic Carbon (TOC) and Total Inorganic Carbon (TIC) for the bulk starting material of unweathered and weathered shale are summarized in Table 3. Higher values for TOC compared to TC was measured for the unweathered -and weathered starting materials, and no TIC was estimated. However, calcite was seen in the SEM analyses and detected in the XRD analyses for unweathered shale.

Table 3: Total Carbon (TC), Total Organic Carbon (TOC) and Total Inorganic Carbon (TIC) for the bulk starting material of unweathered and weathered shale.

Sample	TC (%)	TOC (%)	TIC (%)
Unweathered shale	6.0	6.2	0.0
Weathered shale	4.1	4.2	0.0

4.1.4 Whole rock analysis

The major constituents of the unweathered and weathered starting materials are presented graphically below (Figure 27). The main oxides detected for both shales are SiO_2, followed by Al_2O_3 and K_2O. A higher Loss of Ignition was measured in weathered shale compared to unweathered shale.

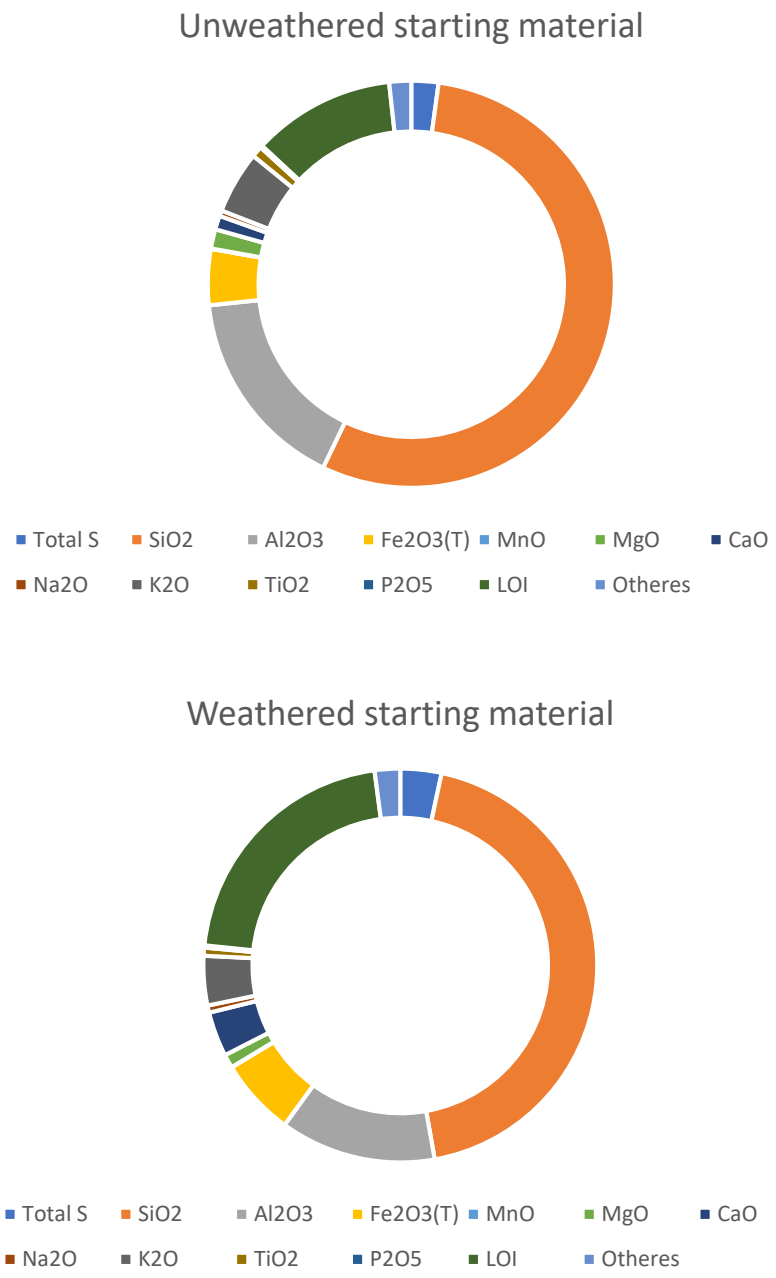

Figure 27: Major oxides and LOI measured in whole rock analysis of the unweathered and weathered starting material. The plots are made from the average values of duplicates of the shales.

Selected trace elements and sulphur content in the starting material of the shales are summarized in Table 4. The unweathered shale had higher concentrations of V, Co, Cd and Sb compared to the weathered shale, whereas the weathered shale had higher concentrations of S, Mo, Ba and U.

Table 4: Some selected trace elements and sulphur content of the unweathered and weathered starting material. Values presented are the average concentration of duplicates of the shales.

	Total S	V	Co	Cd	Mo	Sb	Ba	U
Unit Symbol	%	ppm	ppm	ppm	ppm	ppm	ppm	ppm
Unweathered Kleggerud	2.2	1855	19	7	100	11	778	70
Weathered Taraldrud	3.5	647	11	0.75	>100	5.1	1518	88

Results from the whole rock analyses can be seen in Table A 4 (Appendix) and were used to make triangular plots showing the distribution of relative amounts of elements. Selected triangular plots for the starting material of unweathered – and weathered shale, in addition to samples treated with water for 9 months (Experiment 1), are shown in Figure 28. The diagrams also include reference samples of black mudrocks from the Cambro-Ordovician succession for comparison. All the triangular plots can be seen in Figure A 1 (Appendix). The triangular plots of the unweathered shale from Kleggerud showed some variation in where the samples were distributed in the diagrams. However, most samples were plotted in the same area as horizon 3a. For the weathered shale from Taraldrud, most of the samples were distributed in the areas of horizon 2, but some samples were plotted in the areas of horizon 3a.

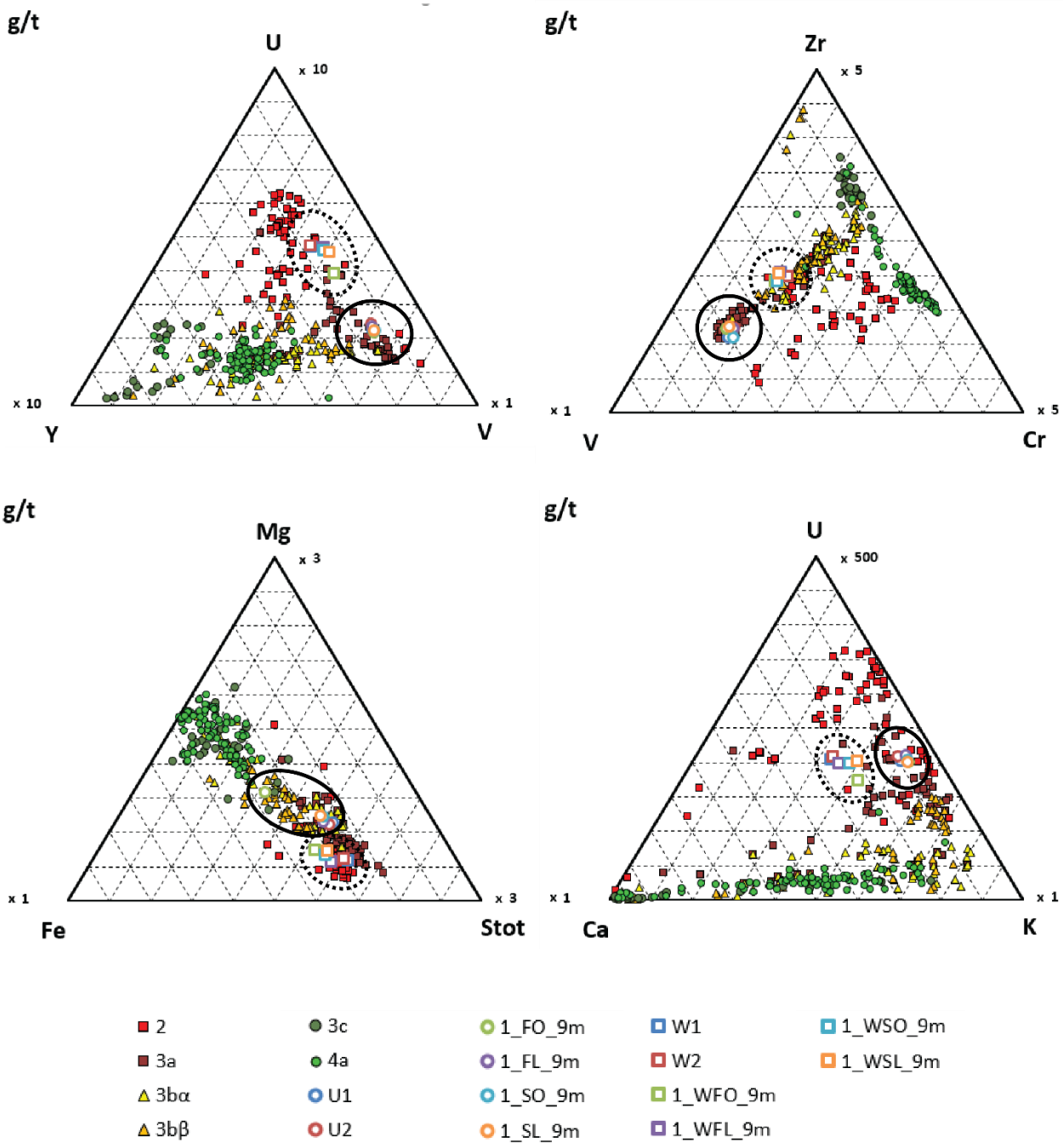

Figure 28: Selected triangular plots obtained from whole-rock analyses with the relative amounts of elements compared to reference samples of black mudrocks within the Cambro-Ordovician succession (Pabst et al., 2017). Solid circle shows where the unweathered shale (Kleggerud) is distributed in the diagrams, and dashed circle show the same for weathered shale (Taraldrud). U: Unweathered shale, W: Weathered shale, F: Freshwater, S: Seawater, O: Oxic: L: Low-oxygen: 9m: Sampled 9 months into Experiment 1.

Neutralization potential (NP) plotted against acidification potential (AP) for the starting material of unweathered – and weathered shale is shown in Figure 29. Both of the shales had NP:AP < 1. The weathered shale had higher AP than the unweathered shale, while none of the samples had any neutralizing potential as the TIC was estimated to 0 %.

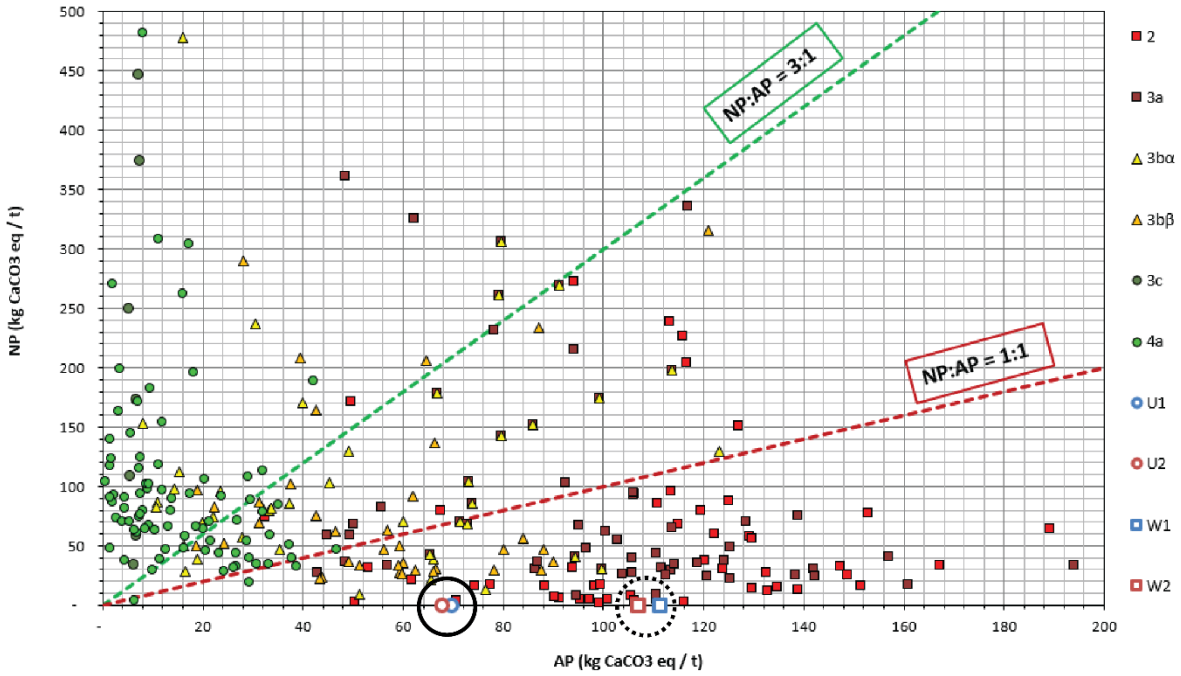

Figure 29: AP-NP diagram with reference samples from the Cambro-Ordovician succession and defined zones. Solid circle shows where the unweathered shale (Kleggerud) is distributed in the diagrams, and dashed circle show the same for weathered shale. U1 and U2: Starting material of unweathered shale, W1 and W2: Starting material for weathered shale.

Fe plotted against total S is shown in Figure 30. The weathered shales plot between Fe:S =1:1 and Fe:S = 1:2 line. Most of the unweathered samples also plot between these two lines, but with a lower Fe and total S content. One unweathered sample (1_FO_9m) plots on the Fe:S = 2:1 line.

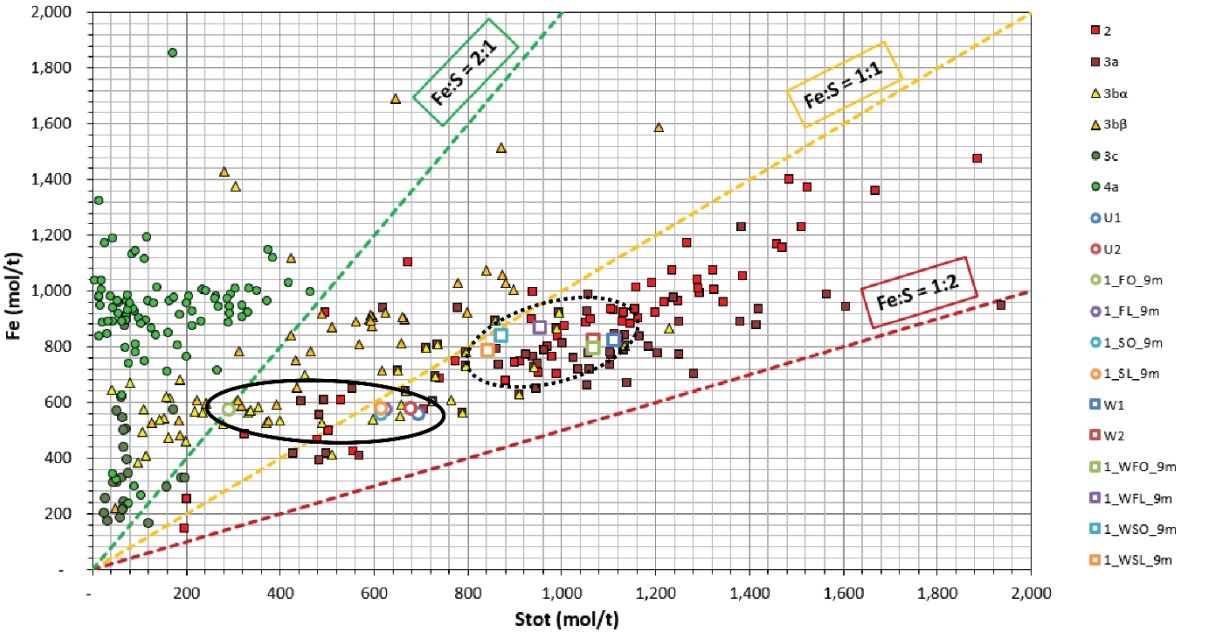

Figure 30: Fe plotted against total S with reference samples from the Cambro-Ordovician succession and defined zones. Solid circle shows where the unweathered shales (Kleggerud) are distributed in the diagrams, and dashed circle show the same for weathered shales. U1 and U2: Starting material of unweathered shale, W1 and W2: Starting material for weathered shale. F: Freshwater, S: Seawater, O: Oxic: L:Low-oxygen.

4.1.5 Grain size distribution

Figure 31 displays the cumulative grain size distribution of the unweathered -and weathered starting materials used in Experiments 1 and 2. The debris of the shales have a similar grain size distribution with a larger fraction of sand-sized particles (63-2000 µm), and a smaller fraction of silt and clay (0-63 µm). The weathered shale has a larger fraction of grains in the interval from 0 - 400 µm compared to the unweathered shale which has a larger fraction of grains in the interval from 400-2000 µm.

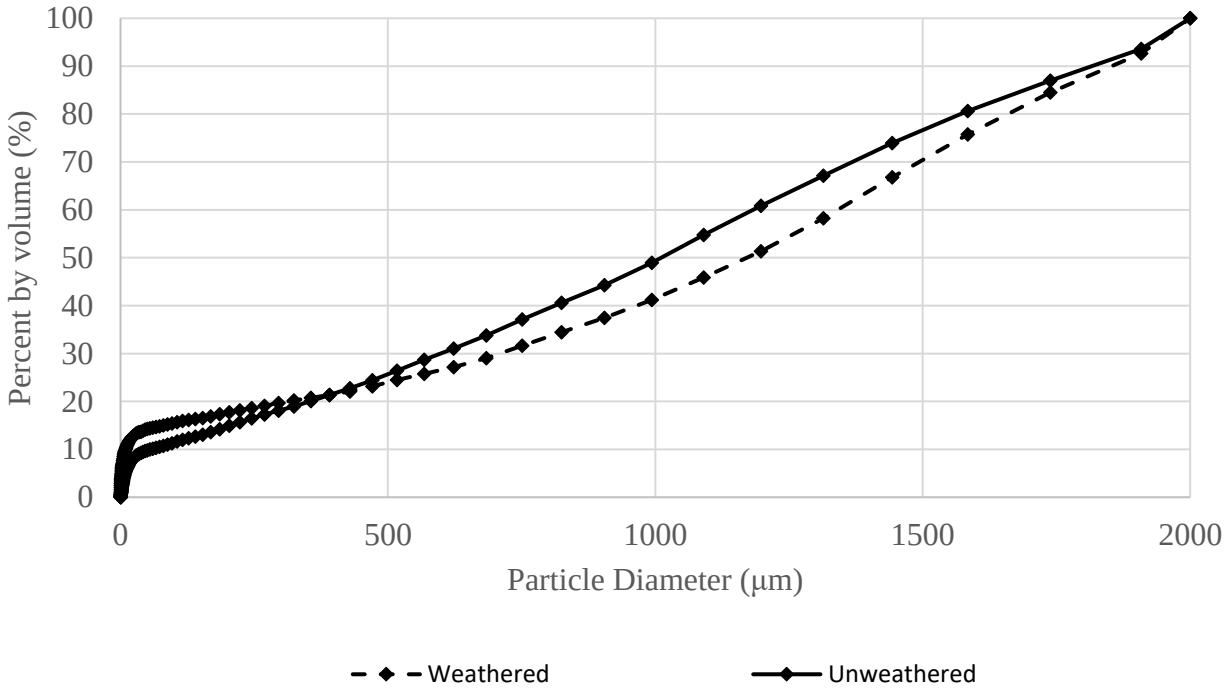

Figure 31: Cumulative grain size distribution of the weathered and unweathered staring materials used in Experiments 1 and 2.

4.2 Water analyses

4.2.1 Water quality before experiment start (Experiment 1)

Field parameters and alkalinity for the starting water before Experiment 1 was started are summarized in Table 5. The initial pH was higher in the starting seawater compared to freshwater (deionized water) (ΔpH = ~2). The conductivity was orders of magnitudes higher for seawater than freshwater. There was no acid neutralizing capacity (alkalinity) in the initial freshwater, while seawater had an initial alkalinity of 2.2 meq/L. The redox potential (Eh) was higher for the starting freshwater compared to seawater (ΔEh = 190 mV).

Table 5: Field parameters and alkalinity for the starting fresh- and seawater before Experiment 1 and 2 were started.

	pH	Eh [mV]	Oxygen [mg/L]	Conductivity [µS/cm]	Alkalinity [meq/L]	Temperature [°C]
Freshwater	5.7	560	8.2	2	n.d.	23.4
Seawater	7.7	370	8.3	42100	2.2	23.7

Major cat- and anions in the starting fresh- and seawater before the experiments start are summarized in Table 6 and Table 7. Minor amounts of the major ions were detected in the starting freshwater. While in seawater, initial concentrations of chlorine (Cl^-), sulphate (SO_4^{2-}), bromine (Br^-), sodium (Na^+), potassium (K^+), magnesium (Mg^{2+}) and calcium (Ca^{2+}) were measured.

Table 6: Major anions measured in the starting fresh- and seawater before Experiment 1 and 2 were started.

	F [ppm]	Cl [ppm]	SO_4^{2-} [ppm]	Br[ppm]	NO3 [ppm]	PO4 [ppm]
Freshwater	n.d.	0.060	0.20	n.d.	0.20	n.d.
Seawater	n.d.	20 414	3 189	224	n.d.	n.d.

Table 7: Major cations measured in the starting fresh- and seawater before Experiment 1 and 2 were started.

	Na [ppm]	K [ppm]	Mg [ppm]	Ca [ppm]
Freshwater	0.10	0.090	n.d.	0.37
Seawater	11446	446	1568	460

Trace elements in the starting fresh- and seawater can be seen in Table 8. No metals were detected in the starting freshwater, while the starting seawater had minor concentrations of barium (Ba), molybdenum (Mo), uranium (U) and zink (Zn).

Table 8: Trace elements measured in the starting fresh- and seawater before Experiment 1 were started.

[µg/L]	Al	As	Ba	Cd	Co	Cr	Cu	Fe	Mn	Mo
Freshwater	<20	<0,5	<1	<0.1	<0.2	<3	<4	<2	<1	<1
Seawater	<20	1.7	6.9	<0.1	<0.2	<3	<4	<2	<1	10.4
[µg/L]	Ni	Pb	Sb	Se	Sn	Tl	U	V	Zn	
Freshwater	<2	<0.2	<1	<6	<10	<0.1	<0.1	<5	<3	
Seawater	<2	<0.2	<1	<6	<10	<0.1	3.0	<5	4.3	

4.2.2 Experiment 1: Method Evaluation

To test if the plastic bottles stored under water in Experiment 1 prevented fast diffusion of oxygen, nitrogen bubbled water with an initial oxygen concentration of 1.2 mg/L were stored in the same way as low-oxygen samples, i.e., in a water filled box, in Experiment 1 for one week.

The oxygen concentration in the nitrogen bubbled water stored in the same way as the low-oxygen samples in Experiment 1, increased from 1.2 to 5.3 mg/L after one week (measured in the glove box). Additionally, a water filled beaker with an initial oxygen concentration of 8.7 mg/L, before flushing the glove box with nitrogen, decreased to 5.6 mg/L after the glove box was flushed for 30-40 minutes.

4.2.3 Field parameters

Measured pH, redox potentials, dissolved oxygen concentrations and conductivity over the sampling period for Experiments 1 and 2 are presented graphically below. Additionally, all values can be seen in Appendix (Table A 5 and Table A 6).

pH

The measured pH in Experiment 1 is displayed in Figure 32. Seawater mixed with unweathered shale (1_SO, 1_SL) had approximately the same pH before and after being mixed with shale. For the unweathered shale treated with freshwater (1_FO, 1_FL), the leachate pH increased from 5.7 in the starting water to above 7 in the first sampling point (after one day). A significant difference in the pH between low-oxygen and oxic treatments (p-value = $9.5 \cdot 10^{-6}$) was observed for unweathered shale in Experiment 1: The pH stabilized around 7.5 for samples treated with fresh- and sea water under low-oxygen conditions (1_FL, 1_SL), while the pH in the oxic samples (1_FO, 1_SO) stabilized at a slightly higher pH of 7.7.

Lower pH was measured for samples containing weathered shale compared to the unweathered shale. In the first sampling point (after one day), the pH was between 2.9 and 4.1 for weathered shale in all treatments. In the duration of the experiment, no noteworthy difference between oxic and low-oxygen samples was observed, but significantly lower pH values were measured for freshwater compared to the seawater treatments for weathered shale (p-value = $3.5 \cdot 10^{-9}$). The pH varied from 2.9 to 3.6 in freshwater treatments and from 3.1 to 4.1 for seawater treatments over the sampling period.

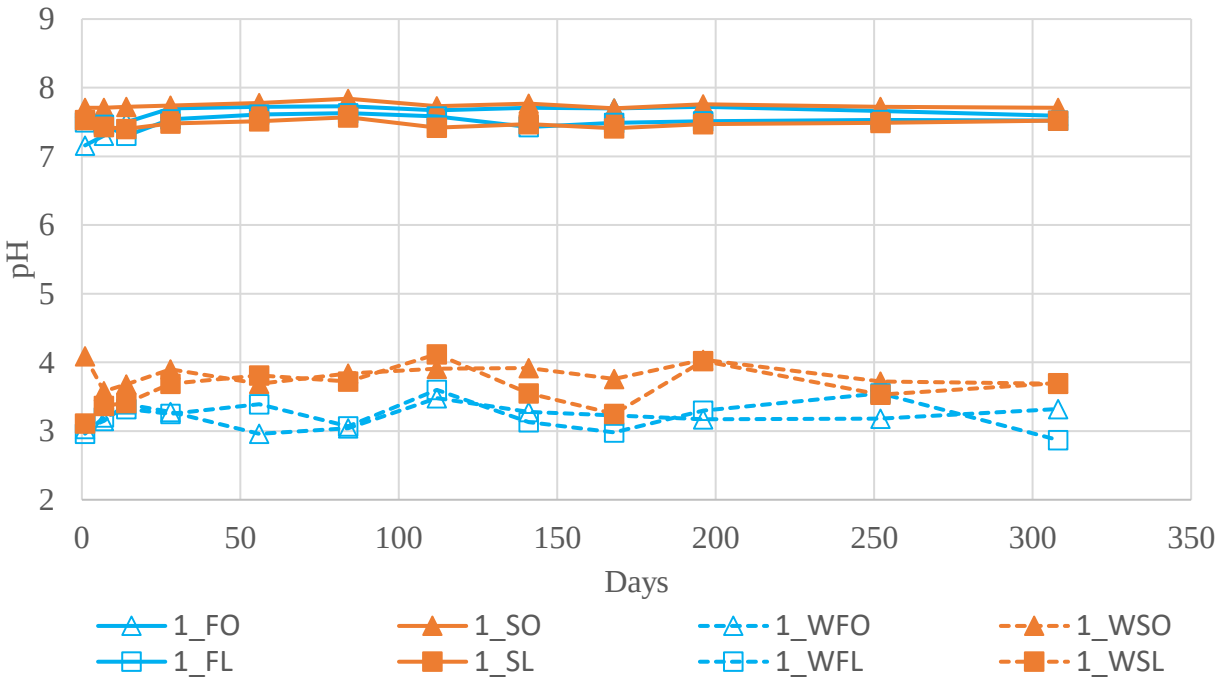

Figure 32: pH measurements in Experiment 1. Blue line: freshwater, orange line: seawater, solid line: unweathered shale, dashed line: weathered shale. Triplicates were performed after 1, 6 and 11 months, and the median values of the triplicates are presented in the plots. (W: Weathered shale, F: Freshwater, S: Seawater, O: Oxic, L: Low-oxygen).

In Experiment 2, only unweathered shale was used, and pH measurements with time are displayed in Figure 33. The treatment with shale kept in seawater under anoxic conditions (2_SA) stabilized at a somewhat lower pH (~7.5) than the other treatments. Oxic seawater and anoxic freshwater in contact with unweathered shale (2_SO, 2_FA) had a pH of ~8 over the sampling period. The highest pH was measured in the treatment with freshwater under oxic conditions (2_FO) at a pH of ~8.2 after 8 weeks.

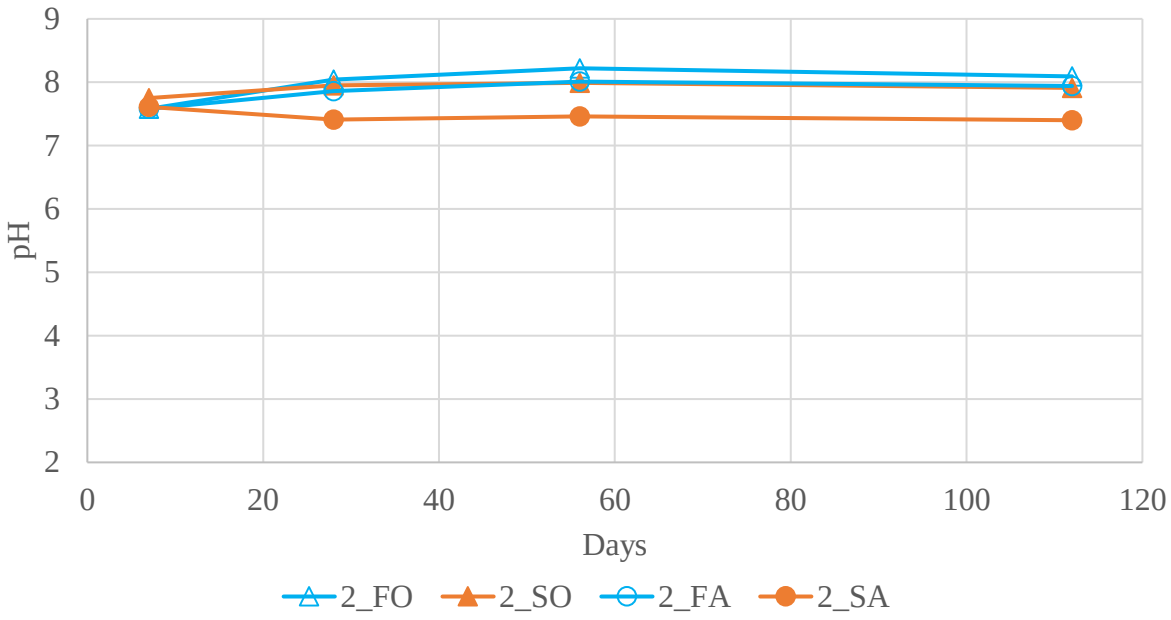

Figure 33: pH measurements in Experiment 2, where only unweathered shale was used. Blue line: freshwater, orange line: seawater. Triplicates were performed at the last measuring point (16 weeks), and their median values are presented in the plots. (F: Freshwater, S: Seawater, O: Oxic, A: Anoxic).

Redox potential (E_h)

Measurements of redox potentials (E_h) with time in Experiment 1 are displayed in Figure 34. Variable E_h were observed for weathered shale during the whole sampling period, while E_h steadily increased for the unweathered shale. Higher E_h was measured for the weathered shale than the unweathered shale with an average difference of ~200 mV. Slightly lower redox potentials were observed for weathered shale treated with seawater than freshwater with an average difference of 87 mV.

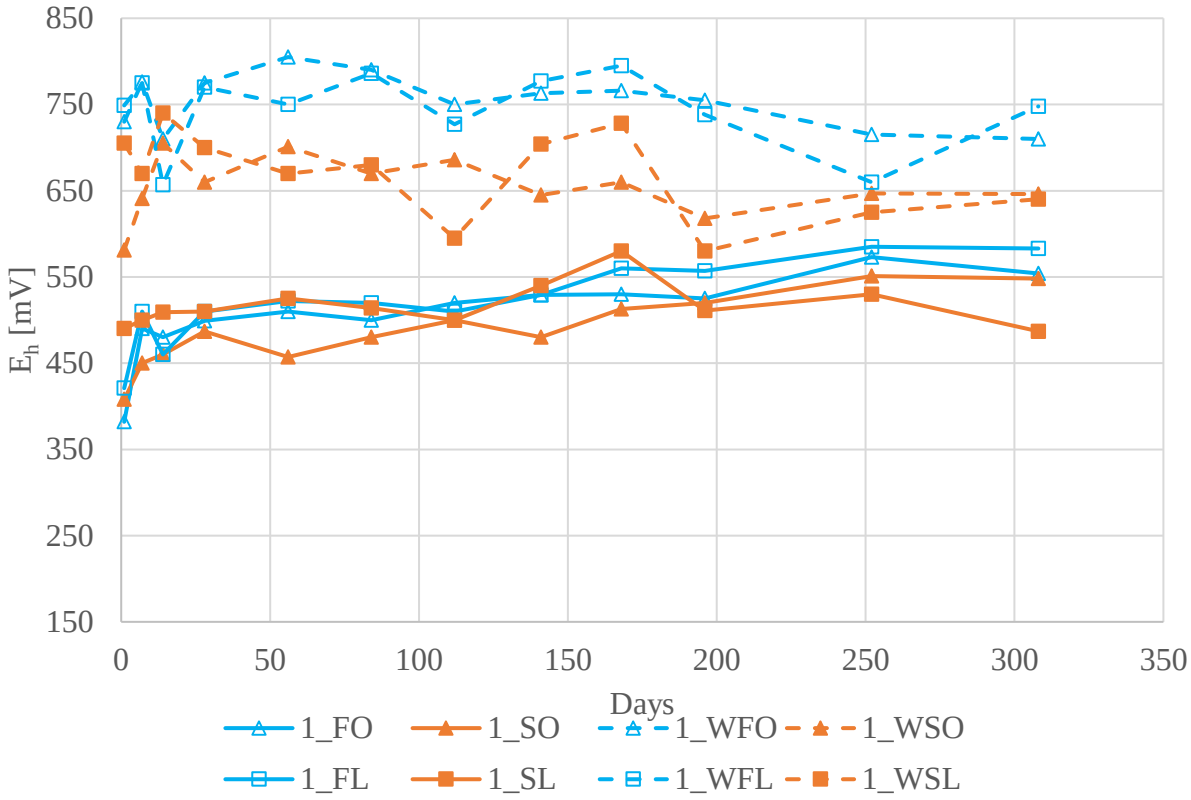

Figure 34: Redox potentials measured in Experiment 1. Blue line: freshwater, orange line: seawater, solid line: unweathered shale, dashed line: weathered shale. Triplicates were performed after 1, 6 and 11 months, and the median values of the triplicates are presented in the plots. (W: Weathered shale, F: Freshwater, S: Seawater, O: Oxic, L: Low-oxygen).

In Experiment 2, only unweathered shale was used. The measured redox potentials (E_h) in Experiment 2 are displayed in Figure 35. Treatments stored under oxic conditions (2_ FO, 2_SO) had the highest E_h-measurements ranging from ~450 to 550 mV over the sampling period. Lower redox potentials were measured for the treatments stored under anoxic conditions (2_SA, 2_FA), whereas the lowest redox potential of 210 mV was measured for seawater treatment stored under anoxic conditions (2_SA) after 4 months.

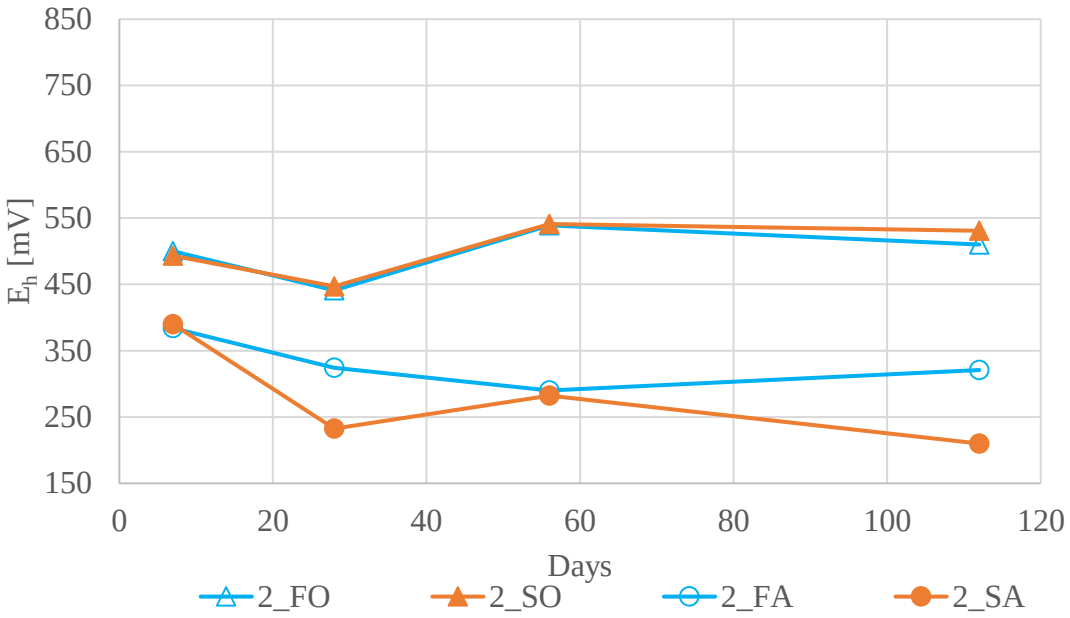

Figure 35: Redox potentials (E_h) measured in Experiment 2, where only unweathered shale was used. Blue line: freshwater, orange line: seawater. Triplicates were performed at the last measuring point (16 weeks), and their median values are presented in the plots. (F: Freshwater, S: Seawater, O: Oxic, A: Anoxic).

Dissolved oxygen

The measured dissolved oxygen concentrations for Experiment 1 are displayed in Figure 36. The oxygen concentrations were relatively constant for unweathered and weathered shale treated with fresh- and seawater during the sampling period. The oxygen concentration in the oxic samples stabilized between 8-9 mg/L, while it stabilized at around 5 mg/L for the low-oxygen samples.

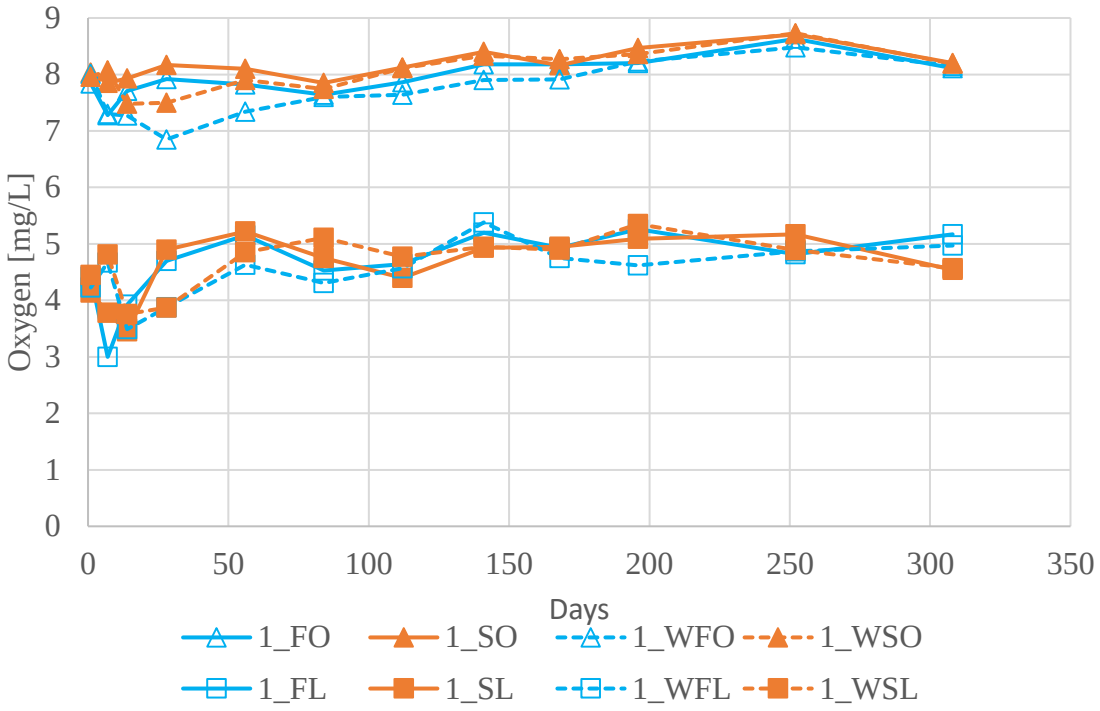

Figure 36: Dissolved oxygen concentrations in Experiment 1. Blue line: freshwater, orange line: seawater, solid line: unweathered shale, dashed line: weathered shale. Triplicates were performed after 1, 6 and 11 months, and the median values of the triplicates are presented in the plots. (W: Weathered shale, F: Freshwater, S: Seawater, O: Oxic, L: Low-oxygen).

The dissolved oxygen concentrations for Experiment 2, where only unweathered shale was used, are summarized in Figure 37. The oxygen concentrations in the oxic samples stabilized around 8-9 mg/L, while the anoxic samples stabilized at around 0.5 mg/L.

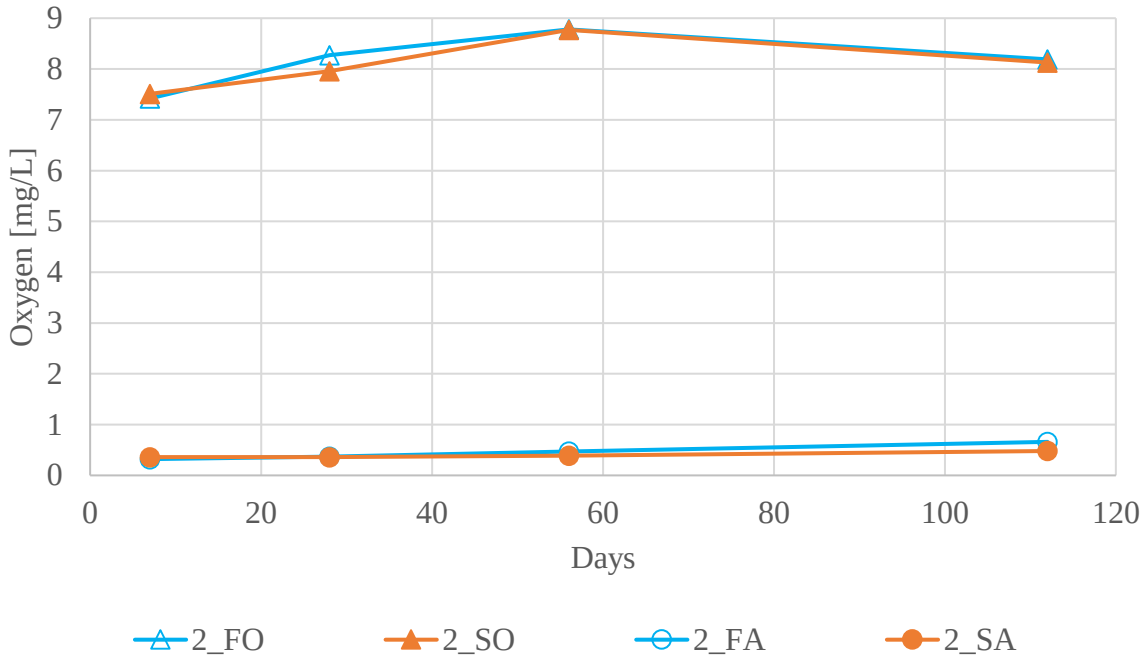

Figure 37: Dissolved oxygen concentrations in Experiment 2, where only unweathered shale was used. Blue line: freshwater, orange line: seawater. Triplicates were performed at the last measuring point (16 weeks), and their median values are presented in the plots. (F: Freshwater, S: Seawater, O: Oxic, A: Anoxic).

Conductivity

The measured conductivity for weathered and unweathered shale treated with freshwater is displayed in Figure 38. For unweathered shale treated with freshwater (1_FO, 1_FL), the conductivity increased to ~250 µS/cm after one day and increased approximately linearly in the following sampling period. For the weathered shale treated with freshwater, the conductivity increased to ~2000-2500 µS/cm after one day, followed by a slight increase before it stabilized around 2750 µS/cm after 5 months. No noteworthy difference between oxic and low-oxygen samples were observed.

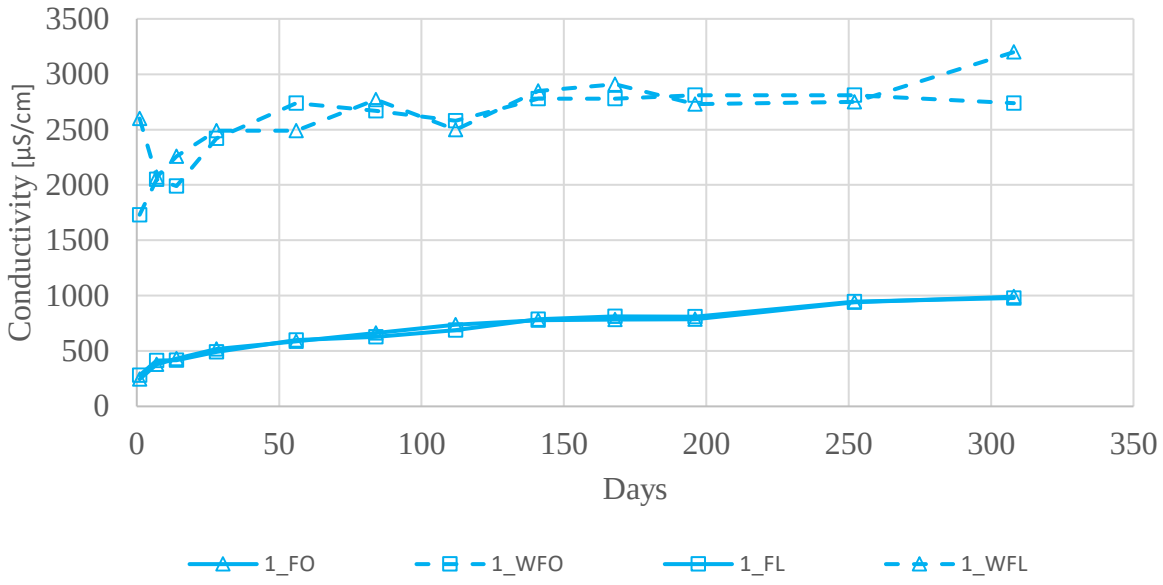

Figure 38: Conductivity measured over the sampling period in freshwater for Experiment 1. Solid line: unweathered shale, dashed line: weathered shale. Triplicates were performed after 1, 6 and 11 months, and the median values of the triplicates are presented in the plots. (W: Weathered shale, F: Freshwater, O: Oxic, L: Low-oxygen).

The conductivity measured in the samples treated with seawater in Experiment 1 is displayed in Figure 39. The conductivity in all the seawater samples, including the seawater blanks, increased with time (Table A 5 in Appendix).

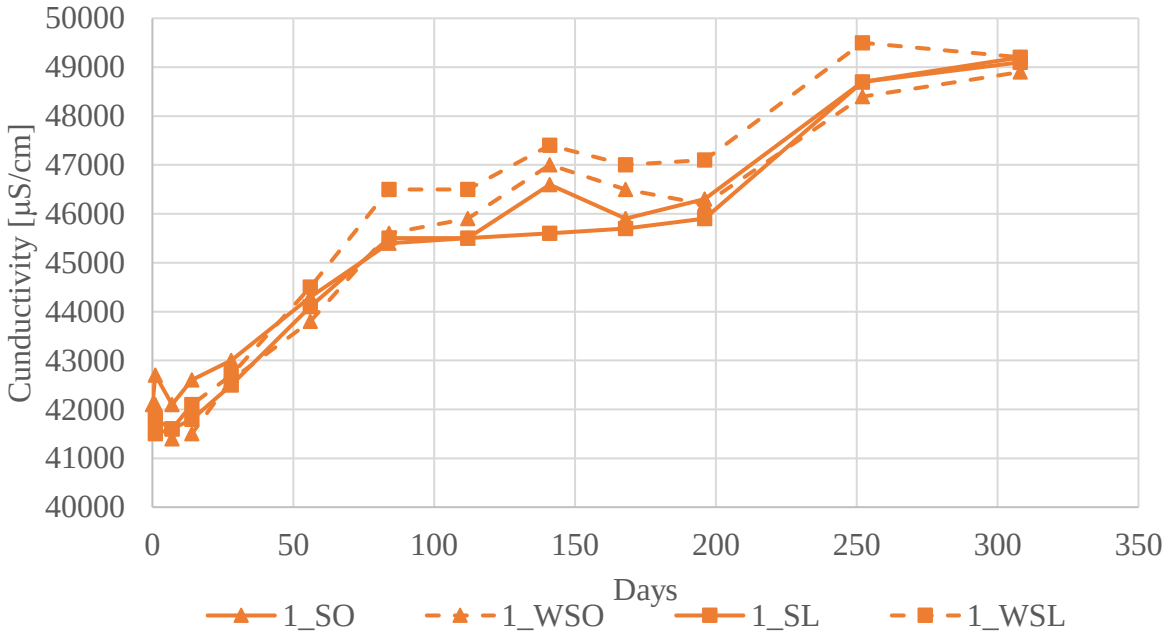

Figure 39: Conductivity measured over the sampling period in seawater for Experiment 1. Solid line: unweathered shale, dashed line: weathered shale. Triplicates were performed after 1, 6 and 11 months, and the median values of the triplicates are presented in the plots. (W: weathered shale, S: Seawater, O: Oxic, L: Low-oxygen).

The measured conductivity for the samples treated with freshwater in Experiment 2, i.e., unweathered shale stored under oxic and anoxic conditions, is displayed in Figure 40. The conductivity increased to ~300-400 µS/cm after one week for freshwater treatments (2_FO and 2_FA). The following conductivity measurements show an increase with time for the oxic samples (2_FO), while a lower conductivity was measured for anoxic samples (2_FA) with a slower increase after ~1 month.

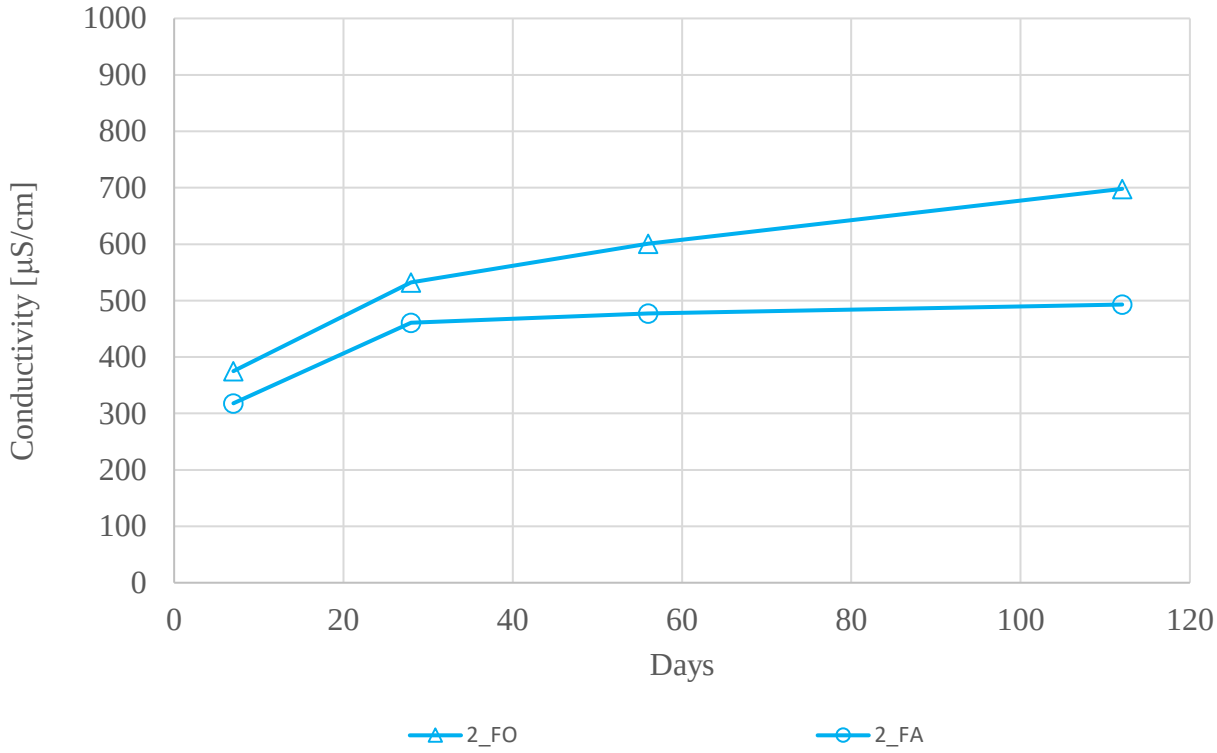

Figure 40: Conductivity measured over the sampling period in freshwater for Experiment 2, where only unweathered shale was used. Triplicates were performed at the last measuring point (16 weeks), and their median values are presented in the plots. (F: Freshwater, O: Oxic, A: Anoxic).

Conductivity measurements for samples treated with seawater in Experiment 2 are displayed in Figure 41. At the first sampling point (after one week), the conductivity was lower for the sample stored under anoxic conditions (2_SA) compared to the one stored under oxic conditions (2_SO). In the following sampling period, the opposite was observed with higher conductivity for 2_SA than for 2_SO.

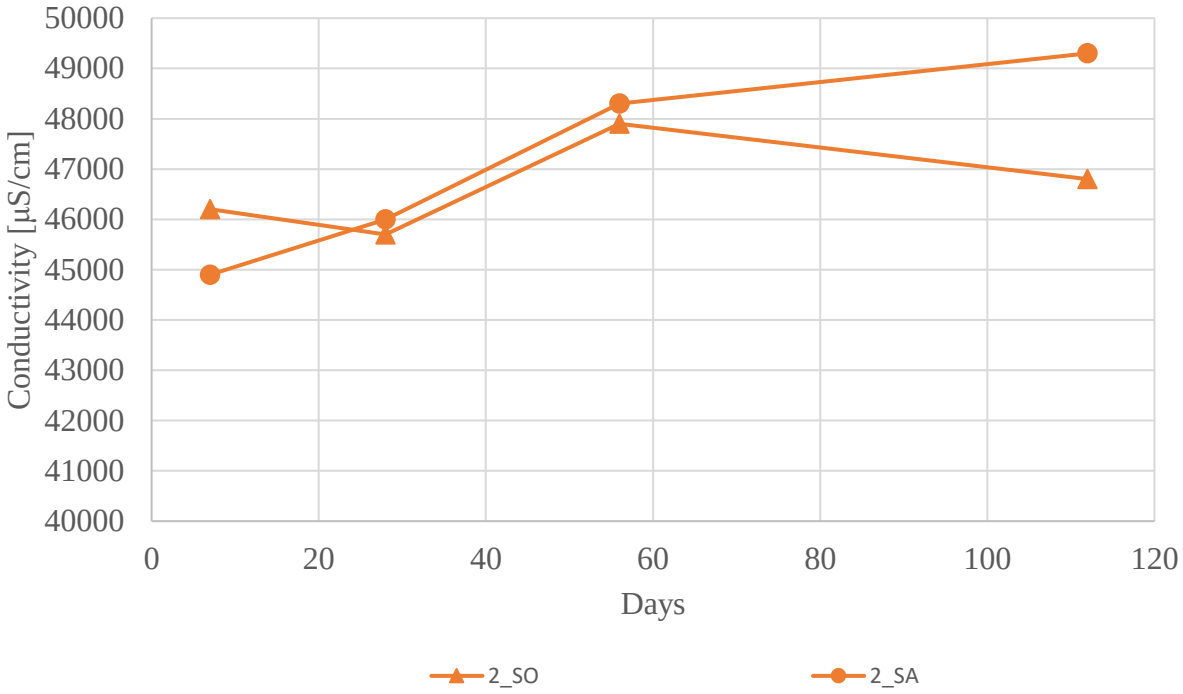

Figure 41: Conductivity measured over the sampling period in seawater for Experiment 2, where only unweathered shale was used. Triplicates were performed at the last measuring point (16 weeks), and their median values are presented in the plots. (S: Seawater, O: Oxic, A: Anoxic).

4.2.4 Alkalinity

The pH measured in the samples containing weathered shale was less than 4.5, which is the endpoint of the alkalinity titration. Therefore, the alkalinity was only measured for the samples containing unweathered shale. The measured alkalinity in Experiment 1 is displayed in Figure 42. The low-oxygen samples had higher alkalinity than the oxic samples for sea- and freshwater treatments. Freshwater treatments had significantly (p-value = $4.6 \cdot 10^{-6}$) lower alkalinity than the seawater treatments stored under the same conditions.

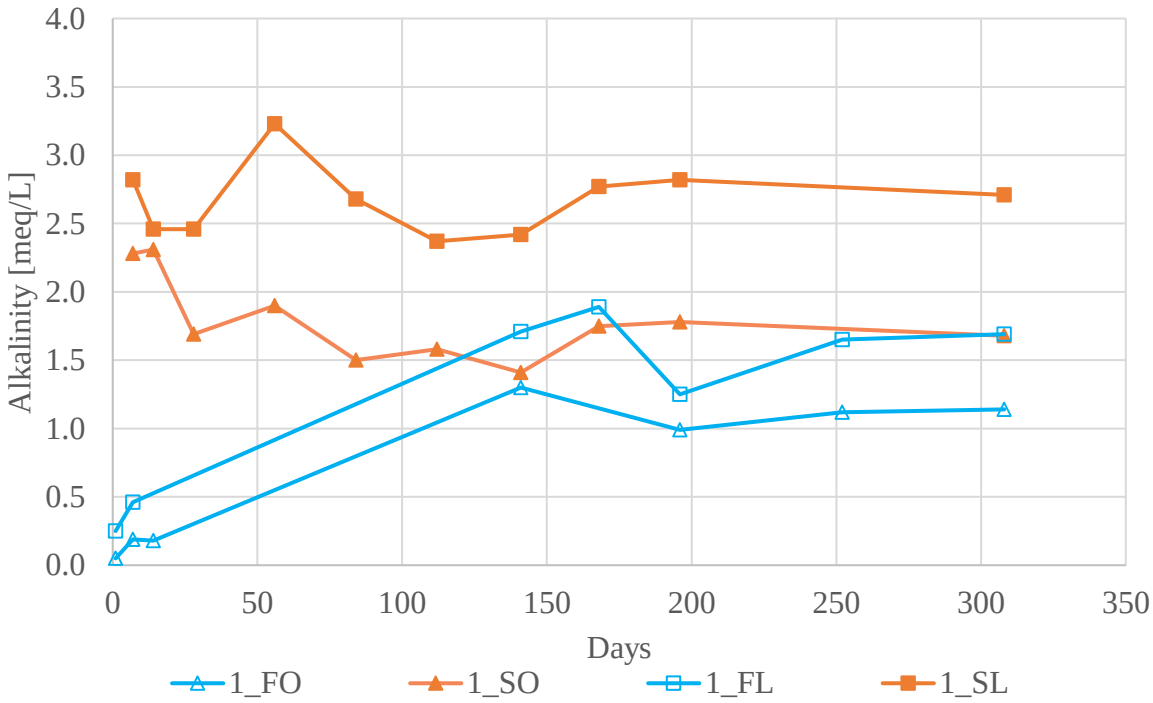

Figure 42 Measured alkalinity in Experiment 1 over the sampling period. Blue line: freshwater, orange line: seawater. Triplicates were performed after 1, 6 and 11 months, and the median values of the triplicates are presented in the plots. (F: Freshwater, S: Seawater, O: Oxic, L: Low-oxygen).

Alkalinity measured in Experiment 2 (unweathered shale stored under oxic and anoxic conditions) is displayed in Figure 43. Freshwater treatments (2_FO, 2_FA) had a lower alkalinity than seawater treatments, and the alkalinity stabilized at around 1 meq/L after 1 month with no noteworthy difference between oxic and anoxic samples. The seawater treatments showed increased alkalinity to a maximum after 2 months followed by a decrease. The greatest increase in alkalinity to ~6.5 meq/L was observed for the seawater treatment stored under anoxic conditions (2_SA) after 1 and 2 months. The equivalent sample stored under oxic conditions (2_SO) also experienced an increase in alkalinity to a maximum of 4.7 meq/L after 2 months.

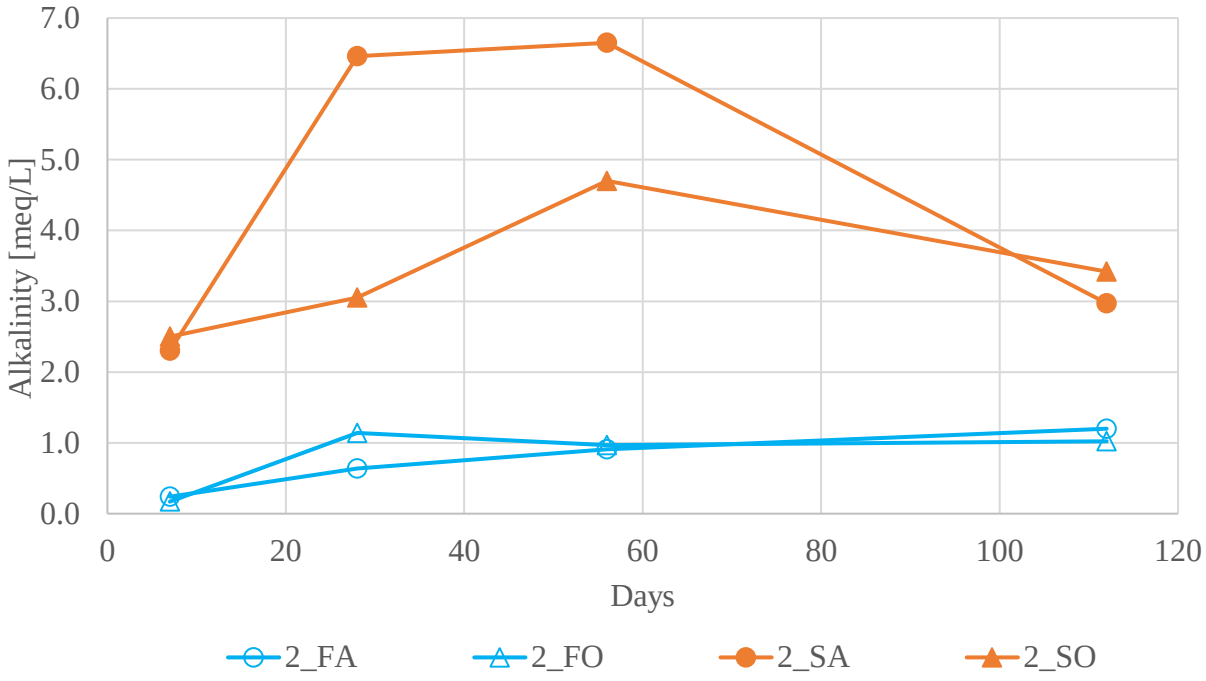

Figure 43: Measured alkalinity in Experiment 2 over the sampling period. Blue line: freshwater, orange line: seawater. Triplicates were performed at the last measuring point (16 weeks), and their median values are presented in the plots. (F: Freshwater, S: Seawater, O: Oxic, A: Anoxic).

4.2.5 Observations

For samples with weathered shale in Experiment 1, a colour difference between fresh-and seawater samples was observed (Figure 44). Weathered shale treated with freshwater developed a red colour, while this was not observed for the seawater treatments. The difference was noticeable after one month and throughout the rest of the sampling period. When the freshwater was transferred from the bottles to beakers for measurements, the red colour was not in the water but sorbed to the surfaces of the bottles.

Air bubbles were observed in the seawater samples, while no to a few air bubbles were observed for freshwater samples.

The shale in the bottles built a layer of approximately 6 mm.

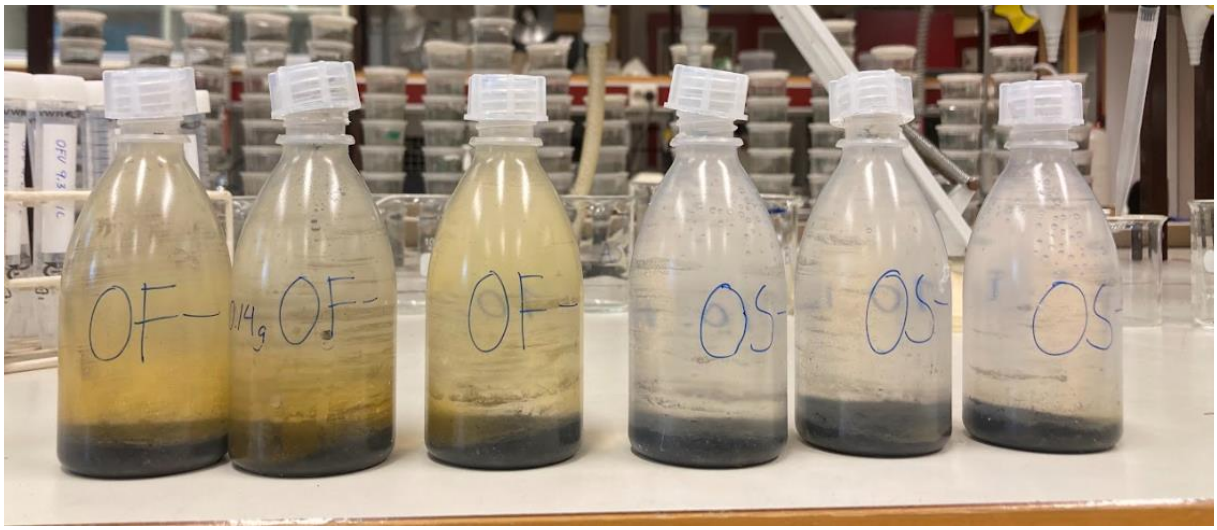

Figure 44: The observed difference between weathered shale treated with fresh -and seawater. The three bottles to the left contained weathered shale treated with freshwater and developed a red colour that stuck to the wall of the bottles. This was not observed for seawater treatments of weathered shale, as seen in the three bottles to the right. Air bubbles were present in the seawater samples, while few air bubbles were observed in the freshwater samples.

4.2.6 Leaching of main ions

The main ions leached from the unweathered and weathered shale in Experiment 1 and 2 were sulphate and calcium, and these results are presented here. For results for other ions, see Appendix (Table A 7 and Table A 8).

Sulphate and calcium concentrations measured in Experiment 1 can be seen in Figure 45 and Figure 46. All samples, except blanks, had a rapid increase in sulphate and calcium concentrations from the starting water, followed by a slower increase in the following

measuring period. No significant difference between oxic and low-oxygen samples were observed for sulphate (p-value = 0.53) or calcium (p-value = 0.69). Leachate from treatments with weathered shale had higher sulphate and calcium concentrations than the unweathered shale. Weathered shale treated with seawater (1_WSO and 1_WSL) leached more sulphate and calcium compared to freshwater treatments (1_WFO and 1_WFL). Leachate of sulphate and calcium from freshwater treatments of unweathered shale (1_FO and 1_FL) had an approximate linear increase during the sampling period. The equivalent samples treated with seawater (1_SO and 1_SL) had more variable concentrations of sulphate and calcium, and when subtracting the concentrations of the starting water, the maximum measured concentrations were higher in seawater compared to freshwater. However, a decrease in sulphate and calcium concentrations was observed after five and six months for all the treatments, but with a greater decline in seawater treatments. After seven months, leachate from seawater treatments of unweathered shale (1_SO and 1_SL) had a lower concentration of calcium than in the first sampling point.

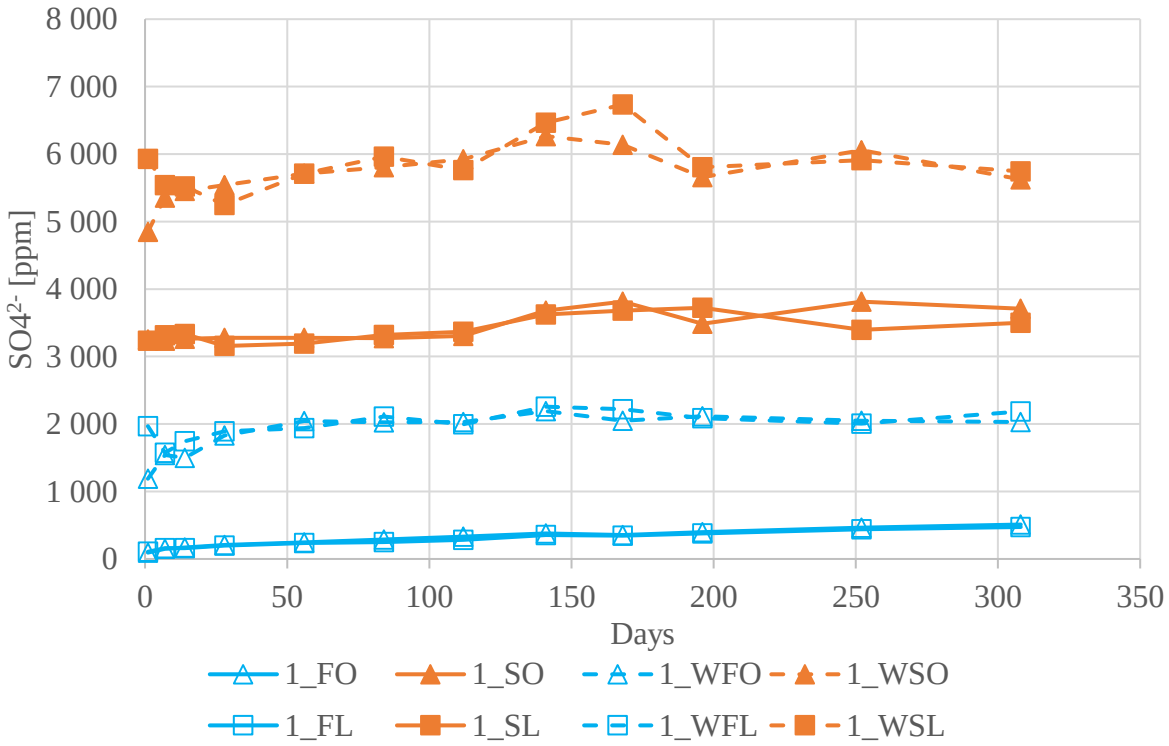

Figure 45: Measured sulphate concentrations in Experiment 1. Blue line: freshwater, orange line: seawater, solid line: unweathered shale, dashed line: weathered shale. Triplicates were performed after 1, 6 and 11 months, and the median values of the triplicates are presented in the plots. (W: Weathered shale, F: Freshwater, S: Seawater, O: Oxic, L: Low-oxygen).

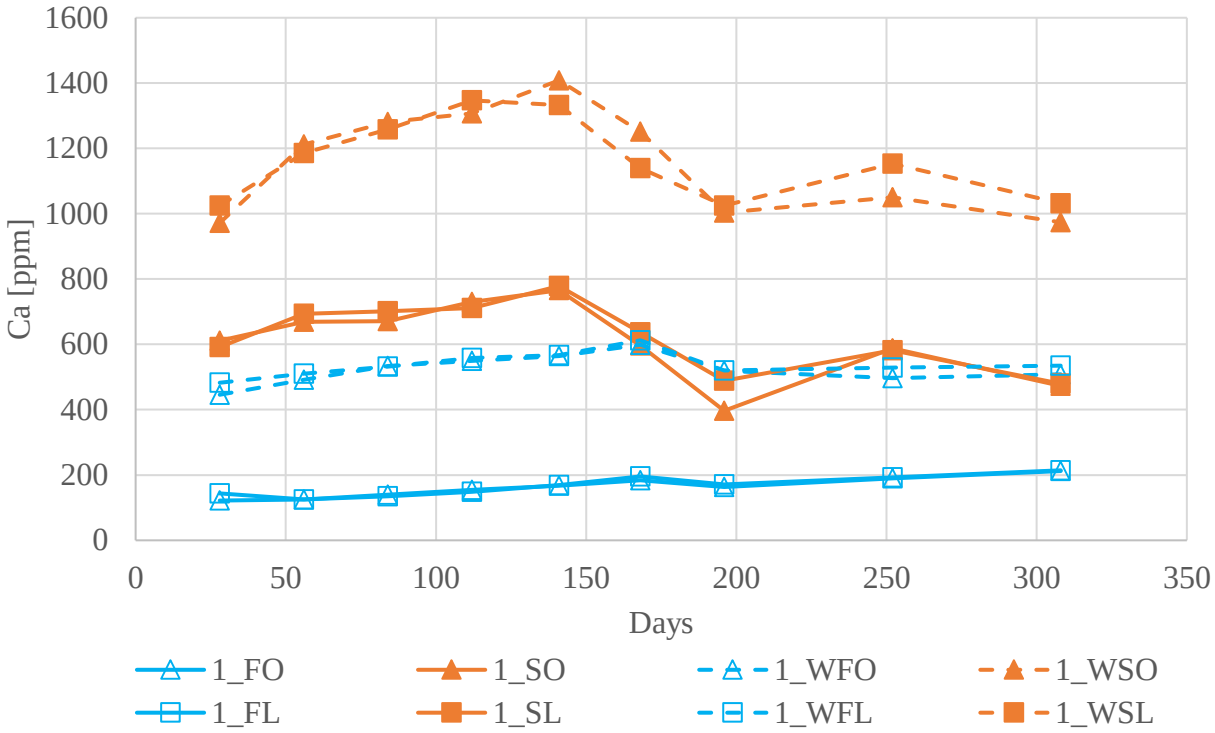

Figure 46 Measured calcium concentrations in Experiment 1. Blue line: freshwater, orange line: seawater, solid line: unweathered shale, dashed line: weathered shale. Triplicates were performed after 1, 6 and 11 months, and the median values of the triplicates are presented in the plots. (W: Weathered shale, F: Freshwater, S: Seawater, O: Oxic, L: Low-oxygen).

Sulphate and calcium concentrations in Experiment 2 can be seen in Figure 47 and Figure 48. Significantly less sulphate (p-value = 0.05) and calcium (p-value = 0.01) are leached from the anoxic compared to oxic freshwater samples. The difference in sulphate (p-value = 0.12) and calcium (p-value = 0.67) between oxic and anoxic samples are not significant for the seawater treatments. However, lower concentration of sulphate is observed for the anoxic seawater treatments. For the freshwater treatments, an increase in the concentrations over the sampling period of SO_4^{2-} and Ca can be seen in the oxic samples. No further increase in sulphate were observed in the anoxic samples after one month. A drop in calcium concentrations in seawater treatments was observed after 2 months under oxic and anoxic conditions.

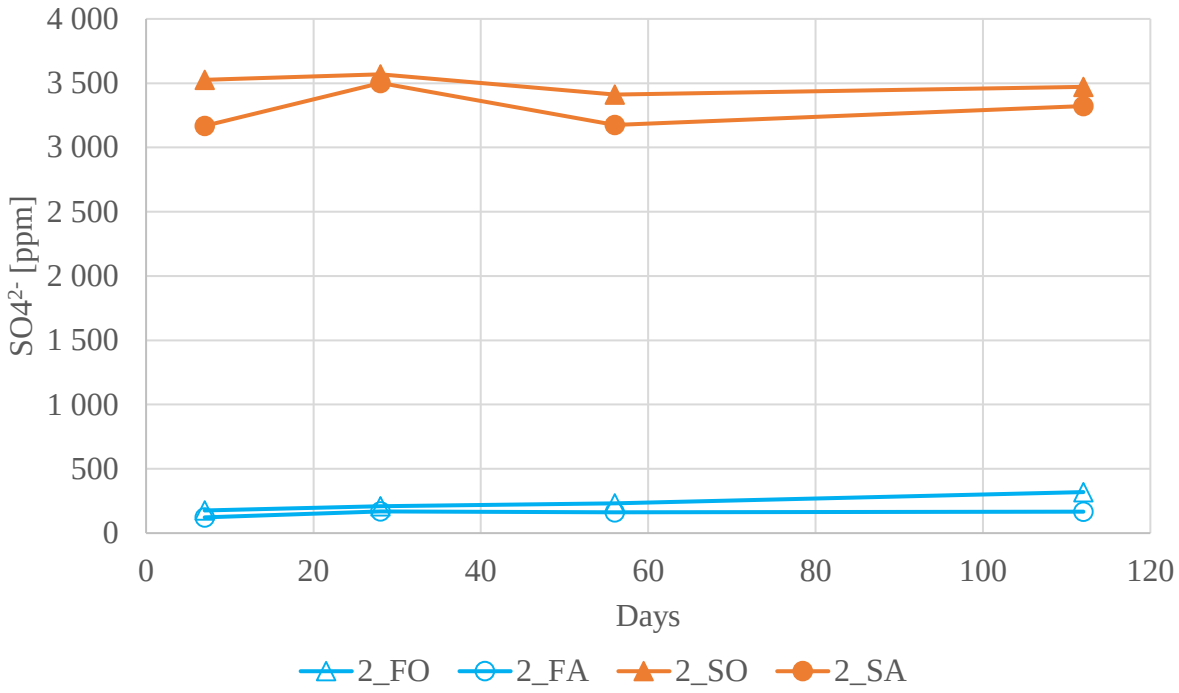

Figure 47: Measured sulphate concentrations in Experiment 2, where only unweathered shale was used. Blue line: freshwater, orange line: seawater. Triplicates were performed at the last measuring point (16 weeks), and their median values are presented in the plots. (F: Freshwater, S: Seawater, O: Oxic, A: Anoxic).

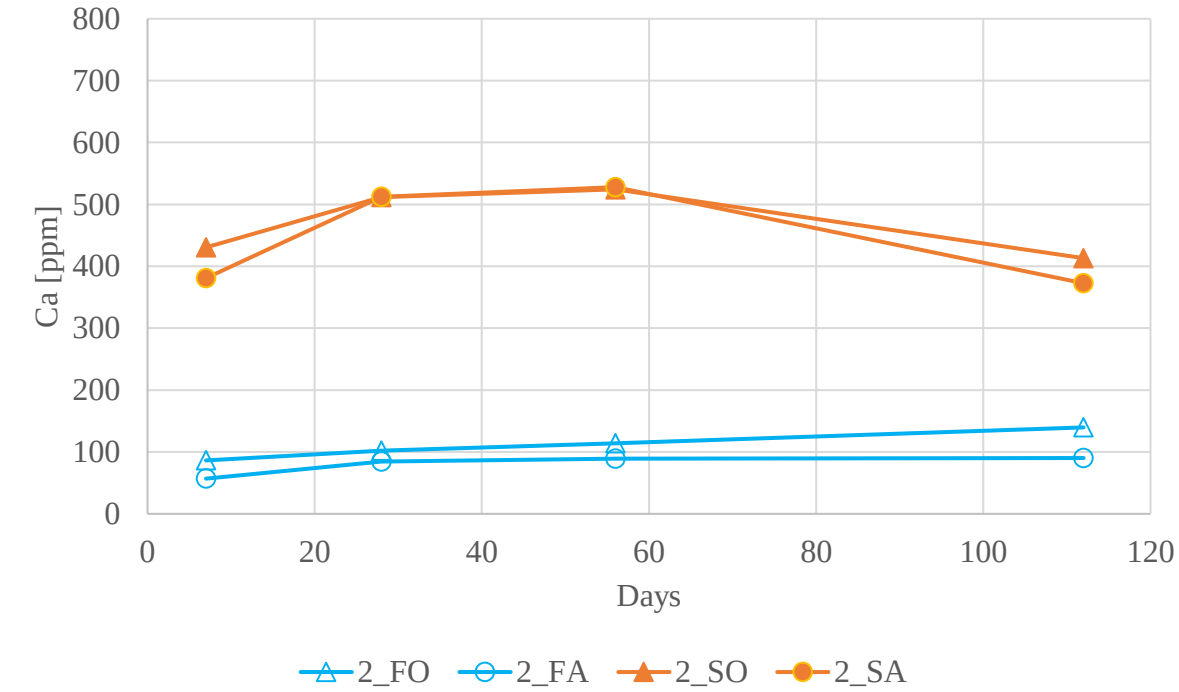

Figure 48: Measured calcium concentrations in Experiment 2, where only unweathered shale was used. Blue line: freshwater, orange line: seawater. Triplicates were performed at the last measuring point (16 weeks), and their median values are presented in the plots. (F: Freshwater, S: Seawater, O: Oxic, A: Anoxic).

4.2.7 Leaching of trace elements

Experiment 1

The concentrations measured in Experiment 1 of the main metals leached from the shale can be seen in Figure 49. In Experiment 1, it was observed higher concentrations of all metals in seawater compared to freshwater treatments of the unweathered shale. This trend was not observed in the leachate from weathered shale.

When examining the metals leached from unweathered shale, the concentrations of most metals steadily increased. However, there were exceptions for Ba and Sb: An immediate drop in Ba concentrations was observed, and a drop in Sb was observed after 2 months.

The concentrations of metals leached from weathered shale did not increase during the sampling period, but the concentrations varied over time. Higher concentrations were observed in the leachate from weathered shale for most metals compared to unweathered shale. The exceptions to this trend were Mo, Sb, Ba, and Cd, which exhibited lower concentrations in the leachate from weathered compared to unweathered shale. Mo and Sb were absent in the leachate from weathered shale but appeared in the leachate from unweathered shale.

Furthermore, higher concentrations of uranium were measured in low-oxygen samples compared to oxic samples in the leachate from unweathered shale. This trend was also observed for Ni, Zn, Co, Mn, and Cd. For the weathered shale, higher uranium concentrations were found in freshwater treatments compared to seawater treatments. The peaks in uranium concentrations coincided with peaks of iron in the freshwater treatments for weathered shale stored under oxic conditions after 1 month (1_WFO_2m) and for the equivalent sample stored under low-oxygen conditions after 11 months (1_WFL_11m).

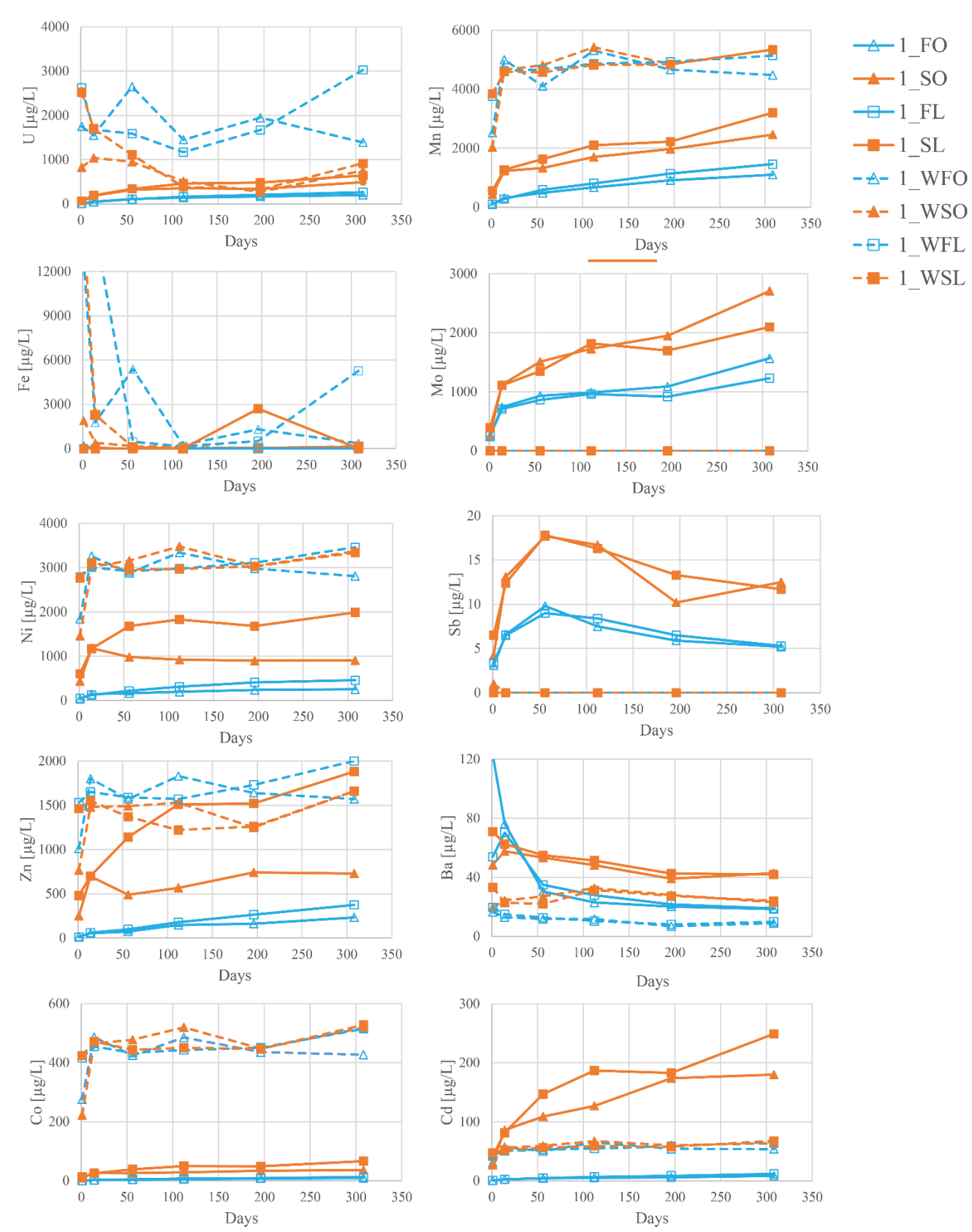

Figure 49: Leaching of metals in Experiment 1. Blue line: freshwater, orange line: seawater, solid line: unweathered shale, dashed line: weathered shale. Triplicates were performed after 1, 6 and 11 months, and the median values of the triplicates are presented in the plots. (W: Weathered shale, F: Freshwater, S: Seawater, O: Oxic, L: Low-oxygen).

Leaching of metals from the shale measured in Experiment 2, using only unweathered shale over a shorter sampling period of 4 months, are presented in Figure 50. Consistent with the findings in Experiment 1, higher concentrations of metals were observed in seawater compared to freshwater treatments.

In contrast to the observations from Experiment 1 regarding the difference in uranium concentration between oxic and low-oxygen samples, no such difference was observed between oxic and anoxic treatments in Experiment 2.

Under anoxic conditions, Cd, Zn, Co, and Ni exhibited a drop in concentration over time in both freshwater and seawater treatments. However, this drop occurred later in seawater treatments compared to freshwater treatments. Additionally, Fe and U concentrations dropped in the sampling points for the freshwater treatment stored under anoxic conditions (2_FA), but no drop was observed in the seawater treatment stored under anoxic conditions (2_SA) after 4 months.

Furthermore, higher concentrations of Sb, Mn, Fe, and Ba were observed under anoxic compared to oxic conditions in fresh- and seawater treatments.

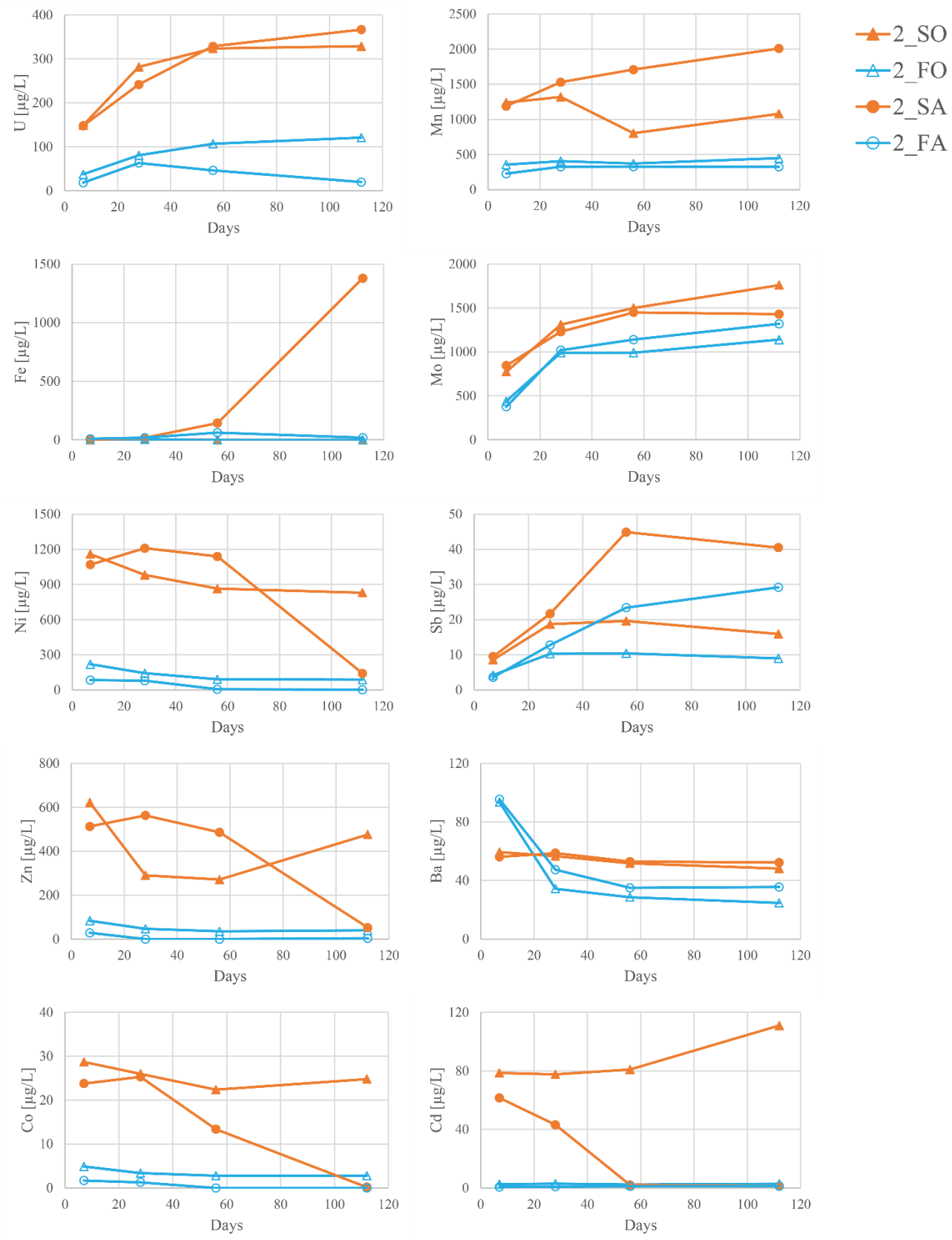

Figure 50: Leaching of metals in Experiment 2, where only unweathered shale was used. Blue line: freshwater, orange line: seawater. Triplicates were performed at the last measuring point (16 weeks), and their median values are presented in the plots. (F: Freshwater, S: Seawater, O: Oxic, A: Anoxic).

4.2.8 Relative standard deviation (RSD%)

The relative standard deviation (RSD%) for selected parameters (conductivity, pH, Eh, alkalinity and concentrations of SO_4^{2-}, Ca and U) for the triplicates in the last measuring point in Experiment 1 (44 weeks) is shown in Figure 51. Higher RSD% for conductivity, pH and uranium was seen for the weathered shale compared to the unweathered shale. For the unweathered shale, more variation in alkalinity was seen in the low-oxygen samples compared to the oxic samples.

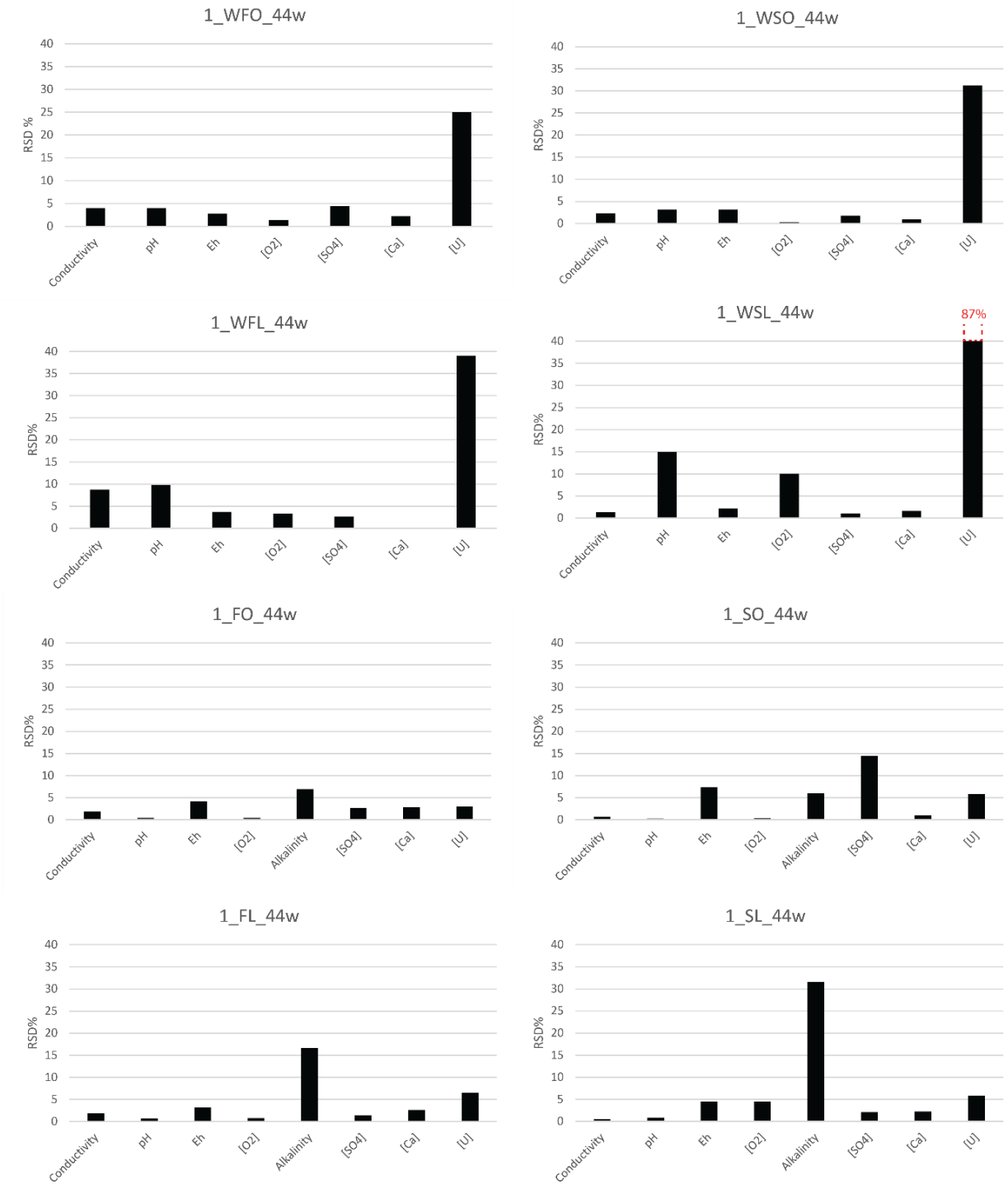

Figure 51: Relative standard deviation (RSD%) for the triplicates in the last measuring point (44 weeks) in Experiment 1 for selected parameters (Conductivity, pH, Eh, alkalinity and concentrations of SO_4^{2-}, Ca and U). Note that for uranium in WSL_44w, the RSD was larger than 40%. W: weathered shale, F: Freshwater, S: Seawater, O: Oxic, L: Low-oxygen.

In Experiment 2 (Figure 52), higher variation in E_h and dissolved oxygen in anoxic compared to oxic samples was observed. High variation in alkalinity (RSD = 47 %) was observed for seawater treatment stored under oxic conditions (2_SO). Also, a high variation (RSD = 62%) was observed for uranium in freshwater treatments stored under anoxic conditions (2_FA).

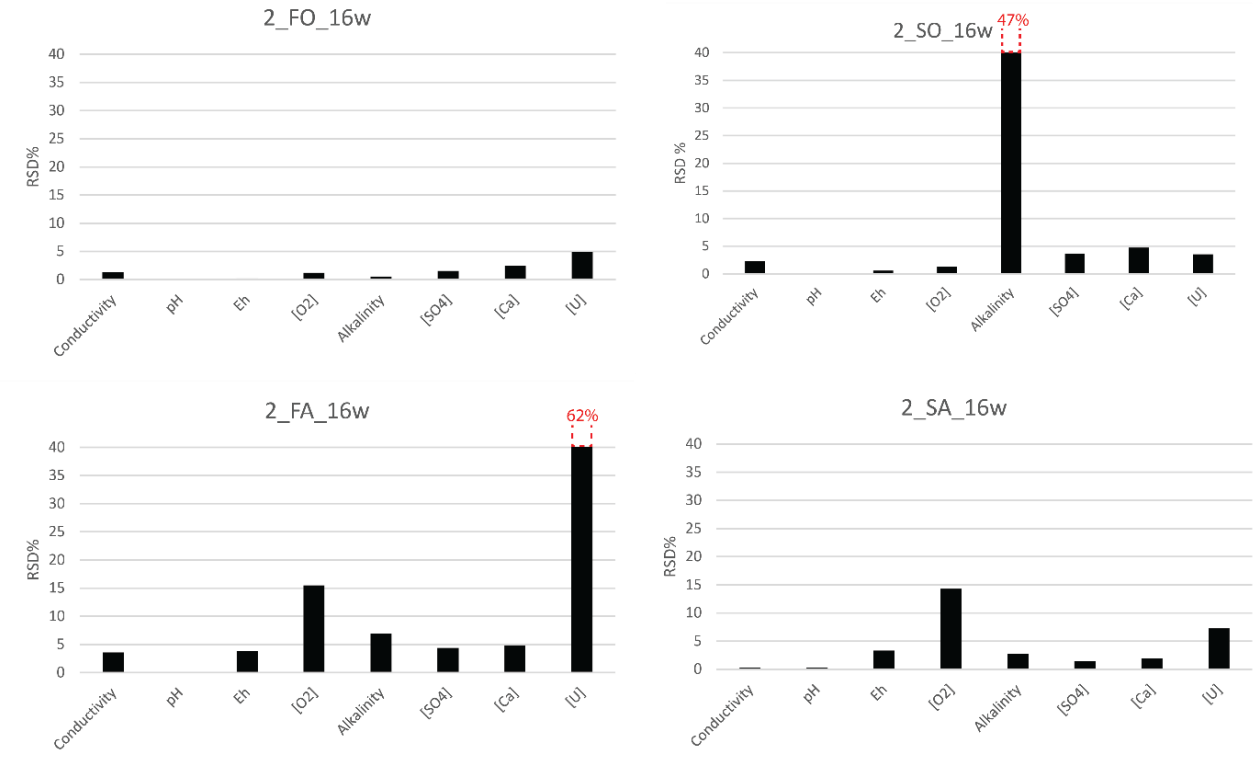

Figure 52: Relative standard deviation (RSD%) for the triplicates in the last measuring point (16 weeks) in Experiment 2 for selected parameters (Conductivity, pH, Eh, alkalinity and concentrations of SO_4^{2-} , Ca and U) Note that for alkalinity in 2_FA and uranium in 2_SO, the RSD was larger than 40%. F: Freshwater, S: Seawater, O: Oxic, L: Low-oxygen.

4.3 Modelling

Calibration model

The model was calibrated according to the results from unweathered shale treated with freshwater under oxic conditions in Experiment 1 (1_FO). Figure 53 shows the measured (blue line) and simulated (black line) concentrations of SO_4^{2-}, Ca, pH and U.

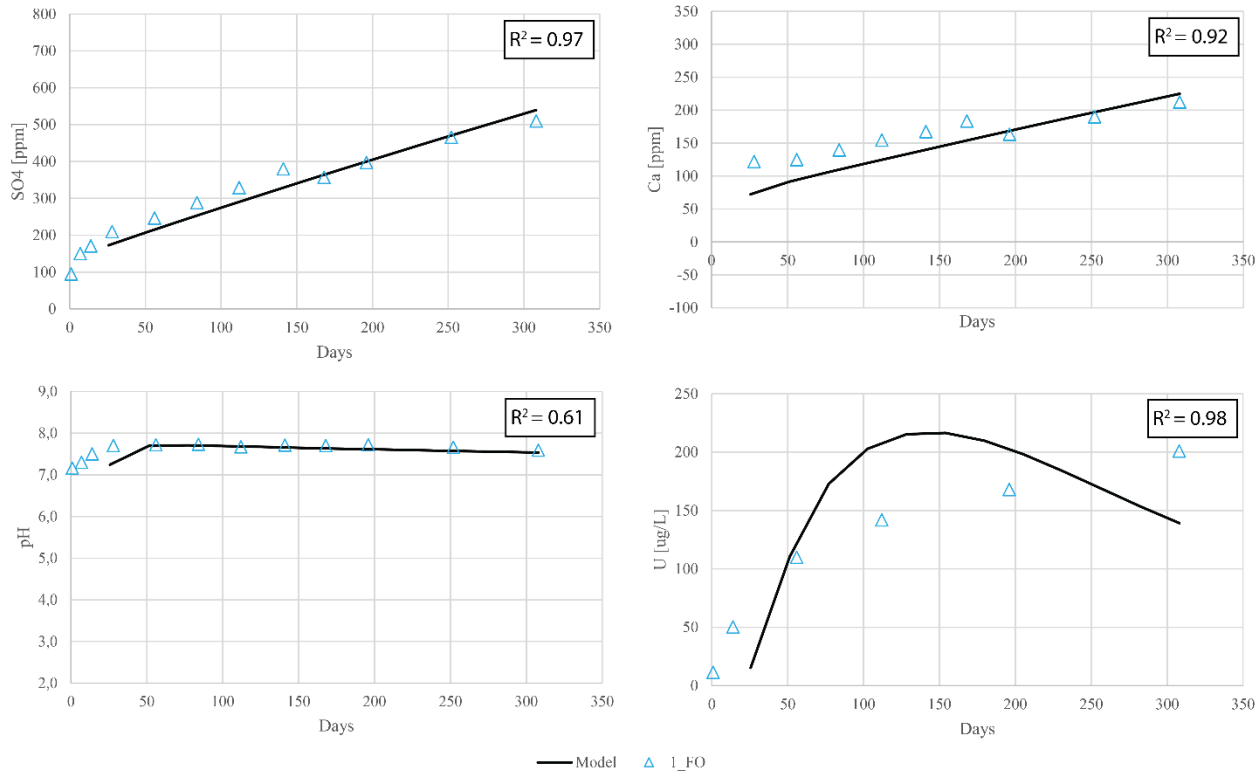

Figure 53: Measured (blue triangles) and simulated (black line) concentrations of SO_4^{2-}, Ca, pH and U for unweathered shale treated with freshwater stored under oxic conditions (1_FO) in Experiment 1.

Validation model

The model vas validated by changing the initial solution from freshwater to seawater and compared with results from the samples of unweathered shale treated with seawater stored under oxic conditions (1_SO) in Experiment 1 (Figure 54). There is a great variability in the measured values (with subtracted background concentrations of SO_4^{2-} and Ca). The deviation between measured and simulated uranium concentrations was greater in seawater than in

freshwater simulations. However, the release of uranium was higher in seawater compared to freshwater for both measured and simulated results.

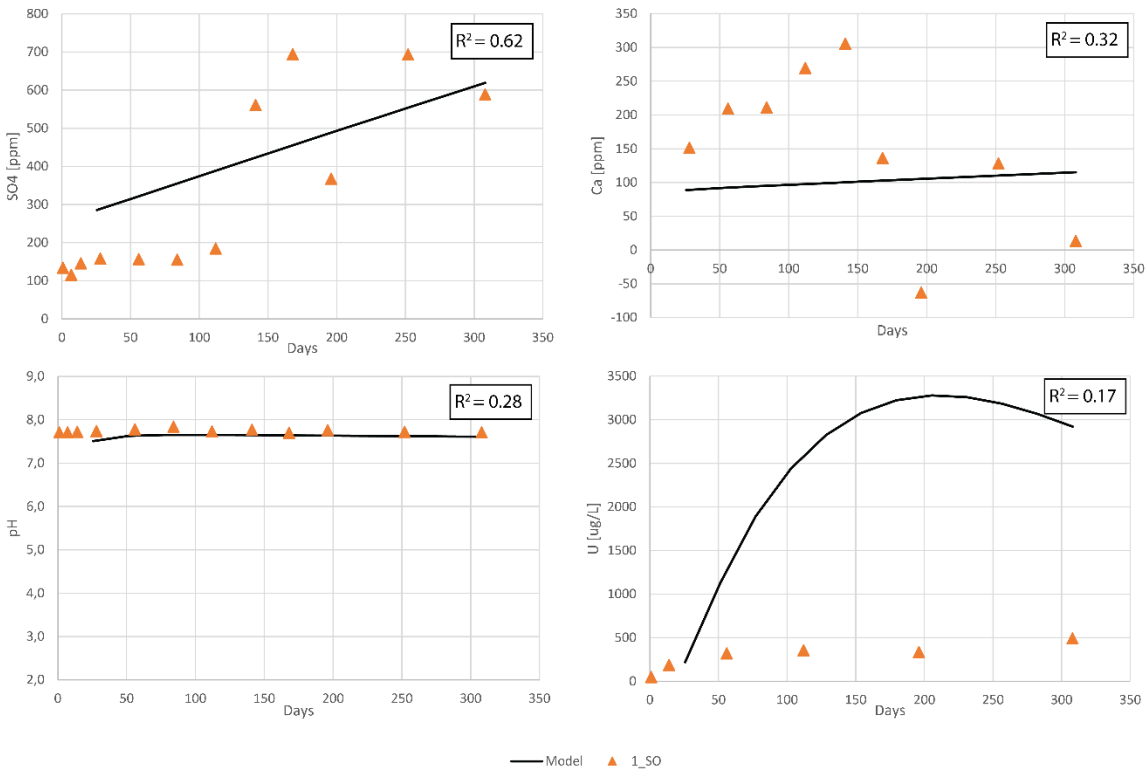

Figure 54: Measured (orange triangles) and simulated (black line) concentrations of SO_4^{2-} , Ca, pH and U for unweathered shale treated with seawater stored under oxic conditions (1_SO) in Experiment 1.

Trace elements

The leaching of trace elements (Cu, Zn, Ba, Mn) simulated in the model plotted with experimental data from Experiment 1 can be seen in Figure 46. The model underestimates the leaching of Zn, Ba and Mn compared to experimental data. Cu is under the detection limit (4 µg/L) in all the sampling points in the experimental measurements, and the model also estimates this. Further, the modelled release of all metals is higher in seawater than in freshwater , which is also mainly the case for the experimental concentrations.

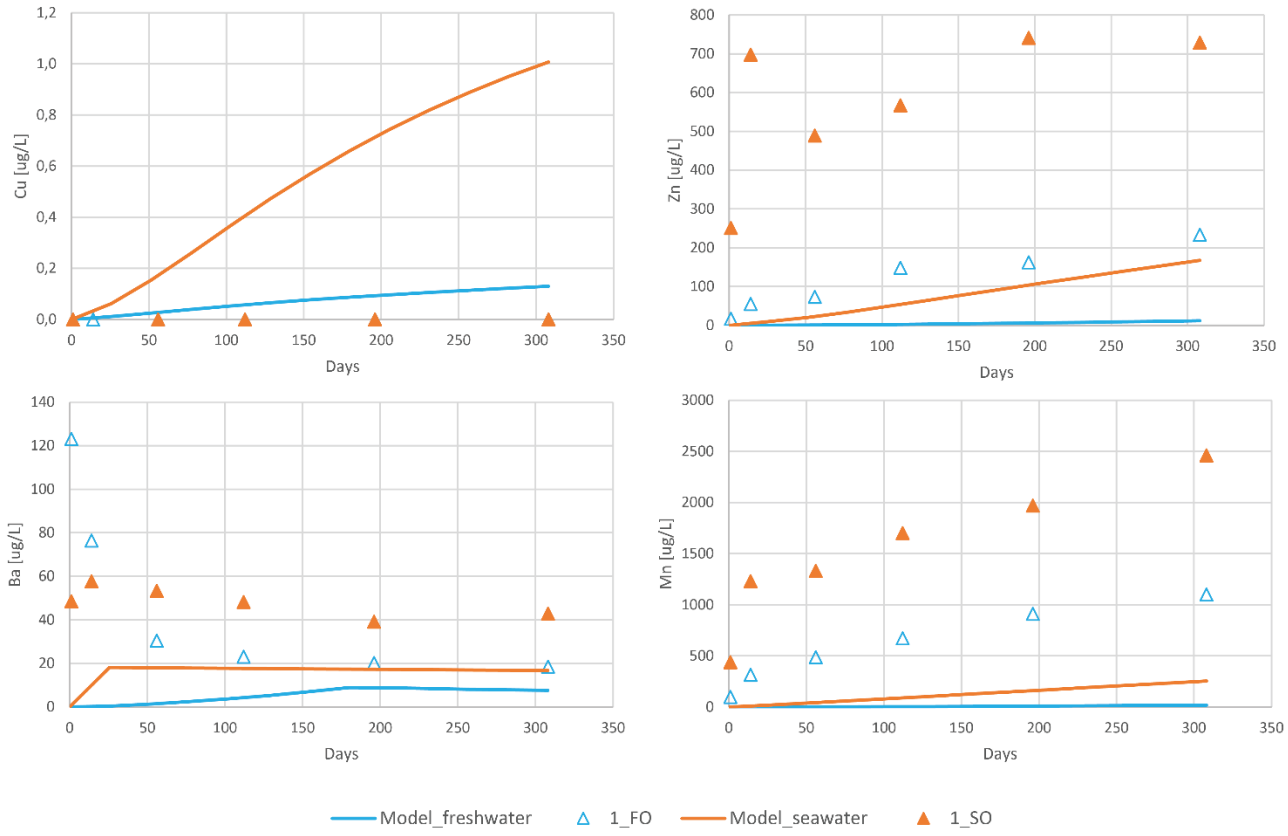

Figure 55: Leaching of trace elements (Cu, Zn, Ba, Mn) simulated in the model plotted with experimental data from Experiment 1.

Extrapolation of calibration and validation model

An extrapolation of the model simulating the batch experiments with unweathered shale treated with fresh- and seawater (calibration and validation) was run for 15 years. The extrapolation of the model estimated that ARD will be produced after ~2 years (Figure 56). The pH drop coincides with the time of completely dissolution of calcite in fresh -and seawater treatments. The simulated drop in pH (and completely dissolution of calcite) occurs somewhat later in seawater than in freshwater treatments. However, after ~4 years, the simulated pH is lower and decreases more rapidly in seawater than in freshwater. The simulated remaining pyrite in the freshwater treatments is steadily decreasing, while the dissolution of pyrite in seawater accelerates after ~8 years and is completely dissolved after ~13 years. This does not happen in the freshwater treatment at a later point in time, and the steady dissolution of pyrite in the freshwater batch over 50 years can be seen in Figure A 2 (Appendix).

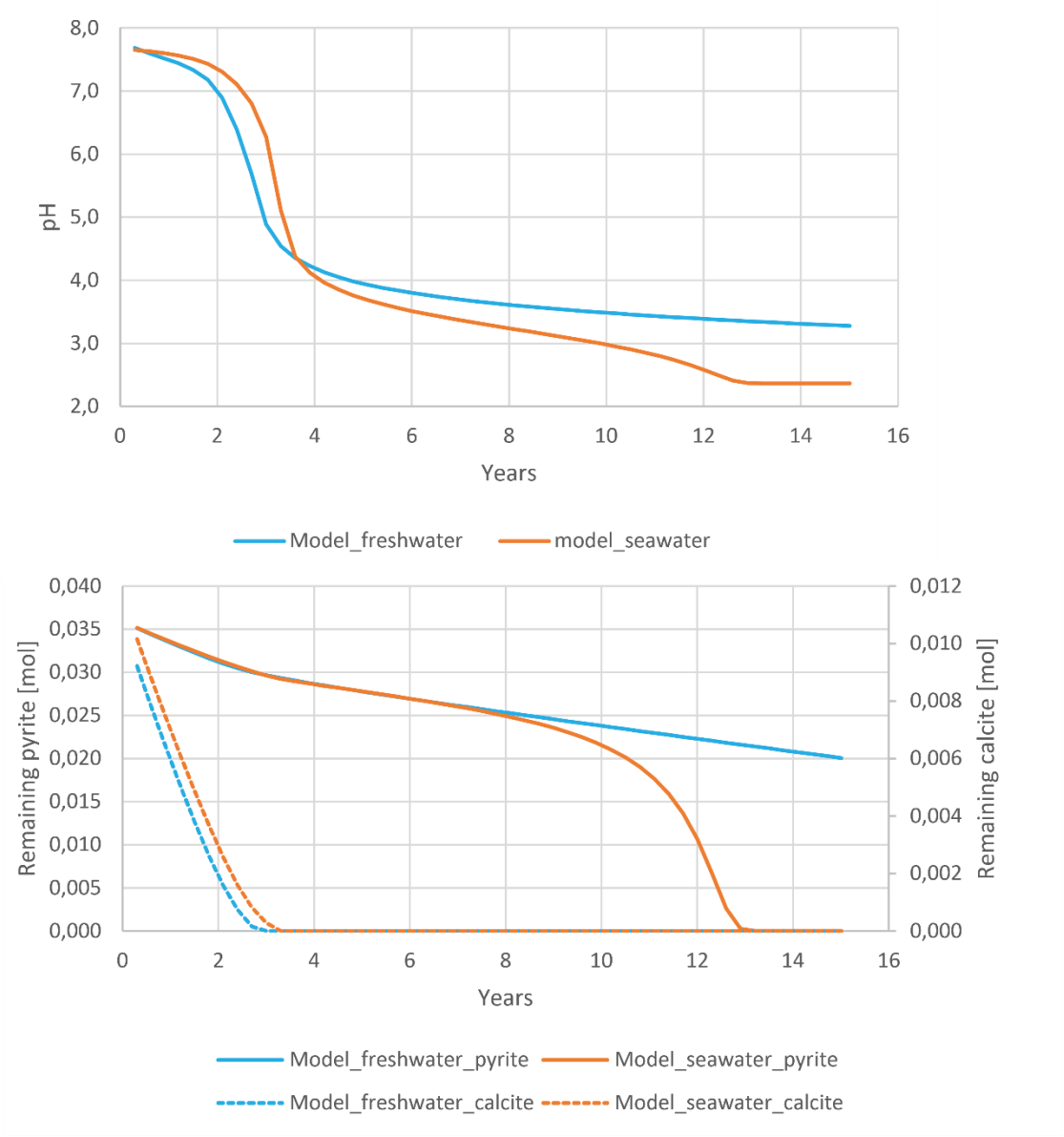

Figure 56: Extrapolation of the model showing the change in pH and dissolution of pyrite and calcite in fresh (blue line) and seawater (orange line) over 15 years.

Drammensfjord

The model was changed to simulate the conditions in the Drammensfjord by implementing the periodic exchange of water and changing the temperature. The model was run for 600 years and showed that oxygen was depleted (Figure A 3 in Appendix) and ARD was not produced (Figure 57). A slight drop in pH (from ~7.7 to 7.2) happens simultaneously as the calcite is completely dissolved. This drop in pH, and completely dissolution of calcite happens faster (~250 years) in the model where the water was exchanged every 3 years compared to when water was

exchanged every 5 years (~450 years). The simulated uranium concentrations in the modelled seawater was steady at ~0.1 µg/L during the 600 years for both three and five year exchange of water.

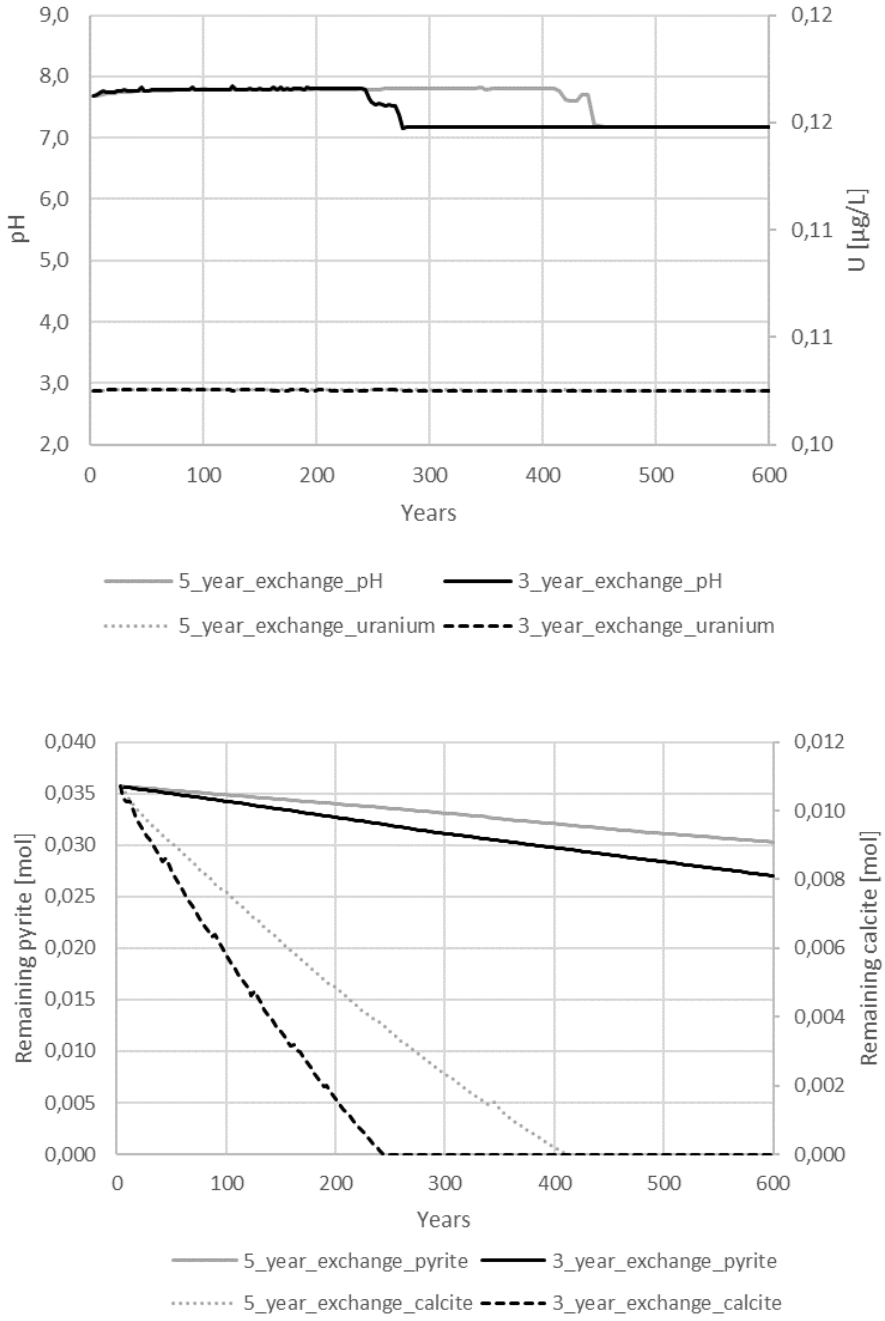

Figure 57: Change in pH, uranium and dissolution of calcite and pyrite with 3 years (black line) and 5 years (grey line) exchange of water in the model simulating the Drammensfjord.

The release of Mn, Ba, Cu and Zn in the Drammensfjord model with exchange of water every three-year (Figure 58) showed that ~0 µg/L of Zn and Cu was released. A steady concentration of ~10 µg/L of Ba was simulated, while the concentration of Mn increased over the time.

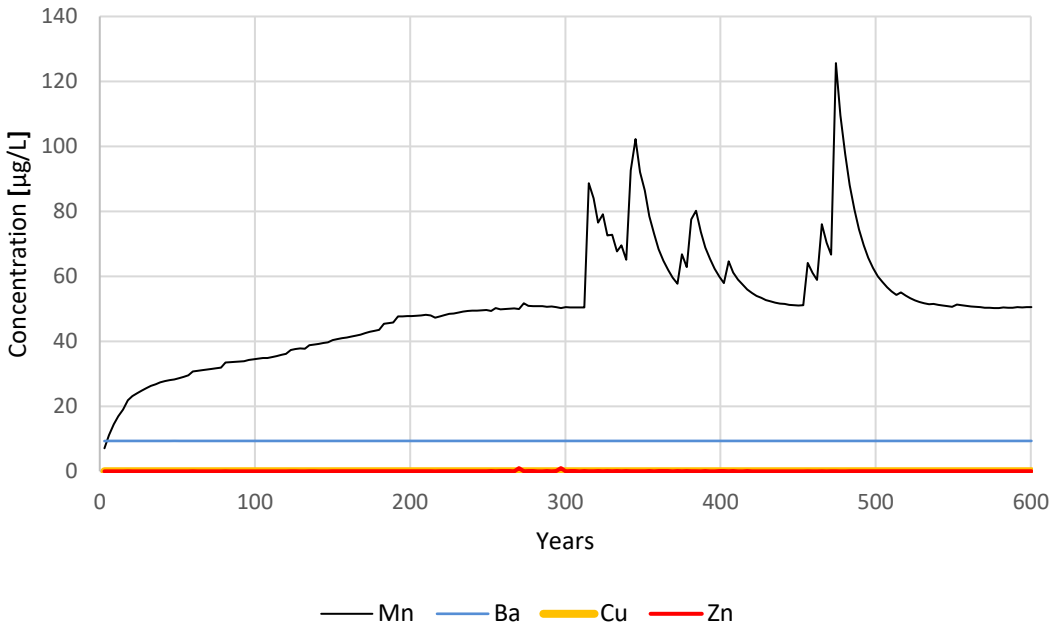

Figure 58: Estimated release of Mn, Ba, Cu and Zn in the Drammensfjord model with exchange of water every three-year.

5. Discussion

5.1 Rock properties and changes with time

5.1.1 Mineralogical composition

Unweathered shale from Kleggerud

SEM and XRD analyses showed that the unweathered starting material mainly consists of quartz, feldspars and clays, as described in the literature for the Alum Shale Formation (e.g., Bjørlykke, 1974). This was supported by the presence of the main oxides, namely, SiO_2, Al_2O_3 and K_2O, measured in “whole rock analysis” (Figure 27).

Iron-sulphides including pyrite (FeS_2) and smaller amounts of pyrrhotite ($Fe_{1-x}S$) were observed in the SEM analyses (e.g., Figure 19.12). The sampling site was intruded by sills (Figure 9), and the pyrrhotite was most likely formed by pyrite alteration due to contact metamorphism (Bjørlykke, 1974).

The sulphur-bearing minerals in the starting material of unweathered shale detected in the XRD were pyrite, pyrrhotite and jarosite [$KFe_3(SO_4)_2(OH)_6$]. The weight percentage of sulphur was calculated from the semi-quantitative amounts obtained from the XRD results (average value of duplicates), giving 3 wt.% pyrite, 1 wt.% pyrrhotite (assumed to be present as Fe_7S_8), and 1.2% jarosite. The total sulphur content calculated from the XRD results gave 2.2 wt.% of sulphur, which is consistent with the amount of total sulphur measured in the "whole rock analysis" (also 2.2% of S). The equal values of total sulphur from the two different analyses suggest that the semi-quantitative amounts obtained from the XRD analysis could be considered reliable.

Secondary sulphate, such as jarosite, was detected in the XRD analysis. This could be a result of the fact that the experiments were started approximately 2 years after the shale was blasted out and meanwhile stored under atmospheric conditions. While the rock masses were stored dry, some oxidation of sulphides can have occurred due to humidity from air. The rapid increase in sulphate observed in the experiments for unweathered shale also supports secondary sulphates to be present. However, in small amounts, since no drop in pH were observed and the produced acid was most likely immediately buffered by, e.g., carbonates.

Total inorganic carbon (TIC) was estimated to be 0 % in the total carbon (TC) analysis. However, calcite was observed in small amounts in the SEM images (e.g., Figure 19.8) and measured with XRD (0-1 wt. %). Wærsted et al. (2023a) measured TIC for the same shale (unweathered shale from Kleggerud) at 0.27 %, suggesting that TIC was under the detection limit for the method used in this study. The results of the XRD analyses are uncertain for minerals of lower abundance (< 3 wt. %, see Kriegel et al., 2020), and the quantitative amount of e.g., pyrrhotite (~1 wt.%) and calcite (0-1 wt.%) are uncertain. Total organic carbon (TOC) was estimated to be 6.2 %, a bit lower than reported in the literature (around 10 %) for the Alum Shale Formation (Andersson et al., 1985). Some of the organic carbon might have matured and expelled from the shale, migrating to the surface due to contact metamorphism under the Permian rifting (Bastiansen et al., 1957). This is supported by the observed magmatic intrusions (sills) at the sampling site (Figure 9).

Weathered shale from Taraldrud

As for the unweathered shale, the main constituents of the starting material were quartz, feldspars, and clay minerals. Pyrite was only detected in one of the outcrops (Figure 21.8), which suggests that most of the pyrite was already weathered before the experiment was started. The cavity observed in the vicinity of pyrite in the outcrop (Figure 21.8) is assumed to be a negative shape of a pyrite grain that has been oxidized and dissolved. No carbonates were measured with XRD or seen in the SEM analysis, nor in the TIC estimated from TC and TOC analysis. If carbonates existed prior to the disposal of the shale at Taraldrud, these carbonates might have been used in the neutralization of the acid generated through sulphide oxidation from earlier weathering. Further, after the initial increase in sulphate concentrations and drop in pH, no noteworthy changes in these parameters were observed during the experiment period, indicating that further sulphide oxidation was not taking place. This supports the assumption that the amount of sulphides present in the starting material of the weathered shale was small. When choosing material for the experiment, middle sized rock pieces (2mm – 8 cm) were selected. This was done to avoid the fine material that was thought to be completely weathered and to avoid the unweathered core of larger rock pieces which could contain enough carbonates to neutralise the pH. These results indicate that larger pieces of rock should have been selected.

A high RSD (relative standard deviation, given in %) of conductivity, pH, and uranium concentrations was seen for the weathered shale, suggesting that the mixed fraction of

weathered shale was not sufficiently homogenized. It was a mixture from three different sample shafts collected by NGI at Taraldrud in 2020.

The sulphur content measured in the "whole rock analysis", with an average of 3.5% S, was assumed to be present as secondary sulphate minerals due to the oxidation of pyrite before the start of the experiment. This was indicated by the SEM analyses (Figure 21.1) where "Unknown sulphate" appears as a crust on a rock fragment and is assumed to be a secondary iron-sulphate caused by earlier weathering of sulphides and precipitation. The spectrum of "unknown sulphate" (Figure 22) suggests that it is rozenite [$Fe(SO_4)\cdot 4H_2O$] or schwermanite [$Fe_8O_8(OH)_6(SO_4)\cdot nH_2O$]. Phosphorus, aluminium and calcium could be sorbed to the surface of the mineral, as no mineral with the composition (seen in the crust) of O, S, F, Al, P and Ca exists (Mindat.org, 2023). Another explanation could be that the EDS spectrum (Figure 22) is a result of mixing between two or more phases, as the X-rays penetrate 1-3 µm into the sample (Klein et al., 2008). A thin layer of a secondary sulphate phase could be overlying another phase, and both sulphate and the underlying phase are detected in the EDS analysis. The presence of soluble secondary iron-sulphates was supported by observations in Experiment 1, where an immediate drop in pH and a rapid increase in sulphate concentrations were observed for all samples with weathered shale. Jarosite [$KFe_3(SO_4)_2(OH)_6$] and the already mentioned secondary sulphate minerals were measured in the XRD analysis of the weathered shale, where jarosite was the most abundant, followed by schwertmannite and rozenite (Table A 3 in Appendix).

Change in mineralogical composition after 7 and 9 months

Relatively more feldspar and smaller amounts of clay minerals were observed in the XRD analyses for the samples that had been treated with seawater for 7 and 9 months (Figure 25 and Figure 26). The relative increase in feldspars could result from early diagenetic precipitation of K-feldspar (Morad, 1978). Table A 2 and Table A 3 (Appendix) shows that the relative amount of microcline [$KAlSi_3O_8$] increased in the shales after being treated with seawater for 7 and 9 months. Around 450 ppm potassium (Table 7) was present in the starting seawater and absent in the starting freshwater. This could explain why precipitation of early diagenetic K-feldspar occurs in seawater, but not in freshwater treatments. The more pronounced increase of K-feldspar in weathered compared to unweathered shale treated with seawater could be caused by higher potassium availability. This could be explained by desorption and dissolution of clay minerals under acidic conditions resulting in more precipitation of K-feldspars as microcline.

5.1.2 Horizons of origin

The characterization using triangular diagrams derived from "whole rock analysis" showed that both unweathered and weathered shale belonged to the Alum Shale Formation (Horizon 2 and 3a) (Pabst et al., 2017). The unweathered shale from Kleggerud was identified as horizon 3a, which was consistent with the characterization done by Wærsted et al. (2023a), that characterized the same batch of shale as horizons 2 and 3a. The weathered shale, which was primarily plotted in the areas within horizon 2 and horizon 3a, was probably a mix of horizons as the bulk material was a mixture of shale from three different shafts: ~40 % was from shaft 5 as described by Sørmo et al. (2017) as horizon 3bα/3bß. The remaining ~60 % was from shaft 9 and 16 and are characterized as horizon 2 and 3a.

5.1.3 Potential for Acid Rock Drainage (ARD)

Both unweathered -and weathered shale were characterized as horizon 2 and 3a which is known to have the potential to produce acid rock drainage (ARD) (Pabst et al., 2017). The weathered shale produced ARD immediately after being mixed with water, resulting in low pH (<4), elevated levels of heavy metals and sulphates and high electrical conductivity. ARD was not produced in the samples containing unweathered shale in the experiments. Based on the rock characterization, it is estimated that the unweathered shale has the potential to produce ARD as NP:AP < 1 (Figure 29). This implies that pH would have dropped with time if the access to oxygen had been sufficient. This was demonstrated in a recent study done by Totland et al. (2023), where a column experiment that utilized unweathered shale, also from Kleggerud, was kept unsaturated, with periodic water addition. After approximately one year, a significant decrease in pH was observed in the leachate from the column. The pH stabilized around 2.5 after two years.

When estimating the ARD potential by comparing AP with NP, kinetics are not considered, and when ARD would have occurred in the batch experiments is uncertain. The pyrite in the unweathered shale was mainly present as framboidal pyrite (Figure 19.1), which usually is more reactive than cubic pyrite (Jeng, 1991). Additionally, pyrrhotite was also detected and is thought to be more reactive than pyrite and could produce ARD faster (Pabst et al., 2017). Another factor affecting the kinetics of ARD development is the dissolution of calcite and other acid-neutralising minerals.

5.2 Water chemistry

5.2.1 Leaching of main ions

Sulphate and calcium were the main ions leached from the unweathered shale in Experiment 1 and 2. The rapid increase in sulphate concentrations implies that secondary sulphate minerals were originally present in the unweathered shale and dissolved quickly in contact with water. The following slower increase in the sulphate concentration is most likely due to pyrite oxidation. However, the pH stood at circumneutral pH throughout the sampling period of 44 weeks, indicating that the acid produced from pyrite oxidation was neutralized. The acid generated in the system was likely buffered by carbonates that originated from the dissolution of calcite. The rise in calcium concentration followed the same trend as sulphate concentrations, supporting the assumption of calcite dissolution caused by buffering of produced acid.

For the samples with weathered shale in Experiment 1, substantially higher leachate concentrations of sulphate and calcium were observed at the first sampling point (after one day) for all treatments, compared to the leachate in samples with unweathered shale. The high concentrations of sulphate observed were probably released from soluble secondary iron sulphates. This is supported by the rapid decrease in leachate pH, compared to the starting water, in the first sampling point. The rock analysis implied that no carbonates were present in the weathered shale, thus, the high calcium concentration could originate from desorption from clays due to the low pH (~ 4). It could also originate from the dissolution of gypsum, which also dissolves under low pH conditions (Rahimi et al., 2022). Gypsum was detected in the XRD analyses and likely formed in the earlier weathering processes.

A decrease in sulphate and calcium concentrations was observed after ~5-6 months for all the samples in Experiment 1. The decrease was more pronounced for seawater than freshwater samples. This could result from precipitation of gypsum [$CaSO4 \cdot 2H_2O$]. Calculations of the saturation index (SI) for 1_SO (unweathered shale treated with seawater under oxic conditions), using the measured concentrations and the equilibrium constant of gypsum $K = 10^{-4.58}$ (Bouchelaghem, 2010), gave SI = 1.4 for 1_SO_5m (before the drop - 5 months) and SI=1.1 for 1_SO_7m (after the drop -7 months). The calculations show that gypsum was oversaturated (SI>0) in the system, and that gypsum could have precipitated. However, concentrations were used instead of activity for the calculations, which overestimates ions

available for reactions, thus the saturation state. When the main cations and anions for the solutions are implemented in a PHREEQC script (Code A 1 and Code A 2 in Appendix), where activity and speciation are taking into account, the saturation index of gypsum was calculated to be SI = -0.78 for 1_SO_5m and SI = -0.52 for 1_SO_7m, indicating that the system is undersaturated in gypsum (SI<0).

Another explanation for the observed drop in calcium and sulphate concentrations could be caused by inaccurate dilution of the water samples. The drop is more pronounced in seawater than in freshwater samples, and the uncertainties could come from the high background concentration of Ca and SO_4^{2-}, which made it necessary to dilute the seawater samples to 1:1000 for IC analysis.

Alkalinity

Higher alkalinity was measured in the samples stored under low-oxygen compared to oxic conditions in Experiment 1 (Figure 42). This could result from less pyrite oxidation in the low-oxygen compared to oxic samples, and less neutralization of produced acid was required giving higher alkalinity. However, no significant difference in the sulphate concentrations between the oxic and low-oxygen samples was observed, indicating no significant difference in pyrite oxidization between the samples.

Another explanation for the observed difference in alkalinity between low-oxygen and oxic samples could be increased dissolution of calcite due to higher partial pressure of CO_2 in the closed bottles. The excess source of CO_2 comes from the dissolution of calcite itself (Equation 9), or biological activity. Wærsted et al. (2023b) observed this in a comparable batch experiment, i.e., batch experiments with alum shale treated with freshwater stored under different oxygen conditions, where increased CO_2 pressure was measured in closed bottles. The difference in pH between the low-oxygen (pH ~7.5) and oxic samples (pH ~7.7) supports the hypothesis of higher CO_2 pressure in the closed bottles. The increased pressure of CO_2 could give a lower pH as the solubility of CO_2 depends on the partial pressure and produces carbonic acid (H_2CO_3) when it dissolves in water (VanLoon, 2011).

5.2.2 Leaching of trace elements

Higher concentrations of trace metals were observed in treatments of unweathered shale in seawater compared to freshwater in Experiments 1 and 2. This is most likely due to the high ionic strength in seawater compared to freshwater. Higher ionic strength can increase the solubility of phases as it results in a lower effective concentration (activity) and affects the equilibrium (Appelo and Postma, 2005). Additionally, more ions can outcompete already sorbed trace elements from available sorption sites, releasing more trace metals into solution. Complexation with ions, such as chlorine and carbonates, forming more stable aqueous complexes can also keep the metals in solution.

The higher release of trace metal concentrations in seawater, compared to freshwater treatments, was not observed for the weathered shale in Experiment 1. Higher concentrations of U, Mn, Ni, Zn, and Co were found in the leachate from weathered shale compared to unweathered shale. These metals could have been mobilized during previous weathering processes and subsequently sorbed onto precipitated iron(oxy)hydroxides or incorporated into secondary-formed iron sulphates within the weathered shale. Iron sulphates are soluble and immediately produce acidic water upon dissolution in water (Hammarstrom et al., 2005). The rapid increase in the concentrations of these metals and the rapid decrease in pH support the assumption that these metals originated from desorption due to the lower pH or from the secondary iron sulphates themselves - possibly a combination of both.

On the other hand, Mo and Sb were almost absent in leachate from the weathered shale, while it was present in the leachate from the unweathered shale. This suggests that Mo and Sb are more mobile than U, Mn, Ni, Zn, and Co and that the mobile phase of Mo and Sb were already washed out of the weathered shale due to previous weathering. Another explanation could be that the shales have different origins and different compositions. Alum shale from the same horizon can vary a lot in composition, even over short distances (Pabst et al., 2017). It could be that the weathered shale originally didn’t contain mobile species of these elements.

After the initial increase, no noteworthy changes during the sampling period were seen for the trace metals leaching from weathered shale. However, the concentrations were varying over the sampling period suggesting that the starting material of weathered shale was not sufficiently homogenized.

Some metals (Cd, Zn, Co, Ni) leached from unweathered shale decreased in concentration over time in fresh- and seawater treatments under anoxic conditions (Experiment 2). This implies that these elements are precipitated from the solution, potentially as sulphides. The decrease occurred earlier in freshwater than in seawater treatments. This can be due to the high ionic strength of seawater, giving lower effective concentrations (activity) for the solutes (Appelo and Postma, 2005). It is shown by Wang et al. (2014) that ionic strength can decrease the rate of sulphide precipitation, as FeS, under anoxic conditions. Inhibiting factors on rate of precipitation can result from complexation with, e.g., organic complexes (Wang et al., 2005) or inorganic complexes like chlorine.

Uranium

A decrease in uranium concentrations was also observed in the freshwater treatment of unweathered shale but did not appear in the seawater treatment. One explanation for the decrease is the reduction of water-soluble U(VI) to insoluble U(IV) (Schovsbo, 2002). It is possible that uranium would have precipitated with time also in the seawater treatments, as the reduction of U(VI) to U(IV) has slow kinetics and will first take place in the sulphate reduction zone.

Higher uranium concentrations were measured in low-oxygen compared to oxic samples in the leachate from unweathered shale in Experiment 1 (Figure 49). This difference could result from carbonate complexation (Hsi and Langmuir, 1985), as the alkalinity measured in the low-oxygen samples was higher than in the oxic samples. Carbonated uranium species (e.g., $UO_2(CO_3)_2^{2-}$) are less prone to sorb to surfaces, and hence uranium will stay in solution. Differences in the uranium leached from the weathered shale between low-oxygen and oxic samples were not observed. No carbonates (measured as alkalinity) were present in the leachate from weathered shale, supporting the hypothesis that carbonate complexation of uranium is the cause of higher uranium concentrations observed in the low-oxygen samples containing unweathered shale.

For the weathered shale, higher uranium concentrations were observed in freshwater compared to seawater treatments, opposite as what was observed for the unweathered shale. This can be due to the higher pH observed in seawater compared to freshwater samples, caused by the initial buffering capacity of seawater. Lower pH can affect the system by: i) More H^+ in solution can outcompete uranium from the available sorption sites so that more uranium stays in solution,

or ii) iron(oxy)hydroxides can dissolve if pH < ~4 giving less sorption sites for scavenging uranium from solution. The latter explanation is supported by the coinciding uranium and iron peaks in the freshwater treatments of weathered shale in Experiment 1 (Figure 49).

Environmental guidelines

The Norwegian Environment Agency have developed a classification system and threshold concentrations for some metals (As, Cd, Cr, Cu, Ni, Pb, and Zn) in natural waters. The classification system includes five classes (I, II, III, IV and V) ranging from Class I, which represents "background" concentrations to Class V which represents "very poor" conditions. The threshold values varies for seawater and freshwater, and can be seen in the Table A 11 and Table A 12 (Appendix). Threshold values of uranium are not included in the quality standards developed by the Norwegian Environment Agency; however, the World Health Organization (WHO) has established a threshold value of 30 µg/L of U, representing the maximum contamination level of uranium in drinking water (WHO, 2017).

Table 9 shows the metal concentrations in samples containing weathered shale. Cd, Cu, Ni, and Zn concentrations were classified as Class V, and U significantly exceeds the threshold value of 30 µg/L. Cr is also classified as Class V in some samples.

Table 9: Classification of metals for samples with weathered shale measured in Experiment 1 based on quality standards developed by Norwegian Environment Agency (2016) and the drinking water limit for uranium by (WHO, 2017). W: weathered shale, F: Freshwater, S: Seawater, O: Oxic, L: Low-oxygen.

	As	Cd	Cr	Cu	Ni	Pb	U	Zn
1_WFO_1d	1.3	31	26	833	1840	0.50	1750	1010
1_WFO_2w	<0.5	58	7.6	925	3260	<0.2	1550	1800
1_WFO_2m	<0.5	50	17	1500	2880	<0.2	2650	1570
1_WFO_4m	<0.5	65	<3	852	3340	<0.2	1450	1830
1_WFO_7m	<0.5	54	5.4	1110	2980	<0.2	1950	1640
1_WFO_11m	<0.5	54	<3	871	2810	<0.2	1390	1570
1_WSO_1d	<0.5	27	<3	423	1460	0.80	827	765
1_WSO_2w	<0.5	56	<3	435	3020	0.50	1040	1480
1_WSO_2m	0.70	59	<3	300	3160	<0.2	951	1490
1_WSO_4m	0.70	67	<3	154	3480	<0.2	511	1530
1_WSO_7m	0.80	60	<3	80	3040	<0.2	271	1250
1_WSO_11m	0.50	64	<3	184	3370	<0.2	756	1660
1_WFL_1d	5.3	45	61	1340	2790	0.40	2620	1530
1_WFL_2w	<0.5	51	15	979	3010	0.90	1680	1650
1_WFL_2m	<0.5	53	6	1030	2920	<0.2	1590	1590
1_WFL_4m	<0.5	55	<3	580	2980	<0.2	1170	1570
1_WFL_7m	<0.5	59	<3	969	3110	<0.2	1670	1730
1_WFL_11m	<0.5	66	18	1470	3460	<0.2	3030	2000
1_WSL_1d	1.8	47	39	1220	2770	2.5	2520	1460
1_WSL_2w	0.50	52	12	709	3110	1.0	1700	1550
1_WSL_2m	0.50	56	4	425	2960	0.3	1110	1370
1_WSL_4m	0.50	59	<3	145	2970	<0.2	386	1220
1_WSL_7m	<0.5	58	<3	102	3030	0.2	326	1260
1_WSL_11m	0.50	68	<3	231	3340	<0.2	917	1660
	Class I	Class II	Class III	Class IV	Class V	n.d	U<30 µg/L	U>30 µg/L

For unweathered shale in Experiment 1 (Table 10), Ni and Zn were classified as Class V, and U exceeded the threshold value of 30 µg/L in most of the samples. The concentration of Cd is classified as Class V in the seawater samples and Class IV in the freshwater samples.

Table 10: : Classification of metals for samples with unweathered shale measured in Experiment 1 based on quality standards developed by Norwegian Environment Agency (2016) and the drinking water limit for uranium by (WHO, 2017). F: Freshwater, S:Seawater, O: Oxic, L: Low-oxygen.

	As	Cd	Cr	Cu	Ni	Pb	U	Zn
1_FO_1d	<0.5	0.5	<3	<4	37	0.20	11	16
1_FO_2w	<0.5	2.6	<3	<4	142	<0.2	50	55
1_FO_2m	<0.5	4.3	<3	<4	161	<0.2	110	73
1_FO_4m	<0.5	5.2	<3	<4	196	<0.2	142	148
1_FO_7m	<0.5	6.0	<3	<4	238	<0.2	168	162
1_FO_11m	<0.5	8.5	<3	<4	252	<0.2	201	233
1_SO_1d	0.90	31	<3	<4	435	0.20	49	251
1_SO_2w	0.70	86	<3	5.4	1180	0.20	187	698
1_SO_2m	0.90	109	<3	<4	980	<0.2	319	489
1_SO_4m	1.2	127	<3	<4	920	<0.2	355	567
1_SO_7m	0.50	174	<3	<4	898	<0.2	336	741
1_SO_11m	1.3	180	<3	<4	905	<0.2	491	729
1_FL_1d	<0.5	0.80	<3	<4	47	<0.2	9	10
1_FL_2w	<0.5	2.6	<3	<4	123	<0.2	45	60
1_FL_2m	<0.5	4.8	<3	<4	218	<0.2	106	98
1_FL_4m	<0.5	6.7	<3	<4	310	<0.2	162	179
1_FL_7m	<0.5	8.5	<3	<4	408	<0.2	204	264
1_FL_11m	<0.5	12	<3	<4	457	<0.2	264	375
1_SL_1d	0.70	42	<3	<4	606	<0.2	69	480
1_SL_2w	0.60	81	<3	<4	1170	<0.2	196	700
1_SL_2m	0.50	147	<3	<4	1680	<0.2	342	1140
1_SL_4m	0.70	187	<3	<4	1830	<0.2	462	1510
1_SL_7m	0.60	183	<3	<4	1680	0.20	484	1520
1_SL_11m	0.90	249	<3	<4	1990	<0.2	642	1880
	Class I	Class II	Class III	Class IV	Class V	n.d	U<30 µg/L	U>30 µg/L

For Experiment 2, where only unweathered shale was used, the same observations as for Experiment 1 were seen, with two exceptions (Table 11): Unweathered shale treated with freshwater stored under anoxic conditions (2_FA) had concentrations of metals classified as "good" or under the detection limit (except for Cd classified as Class III) in the last measuring point (16 weeks). Also the trace metal concentrations in the seawater sample containing unweathered shale stored under anoxic conditions (2_SA) showed improving conditions over the sampling period. However, the trace metal concentrations in the last sampling point for 2_SA were still classified as class IV and V, and the concentration of uranium significantly exceeded the drinking water limit.

Table 11: Classification of metals for samples with unweathered shale measured in Experiment 2 based on quality standards developed by Norwegian Environment Agency (2016) and the drinking water limit for uranium by (WHO, 2017).
F: Freshwater, S: Seawater, O: Oxic, A: Anoxic.

	As	Cd	Cr	Cu	Ni	Pb	U	Zn
2_SO_1w	1.2	79	<3	<4	1160	<0.2	149	622
2_SO_1m	1.0	78	<3	<4	982	0.20	282	290
2_SO_2m	1.0	81	<3	<4	865	<0.2	324	271
2_SO_4m	<0.5	111	<3	<4	830	<0.2	329	476
2_FO_1w	<0.5	2.6	<3	<4	220	<0.2	38	84
2_FO_1m	<0.5	3.0	<3	<4	143	<0.2	81	47
2_FO_2m	<0.5	2.4	<3	<4	91	<0.2	107	35
2_FO_4m	<0.5	2.9	<3	<4	88	<0.2	121	40
2_SA_1w	1.2	62	<3	<4	1070	<0.2	148	513
2_SA_1m	1.0	43	<3	<4	1210	<0.2	242	563
2_SA_2m	0.90	2.1	<3	<4	1140	<0.2	329	486
2_SA_4m	<0.5	1.4	<3	<4	142	<0.2	367	52
2_FA_1w	<0.5	0.80	<3	<4	84	<0.2	19	28
2_FA_1m	<0.5	1.0	<3	<4	79	<0.2	63	<3
2_FA_2m	<0.5	1.2	<3	<4	6.2	<0.2	47	<3
2_FA_4m	<0.5	1.2	<3	<4	2.1	<0.2	20	3.8
	Class I	Class II	Class III	Class IV	Class V	n.d	U<30 µg/L	U>30 µg/L

5.2.3 Oxic, low-oxygen and anoxic: Evaluation of the method

As illustrated in the chapter "Experiment 1: Method Evaluation", oxygen diffused from the water-filled beaker as the glove box was flushed with nitrogen. Thus, the dissolved oxygen concentrations measured in the glove box (Figure 36 and Figure 37), were not necessarily representative of what was present in the samples. The actual oxygen concentrations in the low-oxygen samples may have been closer to the oxygen concentrations in the oxic samples in Experiment 1. This is supported by the observation of no significant difference in the release of calcium and sulphate between the low-oxygen and oxic samples. The similar release rates indicate similar sulphide oxidation rates.

In Experiment 2 where glass bottles were used, oxygen concentrations were substantially lower than the oxic and low-oxygen treatments (Figure 36 and Figure 37), and measured E_h was also lower. Additionally, there are other indications that anoxic conditions developed: Lower sulphate concentrations were measured in the anoxic samples compared to the equivalent oxic samples. No further increase in the concentrations of sulphate and calcium was observed after one month (28 days) in the anoxic samples. This suggests that pyrite oxidation occurred in the first part of the experiment, contributing to depleting the oxygen and the development of anoxic conditions, and the pyrite oxidation ceased. Calcium was likely released as calcite dissolved when buffering the produced acid, and calcium concentrations in the leachate stabilized when acid was no longer produced.

Dissolved iron was present in the anoxic samples, but not in the oxic and low-oxygen samples in Experiments 1 and 2 (Figure 49 and Figure 50), further supporting that the anoxic samples were truly anoxic. The anoxic freshwater treatment (2_FA) seemed to follow the same trend as the concept of change in porewater chemistry caused by the redox-sequence (Figure 59): Microorganisms first utilize oxidants with the highest redox potential during oxidation, as it yields more energy in their metabolism (Appelo and Postma, 2005). Due to its large redox potential, oxygen is reduced first, followed by nitrate (NO_3^-). Further, solid forms of Mn(IV) and Fe(III) oxides are utilized, releasing Mn^{2+} and Fe^{2+} into solution. In the presence of sulphate and under reducing conditions, sulphate is reduced to H_2S, which can react with Fe^{2+} to form pyrite (precipitated from solution), causing a decrease in the concentration of Fe^{2+}. The absence of aqueous iron in the oxic and low-oxygen treatments is most likely caused by oxidation of released ferrous (from iron sulphide oxidation) to ferric iron (Equation 3) followed by hydrolysis and precipitation of iron(oxy)hydroxide (Equation 4). This is supported by the

observation of more antimony (Sb) in anoxic samples than in oxic samples (Figure 50), as Sb is prone to be sorbed to iron(oxy)hydroxides (Zhang et al., 2022). Sb can be removed from the solution by sorption to precipitated iron(oxy)hydroxides in the oxic samples. While for the anoxic samples, less iron(oxy)hydroxide was precipitated. This could explain the higher concentrations of Sb measured in the anoxic samples and support the assumption of anoxic conditions in Experiment 2.

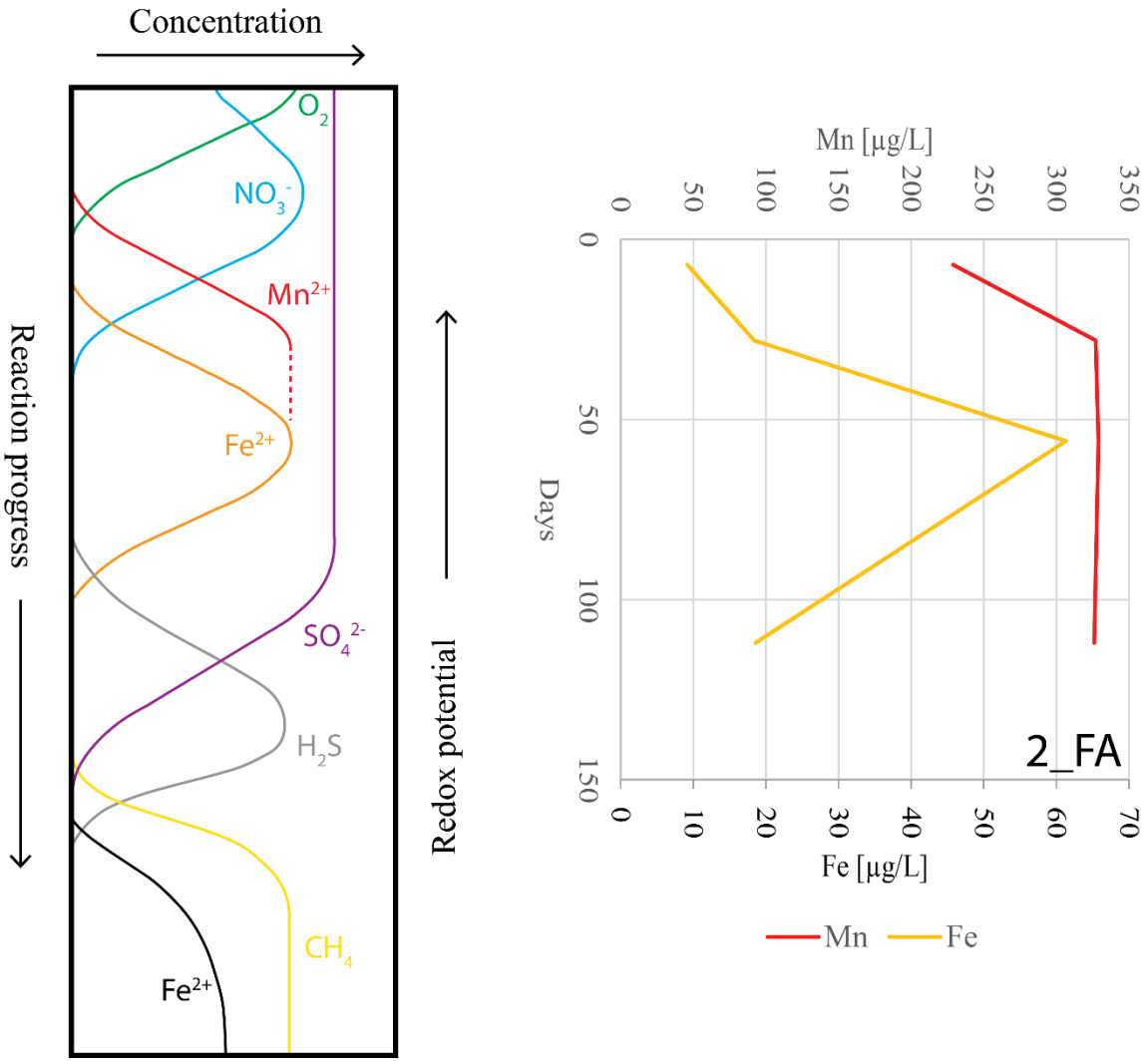

Figure 59: To the left: Concept of change in porewater chemistry caused by the sequence of redox reactions (Modified from Appelo and Postma (2005)). To the right: Leaching of Mn and Fe over time in the batch with unweathered shale treated with freshwater stored under anoxic conditions in Experiment 2 (2_FA).

Redox potential (E_h)

Although the trace metal concentrations indicated development of anoxic or even reducing conditions in Experiment 2, the E_h measurements did not show the same trend (Negative E_h values expected for reducing conditions). Obtaining accurate and reasonable Eh measurements in most natural waters is known to be challenging (Appelo and Postma, 2005), and the Eh measurements could be uncertain. This could be attributed to the lack of equilibrium between the redox couples in the solution or potential analytical issues with the electrode.

The measured E_h and pH values in the experiments plotted in a diagram showing typical E_h-pH relations in natural waters and in a stability diagram for the FeS_2-H_2O system are shown in Figure 60. The weathered samples had lower pH and higher E_h than the unweathered samples and plotted in the areas of "acid mine water". The unweathered shale treated with sea –and freshwater stored under oxic and low-oxygen conditions plotted in the areas of "normal ocean water" and "groundwater". Some of the anoxic samples treated with seawater plotted within the field of "interstitial marine sediments".

The speciation shown in the diagrams is just an indicator of the speciation of the compounds as the diagram was plotted for dissolved species at a concentration of 10^{-5} M. In the experiments the concentrations of iron were, for most of the samples, in the range from ~$7 \cdot 10^{-8}$ M to ~$9 \cdot 10^{-5}$ M and for sulphur it mostly ranged from ~$1 \cdot 10^{-3}$ M to ~$4 \cdot 10^{-2}$ M. However, the diagram predicts that predominant species in the samples with unweathered shale were $Fe(OH)_3$ and $SO4^{2-}$. For the weathered shale, the predominant species of iron in aqueous phase were $Fe(OH)^{2+}$ or Fe^{2+}.

The freshwater treatments of weathered shale in Experiment 1 were closer to the stability field of Fe^{3+} than the seawater treatments according to Figure 60. This is supported by the observation of a reddish colour in the bottles that contained weathered shale mixed with fresh water, which was not observed for the equivalent seawater treatments (Figure 44). The red colour may indicate that, at a certain point in time during the experimental period, the fresh water samples had E_h-pH conditions where Fe^{3+} was stable and in solution, precipitating as poorly crystalline iron(oxy)hydroxides (Equation 4). These iron(oxy)hydroxides probably sorbed to the surfaces of the bottles, resulting in the observed red colour. This condition was not long-lasting, as the water did not have a reddish color when it

was pipetted out of the bottles. This probably didn't happen for the seawater treatments as the natural buffer capacity of seawater resulted in a slightly higher pH.

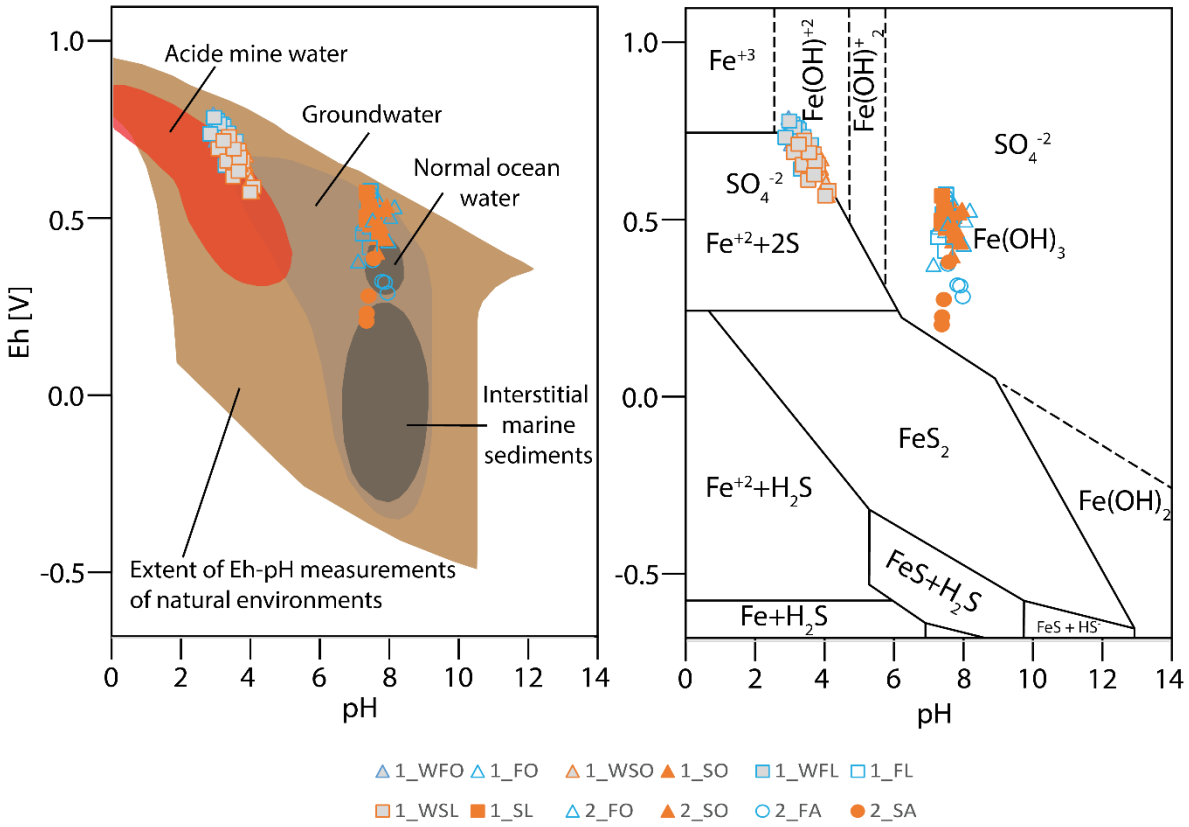

Figure 60: pH and Eh measured in Experiments 1 and 2 plotted in stability diagrams. The diagram to the left shows typical E_h-pH relations in natural waters modified from Bjørlykke (2015). The diagram to the right shows a stability diagram for FeS_2-H_2O system for 10^{-5}M dissolved species at 25 °C, which is modified from Moslemi and Gharabaghi (2017). (1: Experiment 1, 2: Experiment 2, W: Weathered shale, F: Freshwater, S: Seawater, O: Oxic, L: Low-oxygen, A: Anoxic).

5.3 Modelling

Trace metals

As observed in the experiments with unweathered shale, the calibration and validation model gave a higher release of trace metals in seawater than in freshwater under oxic conditions (Figure 55). In the Drammensfjord model, anoxic conditions developed as oxygen was depleted by oxidation of pyrite and TOC (in the sediments). As anoxic conditions developed in the Drammensfjord model, uraninite (UO_2) and pyrite (with impurities of Cu, Zn, Ba, and Mn) were relatively stable, and no leaching of uranium, copper or zinc were simulated. Under anoxic experimental conditions (Experiment 2), no copper was measured in the leachate, and the concentration of zink decreased with time in both freshwater and seawater treatments. The uranium concentration decreased after one month in the freshwater treatment (2_FA) and is expected to decrease in the seawater treatments at a later point in time. These observations support the model's prediction of immobilisation of U, Cu, and Zn under reducing conditions.

Barium reached a stable concentration of ~10 µg/L in the Drammensfjord model, which is within the range of Ba measured in the seawater blanks in Experiment 1 and 2 (~ 6 - 29 µg/L) (Table A 9 and Table A 10 in Appendix). Mn increased in concentration under anoxic conditions in the Drammensfjord model. This was also observed in Experiment 2, where higher concentrations of Mn were measured under anoxic compared to oxic conditions in seawater treatments. Mn is expected to precipitate as MnO_2 under oxic conditions (Bjørlykke, 1974).

The model failed to predict the correct leaching concentrations of Zn, Mn, Ba and U (Figure 54 and Figure 55). This may result from the uncertainty in which mineral phase the different trace metals are associated with. Cu, Zn, Mn and Ba were implemented as impurities in pyrite. These trace metals could originally be present in other mineral phases with faster dissolution kinetics than pyrite, which could explain the underestimation in the release of Zn, Mn and Ba in the model compared to experimental results. The experimental measurements for copper are under the detection limit (<4 µg/L); the same is simulated in the sea -and freshwater model under oxic conditions. Bjørlykke (1974) states that Cu is correlated with S with a correlation coefficient of 0.67, and the leaching of copper in the model could be realistic.

The leaching of uranium was fitted to the results during the calibration. However, a large deviation (overestimation) occurred when the model was validated with seawater as the initial

solution (Figure 54). Uranium was implemented in the model as uraninite. However, uranium is most likely associated with several mineral phases in the alum shale (Bjørlykke 1974). SEM mapping (Figure 20) supports the assumption that uranium is associated with several phases, where uranium appears in all mineral phases except quartz. In addition, small amounts of zircon (Figure 19.7) were observed which is known to be associated with uranium. Implementing all the uranium as uraninite will, therefore, not give a reasonable estimation of leaching of uranium.

Extrapolated model: difference between sea- and freshwater

According to the extrapolated calibration and validation model, seawater turned acidic at a somewhat later point in time compared to freshwater (Figure 56). However, when the drop in pH occurred, it turned more acidic in the model with seawater compared to freshwater. The later drop in pH simulated in the seawater model was most likely caused by the natural buffer capacity of seawater. The lower pH simulated for seawater could be caused by the higher concentration of ions in seawater compared to freshwater. More cations are available in the seawater solution which can outcompete H^+ for the sorption sites. This makes fewer sorption sites available for H^+, thus, H^+ stays in the solution giving lower pH.

Furthermore, the pyrite was completely dissolving in the model with seawater, whereas this did not happen in the fresh water model (Figure 56). This is probably caused by the lower pH simulated in seawater that increases the solubility of goethite. Fe^{3+} would be available in solution and can act as an oxidation agent on pyrite. Oxidation by Fe^{3+} is faster than oxidation by oxygen, and the oxidation of pyrite is accelerated.

Drammensfjord

The transport model with a shale-to-water ratio of 1:10 could represent the sediment/water interface of a possible alum shale sea-disposal site. The penetration depth of oxygen in costal sediments usually ranges from 1 to 5.5 mm (Revsbech et al., 1980). In the experiments, the crushed debris of alum shale made up a layer of ~6 mm, which is consistent with the oxygen penetration depth suggested by Revsbech et al. (1980). Sediments underneath this oxygen penetration depth, will not be supplied by aqueous oxygen, which is why constant anoxic conditions can be assumed for these deeper sediments (assuming absence of disturbance, e.g., bioturbation). Therefore, it is assumed that the model and the batch experiments simulate the sediments that are potentially affected by an interaction with seawater.

According to the model, ARD will not be produced, and metals will be immobilized under the simulated conditions in the Drammensfjord model due to limited oxygen availability. In the model, the oxygen-consuming processes are: i) oxidation of pyrite and ii) oxidation of organic matter in the shale (TOC). However, in an actual situation, the oxygen would most likely be depleted in the water column above the sediments by degradation of organic matter caused by primary production of, e.g., algae. Thus, the conditions on the seafloor would probably have less oxygen available than what was simulated in this model. Prolonged anoxic conditions will immobilize metals, as they will be precipitated or sorbed to organic matter that sinks to the bottom.

5.4 Sea disposal of alum shale

Drammensfjord as a casestudy

The model, simulating the conditions in the Drammensfjord predicted no production of ARD and immobilizing of metals. However, the sill by Svelvik in the Drammensfjord has been dredged several times to make the water depth above the sill deeper for cargo shipping (Bechmann et al., 2017). Consequently, there are indications that the bottom water of the Drammensfjord has been more oxygenated in recent times. This can negatively affect storage of alum shale.

With time, the deposited masses would be covered by sediments supplied from the river Drammen (and other smaller rivers), which can work as an oxygen barrier to the deposited masses. Alve (1991) estimated the sedimentation rate right in front of the sill to be 1.5 mm/yr. In addition, sediments often contain a certain percentage of carbonates that could buffer potentially produced acid, in addition to organic material which have the potential to sorb potentially leached metals.

Sea disposal of alum shale in Norwegian fjords

The environmental conditions based on quality standards for trace metal concentrations developed by Norwegian Environment Agency (2016) showed that the conditions improved with time under anoxic experimental conditions (Experiment 2) for fresh -and seawater treatments of unweathered shale (Table 11). The conditions were mainly in the Class II and III for trace metal concentrations in the last measuring point for the fresh water sample, while the

seawater samples still had concentrations of metals classified as “very poor”. However, the concentrations of metals would have been way less in a fjord system than what was demonstrated in the batch experiments. This is due to a higher water-to-reactive shale ratio; therefore, dilution and diffusion of metals would have occurred, and the concentration of metals would have been lower than the concentrations measured in the experiments. This also applies to weathered shale, where the alkalinity of seawater was not sufficient to neutralize acid produced from weathered shale when the shale-to-water ratio was 1:10. Further investigations are required to understand how weathered alum shale would behave if disposed of on the seafloor under anoxic conditions. This has not been investigated in experiments or PHREEQC modelling in this work.

From a geochemical perspective, sea disposal of unweathered alum shale looks promising in terms of metal immobilization and preventing ARD production, according to Experiment 2 and the modelling. Leaching of metals from alum shale is greater in seawater than in freshwater, as illustrated in the experiments (Figure 49 and Figure 50). However, the effect of oxygen seems more critical in immobilizing metals. In anoxic seawater treatments, Ni, Zn, Co and Cd concentrations are either similar or lower than those measured in the oxic freshwater treatment of the same unweathered shale.

If the shale is disposed of in a freshwater lake, anoxic conditions may develop over time in the porewater. Nevertheless, the potential oxygen supply in a freshwater lake is likely greater than in a seawater fjord system. This is due to the seasonal mixing in freshwater lakes during autumn and spring when the surface water reaches a temperature of 4 °C, its densest point (VanLoon, 2011). Consequently, this dense water sinks and supplies the bottom water with fresh, oxygenated surface water. The density of water is more influenced by salinity rather than temperature (Sylvette Awoh et al., 2020). In a fjord system, where fresh water is supplied at the top via a river, the high salinity in the bottom water prevents mixing caused by seasonal temperature changes in the surface water. As a result, the oxygen supply is limited compared to a freshwater lake system. Therefore, sea disposal of unweathered alum shale in a fjord can serve as a long-term storage facility with restricted access to oxygen.

6. Conclusion

This study aimed to assess the potential of sea disposal of alum shale from a geochemical perspective. Batch experiments were conducted using both weathered and unweathered alum shale treated with fresh- and seawater, under varying oxygen conditions. The main objectives were to: i) assess if the alkalinity of seawater had the potential to neutralize acid produced from weathered shale, ii) investigate if the higher ionic strength of seawater enhances leaching of trace metals from the alum shale, iii) consider how the availability of oxygen affects mobilization of trace metals in sea- and freshwater, iv) evaluate the long-term implications of sea disposal of alum shale through geochemical modelling using PHREEQC.

Plastic bottles containing alum shale submerged in water did not prevent a rapid diffusion of oxygen, and the oxygen supply exceeded consumption within these bottles. This suggests that using plastic bottles submerged in water is unsuitable for investigating low-oxygen/anoxic conditions. Evidence of the development of anoxic conditions was observed in sealed glass bottles submerged in water. Under these conditions, certain metals (Ni, Zn, Co, and Cd) precipitated in both fresh- and seawater treatments, while the concentration of certain trace metals (U and Fe) decreased only in freshwater treatments. The glass bottle experiment lasted only 16 weeks, and it would be of interest to observe the changes in trace metal concentrations over an extended period.

The batch experiments revealed that the alkalinity of seawater was not sufficient to neutralize acid produced from weathered shale when the shale-to-water ratio was 1:10. The characterization of the weathered shale also implied that the debris used in the experiment did not contain sulphides due to previous weathering. Further investigations are required to understand how weathered alum shale (with remaining pyrite) would react under anoxic conditions.

The batch experiments and modelling implied that seawater caused more leaching of trace metals compared to freshwater treatments when it was mixed with unweathered alum shale. This is probably a result of the higher ionic strength and complexation in seawater affecting the solubility and mobility of trace metals. Despite this, the results from the modelling and the anoxic batch experiments indicated that the effect of limiting the access to oxygen seems to be a more important factor in immobilizing metals rather than the initial water composition.

Therefore, sea disposal of unweathered alum shale in a fjord with restricted access to oxygen has the potential to prevent the production of ARD and immobilize trace metals, and thus work as a long-term storage facility.

Bibliography

Alve, E., (1995). Benthic foraminiferal distribution and recolonization of formerly anoxic environments in Drammensfjord, southern Norway, *Marine micropaleontology*, 25, 169–186. https://doi.org/10.1016/0377-8398(95)00007-N

Andersson, A., Dahlman, B., Gee, D.G., Snäll, S., (1985). *The Scandinavian Alum Shales*. Lund - Sweden: Sveriges Geologiska Undersökning.

Appelo, C.A.J., Postma, D., (2005). *Geochemistry, groundwater and pollution*. 2nd ed. Leiden - Netherlands: Balkema.

Bastiansen, R., Moum, J., Rosenqvist, I.T., (1957). *Bidrag til belysning av visse bygningstekniske problemer ved Oslo-områdets alunskifere*. Oslo - Norway: NGI.

Bechmann, P., Dolven, J., Salomonsen, G.R., Haugestøl, G.L., (2017). *Miljøovervåking av Indre Drammensfjord Sluttrapport for overvåkingen i 2014-2015 og oppsummering av prosjektet «Ren Drammensfjord 2015» (No. 5142611– 02)*. Sandvika - Norway: Norconsult.

Berner, R.A., De Leeuw, J.W., Spiro, B., Murchison, D.G., Eglinton, G., (1985). Sulphate Reduction, Organic Matter Decomposition and Pyrite Formation [and Discussion]. Philosophical transactions of the Royal Society of London, *Series A: Mathematical and physical sciences*, 315, 25–38. https://doi.org/10.1098/rsta.1985.0027

Bierens de Haan, S., (1991). A review of the rate of pyrite oxidation in aqueous systems at low temperature, *Earth-science reviews*, 31, 1–10. https://doi.org/10.1016/0012-8252(91)90039-I

Bjørlykke, K., (2015). Sedimentary Geochemistry: How Sediments are Produced, in: *Petroleum Geoscience: From Sedimentary Environments to Rock Physics*. Berlin/Heidelberg - Germany: Springer, 91–117. https://doi.org/10.1007/978-3-642-34132-8_3

Bjørlykke, K., (2010). Unconventional Hydrocarbons: Oil Shales, Heavy Oil, Tar Sands, Shale Gas and Gas Hydrates, in: *Petroleum Geoscience*. Berlin/Heidelberg - Germany: Springer, 459–465. https://doi.org/10.1007/978-3-642-02332-3_21

Bjørlykke, K., (1974). *Depositional history and geochemical composition of lower palaeozoic epicontinental sediments from the Oslo region*. Trondheim - Norway: Universitetsforlaget.

Borba, B.D., Rohrer, J., (2004). Determination of Inorganic Anions in Environmental Waters Using a Hydroxide-Selective Column, *LCGC North America*, 22, 138–148.

Børresen, M., Stenger, S.R., Slinde, G.A., Wærsted, F.M., Mortensen, P.-A., Baardvik, G., (2022). *E6 Taraldrud alunskifer tiltaksplan* (No. 20210283- 02- R), *Koordinert tiltaksplan for forurenset grunn på eiendommene gnr./bnr. 105/4 og 157/2 på Taraldrud*. Oslo - Norway: NGI.

Bouchelaghem, F., (2010). A numerical and analytical study on calcite dissolution and gypsum precipitation, *Applied mathematical modelling*, 34, 467–480. https://doi.org/10.1016/j.apm.2009.06.004

Bragg, W.H., Bragg, W.L., (1913). The reflection of X-rays by crystals. *Proceedings of the Royal Society of London.* Series, A 88, 428–438. https://doi.org/10.1098/rspa.1913.0040

Doebelin, N., Kleeberg, R., (2015). Profex: a graphical user interface for the Rietveld refinement program BGMN, *Journal of applied crystallography*, 48, 1573–1580. https://doi.org/10.1107/S1600576715014685

Egiebor, N.O., Oni, B., (2007). Acid rock drainage formation and treatment: a review. *Asia-Pacific Journal of Chemical Engineering*, 2, 47–62. https://doi.org/10.1002/apj.57
Engebretsen, A.M., Skrutvold, J., Roseth, R., (2020). *Rv.4 Gran - Jaren. Etterundersøkelser av vannkjemi i grunnvann og resipienter 2017 - 2019* (No. 6/50/2020). Norway: NIBIO.
Falk, H., Lavergren, U., Bergback, B., (2006). Metal mobility in alum shale from A-land, Sweden, *Journal of geochemical exploration*, 90, 157–165. https://doi.org/10.1016/j.gexplo.2005.10.001
Field, R.W., Steck, D.J., Smith, B.J., Brus, C.P., Fisher, E.L., Neuberger, J.S., Platz, C.E., Robinson, R.A., Woolson, R.F., Lynch, C.F., (2000). Residential Radon Gas Exposure and Lung Cancer: The Iowa Radon Lung Cancer Study, *American Journal of Epidemiology*, 151, 1091–1102. https://doi.org/10.1093/oxfordjournals.aje.a010153
Fjermestad, H., Gundersen, E., Hagelia, P., Moen, A.B., Torp, M., (2018). *Rv. 4 på Gran, nyttiggjering av svartskifer* (No. 333). Norway: Statens vegvesen.
Hammarstrom, J.M., Seal, R.R., Meier, A.L., Kornfeld, J.M., (2005). Secondary sulfate minerals associated with acid drainage in the eastern US: recycling of metals and acidity in surficial environments, *Chemical Geology*, 215, 407–431. https://doi.org/10.1016/j.chemgeo.2004.06.053
Hsi, C.D., Langmuir, D., (1985). Adsorption of uranyl onto ferric oxyhydroxides: Application of the surface complexation site-binding model, *Geochimica et cosmochimica acta*, 49, 1931–1941. https://doi.org/10.1016/0016-7037(85)90088-2
Huminicki, D.M., Rimstidt, J.D., (2009). Iron oxyhydroxide coating of pyrite for acid mine drainage control, *Applied geochemistry*, 24, 1626–1634. https://doi.org/10.1016/j.apgeochem.2009.04.032
Jeng, A.S., (1991). Weathering of Some Norwegian Alum Shales, *Acta Agriculturae Scandinavica*, 41, 13–35. https://doi.org/10.1080/00015129109438580
Khaidar Ali, R., Butar-butar, L., Qadaryati, N., Santi, N., (2020). Acid neutralizing capacity minerals in Barani Pit PT Agincourt Resources Martabe, North Sumatera: alternative agent on neutralizing acid mine drainage, *E3S web of conferences*, 202, 2008. https://doi.org/10.1051/e3sconf/202020202008
Klein, C., Dana, J.D., Dutrow, B., (2008). *Manual of Mineral Science*, 23rd ed. Hoboken, N.J: Wiley.
Kriegel, M.J., Rudolph, M., Kilmametov, A., Straumal, B.B., Ivanisenko, J., Fabrichnaya, O., Hahn, H., Rafaja, D., (2020). Formation and Thermal Stability of omega-Ti(Fe) in alpha-Phase-Based Ti(Fe) Alloys, *Metals*, 10, 402. https://doi.org/10.3390/met10030402
Lahrouch, F., Baptiste, B., Dardenne, K., Rothe, J., Elkaim, E., Descostes, M., Gerard, M., (2022). Uranium speciation control by uranyl sulfate and phosphate in tailings subject to a Sahelian climate, Cominak, Niger, *Chemosphere*, 287, 132139–132139. https://doi.org/10.1016/j.chemosphere.2021.132139
Løken, T., (2007). Alunskifer/svartskifer – den forurensende bergarten, *Vann*, 42, 211–218.
Lovdata, (2004). *Forurensningsforskriften*, FOR-2004-06-01-931.
Matusiewicz, H., (2017). Sample Preparation for Inorganic Trace Element Analysis, *Physical Sciences Reviews*, 2, 20178001. https://doi.org/10.1515/psr-2017-8001
Mindat.org, (2023). *Search Minerals By Chemistry*. Available from: https://www.mindat.org/chemsearch.php (accessed 5.30.23).
Morad, S., (1978). Feldspars in sedimentary rocks, in *Sedimentology*. Berlin/Heidelberg - Germany: Springer, 452–457. https://doi.org/10.1007/3-540-31079-7_84

Moslemi, H., Gharabaghi, M., (2017). A review on electrochemical behavior of pyrite in the froth flotation process, *Journal of industrial and engineering chemistry*, 47, 1–18. https://doi.org/10.1016/j.jiec.2016.12.012

Nakrem, H.A., Worsley, D., (2013). Jordas eldste oldtid - Kambrium, Ordovicium og Silur - Et yrende liv i havet; 542-416 millioner år, in: *Landet Blir Til*. Trondheim- Norway: Norges geologiske forening.

Nilsson, P.-N., (1970). *Kvarntorpshögen*. Available from: https://commons.wikimedia.org/wiki/File:Kvarntorpsh%C3%B6gen_-_KMB_-_16001000011687.jpg (accessed 11.7.22).

NOAH AS, (2022). *Farlig avfall / Sanering*. Available from: https://www.noah.no/farlig-avfall/sanering/ (accessed 11.7.22).

NOAH AS, (2014). *Noah Langøya_0014*. Available from: https://www.noah.no/langoya/dcim100mediadji_0014-jpg/ (accessed 11.7.22).

Norwegian Environment Agency, (2016). *Quality standards for water, sediment and biota – revised 2020.10.30* (No. M–608).

Owen, A.W., Bruton, D.L., Bockelie, J.F., Bockelie, T.G., (1990). *The Ordovician successions of the Oslo Region*. Trondheim - Norway: Geological survey of Norway (NGU).

Pabst, T., Sørmo, E., Endre, E., (2017). Geochemical characterisation of Norwegian Cambro-Ordovician black mudrocks for building and construction use, *Bulletin of Engineering Geology and the Environment*, 76, 1577–1592. https://doi.org/10.1007/s10064-016-0941-z

Palandri, J.L., Kharaka, Y.K., (2004). *A Compilation of Rate Parameters of Water-Mineral Interaction Kinetics for Application to Geochemical Modeling* (No. 04–1068). U.S Geological Survey.

Parkhurst, D.L., Appelo, C.A.J., (2013). *Description of input and examples for PHREEQC version 3--a computer program for speciation, batch-reaction, one-dimensional transport, and inverse geochemical calculations.* Reston, Virginia: U.S. Geological Survey.

Parviainen, A., Loukola-Ruskeeniemi, K., (2019). Environmental impact of mineralised black shales, *Earth-Science Reviews*, 192, 65–90. https://doi.org/10.1016/j.earscirev.2019.01.017

Rahimi, M.R., Mohammadi, S.D., Taleb Beydokhti, A., (2022). Laboratory simulation of gypsum rock dissolution at different pressures, water-flow velocities and pH ranges, *Quarterly Journal of Engineering Geology and Hydrogeology*, 56. https://doi.org/10.1144/qjegh2021-120

Revsbech, N.P., Jørgensen, B.B., Blackburn, T.H., (1980). Oxygen in the Sea Bottom Measured with a Microelectrode, *Science*, 207, 1355–1356. https://doi.org/10.1126/science.207.4437.1355

Schovsbo, N.H., (2002). Uranium enrichment shorewards in black shales: A case study from the Scandinavian Alum Shale, *GFF*, 124, 107–115. https://doi.org/10.1080/11035890201242107

Schumacher, B., (2002). Methods for the determination of total organic carbon (TOC) in soils and sediments: ecological risk assessment support center, *Method NCEA-C-1282*. United States Environmental Protection Agency, 1–23.

Sjöberg, V., Karlsson, S., (2015). Impact of organic carbon on the leachability of vanadium, manganese, iron and molybdenum from shale residues, *Minerals engineering*, 75, 100–109. https://doi.org/10.1016/j.mineng.2014.10.018

Skei, J., Sørby, H., (2019). *Mining industry and tailings disposal* (No. 1335). Norwegian Environment Agency.

Sørmo, E., Breedveld, G., Pabst, T., (2015). *Deponering av syredannende bergarter. Grunnlag for veileder* (No. M–385). Oslo - Norway: NGI.
Sørmo, E., Harstad, A.O., Baardvik, G., (2017). *Geokjemisk kartlegging og volumestimat av svartskifer* (No. 20160766- 01- R). Oslo - Norway: NGI.
Sylvette Awoh, A., Mbonimpa, M., Bussière, B., (2020). Water covers, in: *Hard Rock Mine Reclamation: From Prediction to Management of Acid Mine Drainage.* CRC Press.
Thomas, D., Rohrer, J., (2013). *Determination of Inorganic Cations and Ammonium in Environmental Waters by Ion Chromatography Using the Dionex IonPac CS16 Column: Application Note 141*, Sunnyvale, California - USA. Thermo Fisher Scientific.
Thomas, R., (2013). *Practical guide to ICP-MS: a tutorial for beginners*, 3rd ed. Boca Raton, Florida - USA: Taylor & Francis.
Totland, C., Baardvik, G., Wærsted, F.M., (2023). *WP1 - Naturally mixed fractions of black shale and rhomb porphyry* (No. 20200436- 02- R). Oslo - Norway: NGI.
VanLoon, G.W., (2011). *Environmental chemistry: a global perspective*, 3rd ed. Oxford - England: Oxford University Press.
Wærsted, F.M., Berge Hansen, C., Fjermestad, H., Hagelia, P., Baardvik, G., (2023a). *WP1 - Container experiments - Yearly report 2021* (No. 20200436- 09- R). Oslo - Norway: NGI.
Wærsted, F.M., Breedveld, G., Erlend, S., (2022). *Håndtering av potensielt syredannende svartskifer - Miljødirektoratet* (No. M–2105). Oslo - Norway: NGI.
Wærsted, F.M., Reinoso-Maset, E., Salbu, B., Skipperud, L., (2023b). Limited access to oxygen reduces the release of harmful trace elements from submerged alum shale debris, *Science of The Total Environment*, 880, 163035. https://doi.org/10.1016/j.scitotenv.2023.163035
Wakao, N., Mishina, M., Sakurai, Y., Shiota, H., (1982). Bacterial Pyrite Oxidation I, *The Journal of General and Applied Microbiology*, 28, 331–343. https://doi.org/10.2323/jgam.28.331
Wang, L.K., Vaccari, D.A., Li, Y., Shammas, N.K., (2005). Chemical Precipitation, in: Wang, L.K., Hung, Y.-T., Shammas, N.K. (Eds.), *Physicochemical Treatment Processes*, *Handbook of Environmental Engineering*., Totowa, New Jersey - USA: Humana Press, NJ, 141–197. https://doi.org/10.1385/1-59259-820-x:141
Wang, Q. 'Luke,' Zhang, Z., Kan, A., Tomson, M., (2014). Kinetics and Inhibition of Ferrous Sulfide Nucleation and Precipitation, *SPE International Oilfield Scale Conference and Exhibition*, Aberdeen - Scotland: OnePetro. https://doi.org/10.2118/SPE-169748-MS
WHO, (2017). *Guidelines for drinking-water quality, 4th ed*. Geneva - Switzerland: World Health Organization.
Williamson, M.A., Rimstidt, Jd., (1994). The kinetics and electrochemical rate-determining step of aqueous pyrite oxidation, *Geochimica et cosmochimica acta*, 58, 5443–5454. https://doi.org/10.1016/0016-7037(94)90241-0
Zhang, Y., O'Loughlin, E.J., Kwon, M.J., (2022). Antimony redox processes in the environment: A critical review of associated oxidants and reductants, *Journal of Hazardous Materials*, 431, 128607. https://doi.org/10.1016/j.jhazmat.2022.128607
Zumdahl, S.S., DeCoste, D.J., (2017). *Chemical principles*, 8th ed., Boston, Mass - USA: Cengage Learning.
Åhlgren, K., Sjöberg, V., Allard, B., Bäckström, M., (2021). Groundwater chemistry affected by trace elements (As, Mo, Ni, U and V) from a burning alum shale waste deposit, Kvarntorp, Sweden, *Environ Sci Pollut Res*, 28, 30219–30241. https://doi.org/10.1007/s11356-021-12784-2

Appendix

Table A 1: Input parameters and calculations of input parameters for the modelling in PHREEQC.

Input	Value	unit	Based on source
Feldspar	13	wt%	XRD
Pyrite	4.3	wt%	XRD and Wærsted et al. (2023a)
Calcite	1.2	wt%	XRD and Wærsted et al. (2023a)
Cu	93	ppm	Wærsted et al. (2023a)
Zn	379	ppm	Wærsted et al. (2023a)
Ba	778	ppm	Whole rock analysis
MnO	0.028	%	Whole rock analysis
U	70	ppm	Whole rock analysis
% Clay	49	%	XRD
% Org. C	6.00	%	Total carbon (TOC and TIC)
Mass_shale	10	g	
V_porevolume	110	cm3	
density_black shale	2.7	cm3/g	
Volume_shale	3.7	cm3	
V_tot	114	cm3	
CO2_parital_pressure	400	ppm	
O2_partial_pressure	21	%	
All calculations are done for 100 g unweatherd alum shale			Based on source
Calculations	formula	Model input value	
ε (porosity)	V_porevolume/Vtot	0.97	
CEC [meq/kg]	7*(%clay) + 35 *(%C)	553	Appelo and Postma, 2005
CEC [meq/L]	CEC[meq/kgw] * ρb/ε	1543	
CEC [eq/L]	CEC [meq/L]/1000	1.54	
SI_CO2	log(partial_pressure_CO2)	-3.40	
SI_O2	log(partial_pressure)	-0.68	
n_pyrite/100g_shale	m_pyrite/Mm_pyrite	0.04	
n_calcite/100g_shale	m_calcite/Mm_calcite	0.01	
n_K-feldspar/100g_shale	m_feldpar/Mm_feldspar	0.05	
n_uran/100g_shale	m_uran/Mm_uran	0.000029	
nCu/100g_shale	m_copper/Mm_copper	0.00015	
nZn/100g_shale	m_zinc/Mm_zink	0.00058	
nMnO/100g_shale	m_MnO/Mm_MnO	0.00039	
nBa/100g_shale	m_Ba/Mm_Ba	0.00057	
n_OrganicC	m_OC/Mm_C	0.52	
Molratios impurities pyrite:	nCu/n_pyrite	0.0041	
	nZn/n_pyrite	0.016	
	nMn/n_pyrite	0.011	
	nBa/n_pyrite	0.016	
	Fe	0.95	

Table A 2: The relative amount of different minerals measured in the XRD of unweathered shale. The analyses were done for the starting material (U1 and U2) and for the samples stored for 7 and 9 months under different conditions in Experiment 1. F: Freshwater, S: Seawater, O: Oxic, L: Low-oxygen.

Sample	U1	U2	1_FO_7m	1_FO_9m	1_FL_7m	1_FL_9m	1_SO_7m	1_SO_9m	1_SL_7m	1_SL_9m
Unit Symbol	%	%	%	%	%	%	%	%	%	%
Quartz	25	24	26	25	25	25	25	22	25	25
Muscovite	37	30	35	28	36	34	37	36	37	35
Biotite	0.73	0.74	0.61	0.75	0.32	2.4	2.7	1.2	1.3	2.1
Chlorite	1.5	1.6	1.7	1.3	1.4	0.6	1.8	0.6	1.4	2.5
Phlogopite	0.49	0.78	0.50	0.00	0.73	1.23	0.84	0.82	0.00	0.16
Glauconite	3.9	6.1	3.6	8.1	9.9	2.8	0.85	4.0	3.7	0.0
Plagioclase	2.6	1.8	2.1	2.3	1.4	2.1	0.7	3.4	2.1	0.84
Anorthite	0.92	0.80	0.62	0.35	7.4	0.92	2.2	0.92	6.9	2.4
Oligoclase	0.73	1.8	0.00	0.00	0.76	0.93	0.00	0.00	0.00	3.0
Microcline	6.7	4.6	6.8	7.4	2.0	4.8	6.8	6.5	7.0	8.5
Albite	0.00	2.9	0.00	0.00	0.00	0.57	2.3	1.4	0.00	3.2
Illite	13	14	14	15	8.4	14	6.8	13	10	7.7
Kaolinite	0.79	1.8	1.4	1.8	1.7	4.0	4.1	1.5	0.00	2.2
Pyrite	2.9	3.1	3.0	2.7	2.2	2.5	2.3	2.2	2.6	2.6
Pyrrhotite	0.82	1.2	0.56	0.56	0.38	0.50	0.79	0.64	0.61	0.78
Calcite	0.17	1.1	0.96	0.55	0.32	0.75	0.52	1.0	1.2	0.97
Dolomite	0.39	0.83	0.00	0.00	0.00	0.53	1.4	0.00	0.48	0.00
Jarosite	1.3	1.1	1.8	1.5	0.00	2.0	2.2	2.1	0.00	1.6
Rutil	0.66	0.69	0.87	0.73	0.65	0.72	1.2	0.85	0.72	1.4

Table A 3: The relative amount of different minerals measured in the XRD of weathered shale. The analyses were done for the starting material (W1 and W2) and for the samples stored for 7 and 9 months under different conditions in Experiment 1. W: weathered shale, F: Freshwater, S: Seawater, O: Oxic, L: Low-oxygen.

Sample	F1	F2	1_WFO_7m	1_WFO_9m	1_WFL_7m	1_WFL_9m	1_WSO_7m	1_WSO_9m	1_WSL_7m	1_WSL_9m
Unit Symbol	%	%	%	%	%	%	%	%	%	%
Quartz	17	16	19	18	17	16	19	18	19	17
Muscovite	34	36	35	38	38	42	33	31	34	42
Microcline	10	9.4	8.5	11	10	7.1	18	16	16	13
Jarosite	2.7	3.1	2.6	2.9	3.0	2.0	3.9	3.2	3.9	2.6
Plagioclase	2.5	2.9	1.0	3.8	3.8	6.1	4.2	2.6	1.9	3.3
Rozenite	2.1	2.1	1.2	1.6	1.1	1.2	0.66	0.54	0.47	1.0
Schwertmannite	2.4	2.5	1.6	1.6	1.8	1.7	0.22	0.52	0.87	0.92
Gypsum	7.7	7.8	8.0	7.1	7.0	7.2	7.2	6.3	5.9	4.0
Pyrite	0.024	0.27	0.076	0.13	0.053	0.18	0.17	0.15	0.11	0.12
Anorthite	0.40	0.85	1.0	1.0	0.86	0.73	1.9	11	4.4	7.4
Ferrihydrite	0.76	0.21	0.00	1.3	1.0	0.37	2.3	1.7	1.7	1.7
Illite + Kaolinite	13	14	15	13	12	11	5.8	5.4	7.3	2.6
Oligoclase	4.2	3.4	6.3	1.0	2.8	3.9	1.5	0.71	3.4	1.2
Pyrrhotite	0.42	0.31	0.15	0.12	0.19	0.27	0.00	0.33	0.00	0.00
Anhydrite	1.6	0.89	0.59	0.49	1.5	1.5	2.0	1.7	1.3	2.8

Table A 4: Results from whole rock analysis of the starting material of unweathered (U1, U2) and weathered (W1, W2) shale, in addition to samples from Experiment 1 treated with water for 9 months.
W: Weathered shale, F: Freshwater, S: Seawater, O: Oxic, L: Low-oxygen.

Analyte Symbol	Total S	SiO2	Al2O3	Fe2O3(T)	MnO	MgO	CaO	Na2O	K2O	TiO2	P2O5	LOI	Total
Unit Symbol	%	%	%	%	%	%	%	%	%	%	%	%	%
Detection Limit	0.01	0.01	0.01	0.01	0.005	0.01	0.01	0.01	0.01	0.001	0.01		0.01
Analysis Method	CS	FUS-ICP	FUS-ICP	FUS-ICP	FUS-ICP	FUS-ICP	FUS-ICP	FUS-ICP	FUS-ICP	FUS-ICP	FUS-ICP	GRAV	FUS-ICP
U1	2.2	57	17	4.5	0.028	1.6	1.1	0.46	5.2	0.91	0.19	12	99
U2	2.2	56	16	4.6	0.028	1.6	1.1	0.45	5.0	0.88	0.17	12	98
1_FO_9m	0.93	56	16	4.6	0.027	1.5	0.86	0.45	5.1	0.92	0.19	11	97
1_FL_9m	2.0	56	17	4.6	0.026	1.5	0.87	0.44	5.1	0.89	0.18	11	98
1_SO_9m	2.0	56	16	4.5	0.026	1.6	0.89	0.91	5.1	0.87	0.18	12	98
1_SL_9m	2.0	55	16	4.6	0.024	1.7	0.89	1.4	5.0	0.92	0.18	12	98
W1	3.6	45	13	6.6	0.020	1.1	3.9	0.60	4.2	0.68	0.19	22	98
W2	3.4	46	13	6.6	0.020	1.2	3.7	0.61	4.2	0.69	0.19	22	98
1_WFO_9m	2.4	48	14	6.4	0.013	1.1	2.8	0.67	4.6	0.77	0.18	20	99
1_WFL_9m	3.1	46	13	6.9	0.013	1.0	3.5	0.61	4.3	0.71	0.19	22	98
1_WSO_9m	2.8	47	13	6.7	0.014	1.1	3.1	1.3	4.6	0.72	0.18	21	99
1_WSL_9m	2.7	46	14	6.3	0.012	1.2	2.6	1.7	4.4	0.71	0.17	21	98

Analyte Symbol	Sc	Be	V	Cr	Co	Cd	Ga	Ge	As	Rb	Sr	Y	Zr
Unit Symbol	ppm	ppm	ppm	ppm	ppm	ppm	ppm	ppm	ppm	ppm	ppm	ppm	ppm
Detection Limit	1	1	5	20	1	0.5	1	0.5	5	1	2	1	1
Analysis Method	FUS-ICP	FUS-ICP	FUS-ICP	FUS-MS	FUS-MS	TD-ICP	FUS-MS	FUS-MS	FUS-MS	FUS-MS	FUS-ICP	FUS-ICP	FUS-ICP
U1	16	5.0	1910	110	18	7.5	24	< 0.5	25	167	96	45	140
U2	16	4.0	1799	110	20	6.5	24	1.5	51	164	94	42	155
1_FO_9m	16	4.0	1874	100	19	7.7	24	< 0.5	35	158	88	44	155
1_FL_9m	17	4.0	1845	110	21	7.4	25	1.7	52	171	87	43	157
1_SO_9m	16	5.0	1898	120	19	5.5	25	0.50	28	169	90	43	141
1_SL_9m	16	4.0	1817	100	19	6.8	23	1.4	46	160	91	42	155
W1	12	4.0	643	70	11	0.70	22	1.1	87	130	190	32	138
W2	12	4.0	651	80	11	0.80	22	1.1	85	133	183	33	140
1_WFO_9m	12	4.0	701	70	4.0	< 0.5	21	< 0.5	51	129	167	25	131
1_WFL_9m	12	4.0	659	70	6.0	< 0.5	22	1.2	98	133	179	25	140
1_WSO_9m	12	4.0	675	70	6.0	< 0.5	21	< 0.5	60	134	186	26	129
1_WSL_9m	12	4.0	668	70	5.0	< 0.5	22	1.0	81	132	166	23	140

Analyte Symbol	Nb	Mo	In	Sn	Sb	Cs	Ba	La	Ce	Pr	Nd	Sm	Eu	Gd
Unit Symbol	ppm	ppm	ppm	ppm	ppm	ppm	ppm	ppm	ppm	ppm	ppm	ppm	ppm	ppm
Detection Limit	0.2	2	0.1	1	0.2	0.1	2	0.05	0.05	0.01	0.05	0.01	0.005	0.01
Analysis Method	FUS-MS	FUS-MS	FUS-MS	FUS-MS	FUS-MS	FUS-MS	FUS-ICP	FUS-MS	FUS-MS	FUS-MS	FUS-MS	FUS-MS	FUS-MS	FUS-MS
U1	15	100	0.10	1.0	6.1	9.1	793	54	98	12	47	9.3	1.8	8.2
U2	17	> 100	0.10	4.0	16	8.8	763	52	97	12	46	9.2	1.7	8.2
1_FO_9m	12	87	0.10	2.0	17	8.2	788	49	91	11	43	8.6	1.7	7.8
1_FL_9m	18	97	0.10	4.0	17	9.3	786	54	100	12	48	9.5	1.8	8.5
1_SO_9m	15	83	0.10	2.0	9.3	9.3	783	54	99	12	49	9.6	1.7	8.4
1_SL_9m	17	82	0.10	4.0	15	8.4	773	50	93	12	45	9.1	1.7	7.8
W1	16	> 100	0.10	3.0	5.2	5.9	1519	47	87	10	39	7.1	1.3	5.9
W2	17	> 100	0.10	3.0	4.9	5.9	1516	47	88	10	39	7.2	1.3	6.1
1_WFO_9m	11	> 100	0.10	1.0	2.8	6.0	1637	43	78	9.5	36	5.9	1.0	4.3
1_WFL_9m	17	> 100	0.10	3.0	5.3	6.1	1530	47	86	10	37	6.6	1.1	5.1
1_WSO_9m	14	> 100	< 0.1	1.0	2.7	5.8	1712	46	85	10	37	6.2	1.1	4.7
1_WSL_9m	16	> 100	0.10	3.0	5.1	5.9	1564	46	84	10	36	6.1	1.0	4.5

Analyte Symbol	Tb	Dy	Ho	Er	Tm	Yb	Lu	Hf	Ta	W	Tl	Bi	Th	U
Unit Symbol	ppm	ppm	ppm	ppm	ppm	ppm	ppm	ppm	ppm	ppm	ppm	ppm	ppm	ppm
Detection Limit	0.01	0.01	0.01	0.01	0.005	0.01	0.002	0.1	0.01	0.5	0.05	0.1	0.05	0.01
Analysis Method	FUS-MS	FUS-MS	FUS-MS	FUS-MS	FUS-MS	FUS-MS	FUS-MS	FUS-MS	FUS-MS	FUS-MS	FUS-MS	FUS-MS	FUS-MS	FUS-MS
U1	1.3	7.9	1.6	4.5	0.65	4.1	0.63	4.0	1.3	3.3	2.8	< 0.1	17	70
U2	1.4	8.0	1.6	4.5	0.66	4.1	0.65	4.0	1.3	2.2	3.0	0.30	17	71
1_FO_9m	1.2	7.4	1.5	4.1	0.59	3.9	0.58	3.5	1.2	1.5	3.1	< 0.1	15	65
1_FL_9m	1.4	8.4	1.6	4.8	0.69	4.4	0.69	4.2	1.3	2.5	3.2	0.30	18	70
1_SO_9m	1.4	8.1	1.6	4.5	0.65	4.1	0.66	4.0	1.3	2.3	2.0	< 0.1	17	67
1_SL_9m	1.3	7.7	1.5	4.3	0.62	3.9	0.64	4.0	1.2	2.1	1.1	0.20	17	64
W1	1.0	5.6	1.1	3.4	0.46	3.0	0.47	3.5	1.1	2.5	3.7	0.30	12	87
W2	1.0	5.7	1.1	3.3	0.46	3.0	0.49	3.7	1.1	2.6	3.9	0.30	12	89
1_WFO_9m	0.62	3.7	0.74	2.2	0.33	2.2	0.35	3.2	1.1	2.0	3.5	< 0.1	11	62
1_WFL_9m	0.80	4.7	0.94	2.8	0.40	2.6	0.42	3.6	1.1	3.0	3.8	0.30	13	81
1_WSO_9m	0.72	4.2	0.81	2.4	0.35	2.2	0.34	3.4	1.1	2.1	2.5	< 0.1	12	80
1_WSL_9m	0.71	4.1	0.80	2.4	0.34	2.2	0.35	3.4	1.1	2.4	1.6	0.30	12	75

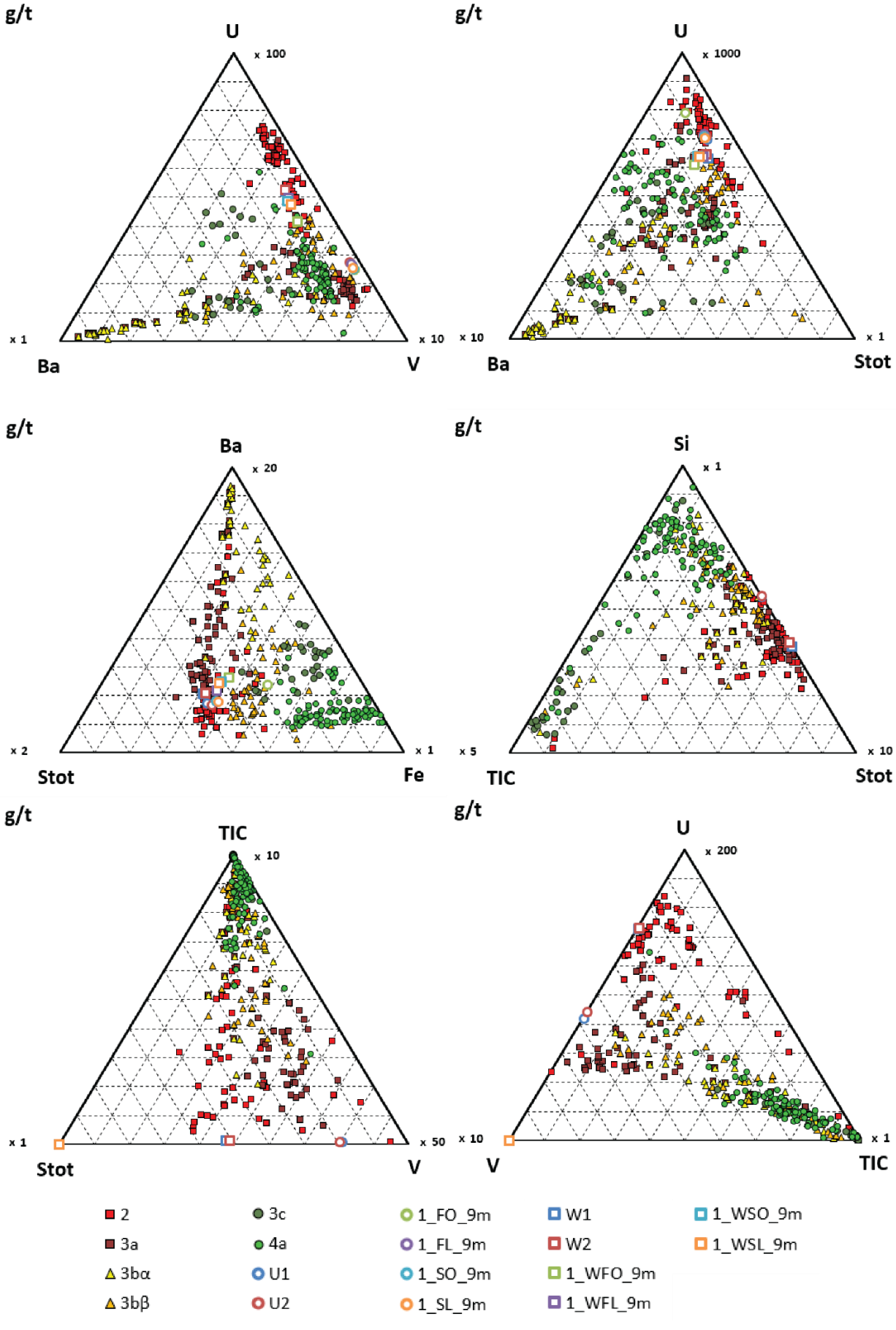
g/t
U
x 100
x 1
Ba
x 10
V
g/t
U
x 1000
x 10
Ba
x 1
Stot
g/t
Ba
x 20
x 2
Stot
x 1
Fe
g/t
Si
x 1
x 5
TIC
x 10
Stot
g/t
TIC
x 10
x 1
Stot
x 50
V
g/t
U
x 200
x 10
V
x 1
TIC
2
3a
3bα
3bβ
3c
4a
U1
U2
1_FO_9m
1_FL_9m
1_SO_9m
1_SL_9m
W1
W2
1_WFO_9m
1_WFL_9m
1_WSO_9m
1_WSL_9m

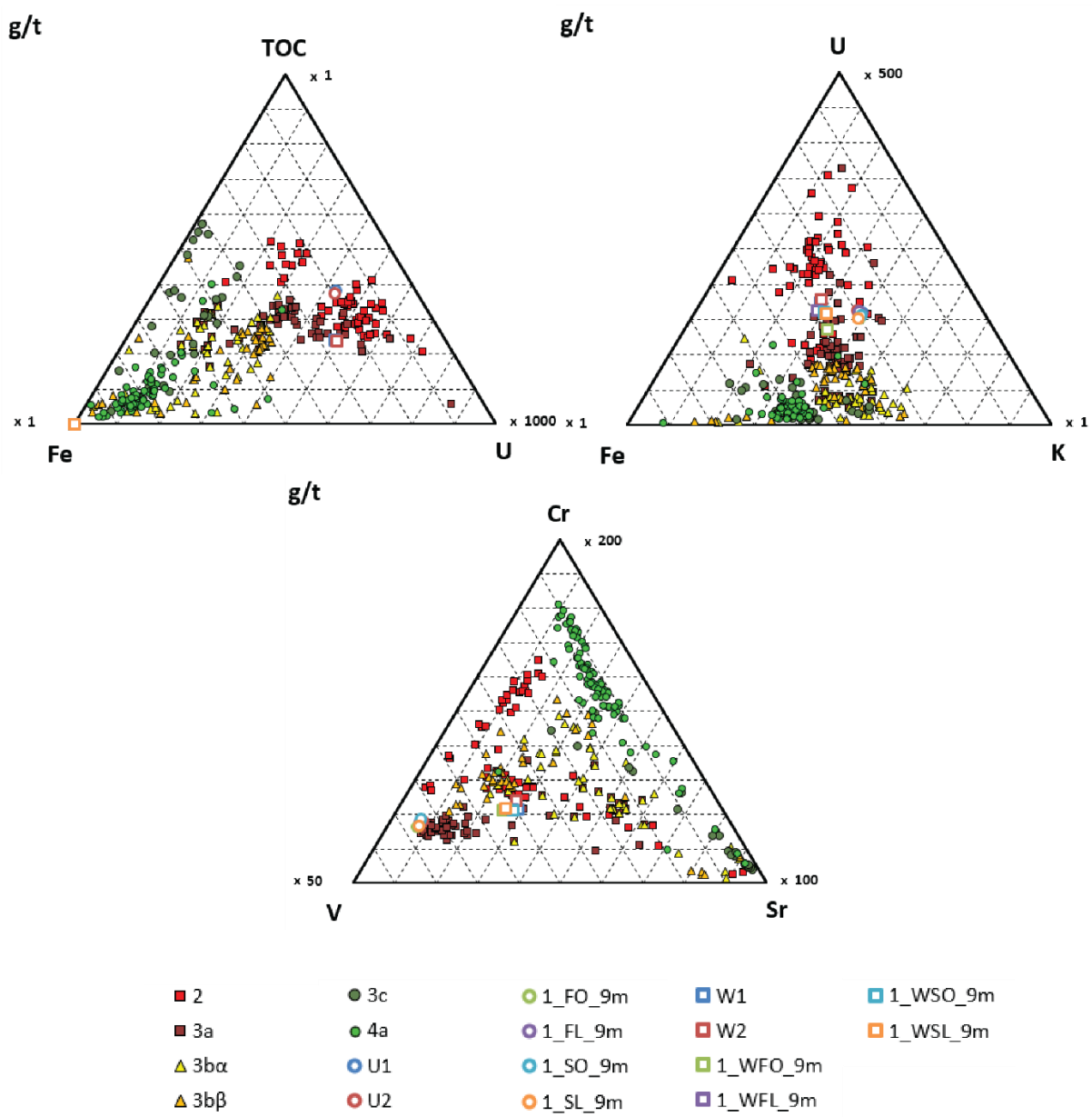

Figure A 1: Triangular plots obtained from whole-rock analyses with the relative amounts of elements compared to reference samples of black mudrocks within the Cambro-Ordovician succession (Pabst et al., 2017).
U: Unweathered shale, W: Weathered shale, F: Freshwater, S: Seawater, O: Oxic: L: Low oxygen.

Table A 5: Weight of shale used for each bottle, and results of field parameters and alkalinity in Experiment 1. B: Blank, W: Weathered shale, F: Freshwater, S: Seawater, O: Oxic, L: Low-oxygen.

	weight shale [g]	Conductivity [µS/cm]	pH	Eh [mV]	Oxygen [mg/L]	Alkalinity [meq/L]	Temperature [°C]
1_WFO_1d	10.1	1731	3.0	730	8.0	n.d.	24
1_WFO_1w	10.1	2050	3.2	776	7.3	n.d.	23
1_WFO_2w	10.1	1990	3.4	710	7.3	n.d.	22
1_WFO_1m	10.2	2420	3.3	775	6.9	n.d.	22
1_WFO_1m	10.1	2380	3.3	776	6.9	n.d.	22
1_WFO_1m	10.1	2370	3.5	768	7.1	n.d.	22
1_WFO_2m	10.1	2740	3.0	805	7.3	n.d.	23
1_WFO_3m	10.2	2670	3.0	790	7.6	n.d.	25
1_WFO_4m	10.1	2580	3.5	750	7.6	n.d.	23
1_WFO_5m	10.1	2780	3.3	763	7.9	n.d.	22
1_WFO_6m	10.1	2780	3.2	766	7.9	n.d.	23
1_WFO_6m	10.1	2590	-	737	8.1	n.d.	23
1_WFO_6m	10.2	2860	3.0	790	8.0	n.d.	23
1_WFO_7m	10.2	2810	3.2	755	8.2	n.d.	22
1_WFO_9m	10.1	2810	3.2	715	8.5	n.d.	19
1_WFO_11m	10.4	2650	3.4	685	7.9	n.d.	23
1_WFO_11m	10.2	2870	3.1	723	8.1	n.d.	23
1_WFO_11m	10.0	2740	3.3	710	8.2	n.d.	23
	weight shale [g]	Conductivity [µS/cm]	pH	Eh [mV]	Oxygen [mg/L]	Alkalinity [meq/L]	Temperature [°C]
1_BFO_1d	0.00	2.0	5.7	560	8.2	n.d.	23
1_BFO_1w	0.00	2.0	5.8	590	8.3	n.d.	23
1_BFO_2w	0.00	2.0	5.7	550	8.3	n.d.	22
1_BFO_1m	0.00	2.0	5.7	618	8.7	n.d.	22
1_BFO_2m	0.00	2.7	5.8	625	8.3	n.d.	23
1_BFO_3m	0.00	2.2	5.7	605	8.1	n.d.	24
1_BFO_4m	0.00	2.0	5.7	615	8.4	n.d.	23
1_BFO_5m	0.00	1.7	5.6	655	8.6	n.d.	22
1_BFO_6m	0.00	2.3	5.7	654	8.6	n.d.	23
1_BFO_7m	0.00	4.0	5.6	688	8.4	n.d.	22
1_BFO_9m	0.00	3.0	5.7	694	8.9	n.d.	19
1_BFO_11m	0.00	4.0	5.6	663	8.3	n.d.	23
	weight shale [g]	Conductivity [µS/cm]	pH	Eh [mV]	Oxygen [mg/L]	Alkalinity [meq/L]	Temperature [°C]
1_FO_1d	10.1	246	7.2	382	7.8	0.050	24
1_FO_1w	10.1	378	7.3	490	7.3	0.19	23
1_FO_2w	10.3	431	7.5	480	7.7	0.18	22
1_FO_1m	10.1	517	7.7	499	7.9	-	22
1_FO_1m	10.1	503	7.7	510	8.0	-	22
1_FO_1m	10.2	525	7.7	510	8.0	-	22
1_FO_2m	10.1	588	7.7	510	7.8	-	23
1_FO_3m	10.1	662	7.7	500	7.6	-	24
1_FO_4m	10.1	738	7.7	520	7.9	-	23
1_FO_5m	10.1	779	7.7	529	8.2	1.3	22
1_FO_6m	10.2	783	7.7	530	8.2	-	23
1_FO_6m	10.1	755	7.7	526	8.2	1.3	23
1_FO_6m	10.2	765	7.7	524	8.0	1.4	23
1_FO_7m	10.1	788	7.7	525	8.2	1.0	22
1_FO_9m	10.1	939	7.7	573	8.6	1.1	19
1_FO_11m	10.2	991	7.6	554	8.1	1.1	23
1_FO_11m	10.1	1029	7.6	600	8.1	1.3	23
1_FO_11m	10.1	1007	7.6	567	8.1	1.1	23
	weight shale [g]	Conductivity [µS/cm]	pH	Eh [mV]	Oxygen [mg/L]	Alkalinity [meq/L]	Temperature [°C]
1_WSO_1d	10.1	42100	4.1	581	8.0	n.d.	23
1_WSO_1w	10.1	41400	3.6	641	8.1	n.d.	23
1_WSO_2w	10.2	41500	3.7	705	7.5	n.d.	23
1_WSO_1m	10.2	42600	3.9	660	7.5	n.d.	22
1_WSO_1m	10.2	43500	3.8	670	7.8	n.d.	22
1_WSO_1m	10.1	43600	4.5	580	7.9	n.d.	22
1_WSO_2m	10.2	43800	3.7	701	7.9	n.d.	23
1_WSO_3m	10.1	45600	3.8	670	7.7	n.d.	24
1_WSO_4m	10.1	45900	3.9	686	8.1	n.d.	23
1_WSO_5m	10.1	47000	3.9	645	8.3	n.d.	22
1_WSO_6m	10.1	46500	3.8	660	8.3	n.d.	23
1_WSO_6m	10.1	46100	3.9	668	8.2	n.d.	23
1_WSO_6m	10.1	46500	3.9	674	8.1	n.d.	23
1_WSO_7m	10.1	46200	4.0	618	8.4	n.d.	22
1_WSO_9m	10.1	48400	3.7	647	8.7	n.d.	19
1_WSO_11m	10.2	48900	3.7	646	8.2	n.d.	23
1_WSO_11m	10.1	48500	3.5	677	8.2	n.d.	23
1_WSO_11m	10.1	46800	3.7	638	8.2	n.d.	23

	weight shale [g]	Conductivity [µS/cm]	pH	Eh [mV]	Oxygen [mg/L]	Alkalinity [meq/L]	Temperature [°C]
1_BSO_1d	0.00	42100	7.8	370	8.4	-	24
1_BSO_1w	0.00	41800	7.9	480	8.3	2.2	23
1_BSO_2w	0.00	41800	7.9	480	8.1	2.2	23
1_BSO_1m	0.00	42700	8.0	482	8.5	2.2	22
1_BSO_2m	0.00	43900	8.0	500	8.3	2.2	23
1_BSO_3m	0.00	45500	8.1	501	8.0	2.1	24
1_BSO_4m	0.00	45500	8.1	510	8.4	2.1	23
1_BSO_5m	0.00	46600	8.1	495	8.5	2.1	22
1_BSO_6m	0.00	45600	8.1	526	8.4	2.8	23
1_BSO_7m	0.00	45600	8.0	526	8.6	2.2	22
1_BSO_9m	0.00	48000	8.0	580	8.9	-	19
1_BSO_11m	0.00	48200	8.0	588	8.3	2.4	23
	weight shale [g]	Conductivity [µS/cm]	pH	Eh [mV]	Oxygen [mg/L]	Alkalinity [meq/L]	Temperature [°C]
1_SO_1d	10.2	42700	7.7	408	8.0	-	23
1_SO_1w	10.1	42100	7.7	450	7.9	2.3	23
1_SO_2w	10.1	42600	7.7	460	7.9	2.3	23
1_SO_1m	10.1	43000	7.7	487	8.2	1.7	22
1_SO_1m	10.1	43000	7.7	490	8.2	2.1	22
1_SO_1m	10.1	43100	7.8	486	8.1	2.2	22
1_SO_2m	10.2	44300	7.8	457	8.1	1.9	24
1_SO_3m	10.1	45400	7.8	480	7.9	1.5	25
1_SO_4m	10.2	45500	7.7	500	8.1	1.6	24
1_SO_5m	10.1	46600	7.8	480	8.4	1.4	22
1_SO_6m	10.1	45900	7.7	513	8.2	1.8	24
1_SO_6m	10.1	45800	7.7	668	8.1	1.9	24
1_SO_7m	10.1	46300	7.8	520	8.5	1.8	22
1_SO_9m	10.1	48700	7.7	551	8.7	-	20
1_SO_11m	10.1	48500	7.7	538	8.1	1.7	23
1_SO_11m	10.1	48900	7.7	615	8.2	1.5	23
1_SO_11m	10.1	49200	7.7	548	8.2	1.6	23
	weight shale [g]	Conductivity [µS/cm]	pH	Eh [mV]	Oxygen [mg/L]	Alkalinity [meq/L]	Temperature [°C]
1_WFL_1d	10.2	2600	3.0	749	4.2	n.d.	23
1_WFL_1w	10.0	2070	3.2	775	4.7	n.d.	23
1_WFL_2w	10.2	2260	3.3	657	3.5	n.d.	23
1_WFL_1m	10.2	2490	3.3	770	3.9	n.d.	22
1_WFL_1m	10.2	2440	3.2	785	2.9	n.d.	22
1_WFL_1m	10.1	2430	3.5	777	3.7	n.d.	22
1_WFL_2m	10.2	2490	3.4	750	4.6	n.d.	24
1_WFL_3m	10.1	2770	3.1	786	4.3	n.d.	25
1_WFL_4m	10.2	2500	3.6	727	4.6	n.d.	24
1_WFL_5m	10.2	2850	3.1	777	5.4	n.d.	22
1_WFL_6m	-	2910	3.0	795	4.8	n.d.	24
1_WFL_6m	-	2810	3.1	794	4.7	n.d.	24
1_WFL_6m	-	2730	3.2	785	4.8	n.d.	24
1_WFL_7m	10.1	2730	3.3	738	4.6	n.d.	22
1_WFL_9m	10.1	2750	3.6	660	4.9	n.d.	20
1_WFL_11m	10.1	3200	2.9	748	5.0	n.d.	23
1_WFL_11m	-	2750	3.4		4.8	n.d.	23
1_WFL_11m	-	3220	2.9	710	5.2	n.d.	23
	weight shale [g]	Conductivity [µS/cm]	pH	Eh [mV]	Oxygen [mg/L]	Alkalinity [meq/L]	Temperature [°C]
1_BFL_1d	0.00	2.6	5.5	610	4.9	n.d.	23
1_BFL_1w	0.00	3.0	5.5	590	5.4	n.d.	23
1_BFL_2w	0.00	2.8	5.4	549	5.5	n.d.	23
1_BFL_1m	0.00	3.0	5.4	620	6.7	n.d.	22
1_BFL_2m	0.00	2.0	5.5	612	6.7	n.d.	24
1_BFL_3m	0.00	3.9	5.4	638	6.4	n.d.	25
1_BFL_4m	0.00	2.4	5.5	638	5.5	n.d.	24
1_BFL_5m	0.00	2.8	5.3	655	6.1	n.d.	22
1_BFL_6m	0.00	3.5	5.4	675	5.7	n.d.	24
1_BFL_7m	0.00	3.0	5.5	649	6.4	n.d.	22
1_BFL_9m	0.00	6.7	5.3	578	6.1	n.d.	20
1_BFL_11m	0.00	4.0	5.5	700	6.0	n.d.	23

	weight shale [g]	Conductivity [µS/cm]	pH	Eh [mV]	Oxygen [mg/L]	Alkalinity [meq/L]	Temperature [°C]
1_FL_1d	10.1	281	7.5	421	4.4	0.25	23
1_FL_1w	10.1	415	7.5	510	3.0	0.46	23
1_FL_2w	10.1	417	7.3	460	3.9	-	23
1_FL_1m	10.2	492	7.5	510	4.7	-	22
1_FL_1m	10.1	495	7.5	545	4.5	-	22
1_FL_1m	10.2	490	7.5	540	4.6	-	22
1_FL_2m	10.1	598	7.6	522	5.2	-	24
1_FL_3m	10.3	627	7.6	520	4.5	-	25
1_FL_4m	10.1	690	7.6	510	4.6	-	24
1_FL_5m	10.1	788	7.4	529	5.2	1.7	22
1_FL_6m	-	813	7.5	560	4.9	1.9	24
1_FL_6m	-	806	7.5	550	4.9	1.8	24
1_FL_6m	-	811	7.6	545	4.8	1.9	24
1_FL_7m	10.2	811	7.5	557	5.3	1.3	22
1_FL_9m	10.1	947	7.5	585	4.8	1.7	20
1_FL_11m	10.2	979	7.5	583	5.2	1.6	23
1_FL_11m	-	1006	7.5	590	5.2	1.2	23
1_FL_11m	-	1014	7.6	555	5.3	1.5	23
	weight shale [g]	Conductivity [µS/cm]	pH	Eh [mV]	Oxygen [mg/L]	Alkalinity [meq/L]	Temperature [°C]
1_WSL_1d	10.1	41800	3.1	705	4.5	n.d.	23
1_WSL_1w	10.2	41600	3.4	670	4.8	n.d.	23
1_WSL_2w	10.2	42100	3.4	740	3.8	n.d.	23
1_WSL_1m	10.2	42700	3.7	700	3.9	n.d.	22
1_WSL_1m	10.1	42900	3.8	687	4.3	n.d.	22
1_WSL_1m	10.1	43100	3.8	691	4.2	n.d.	22
1_WSL_2m	10.1	44500	3.8	670	4.9	n.d.	24
1_WSL_3m	10.1	46500	3.7	680	5.1	n.d.	25
1_WSL_4m	10.1	46500	4.1	595	4.8	n.d.	24
1_WSL_5m	10.2	47400	3.6	704	5.0	n.d.	22
1_WSL_6m	-	47000	3.3	728	4.9	n.d.	24
1_WSL_6m	-	47000	3.7	700	4.9	n.d.	24
1_WSL_7m	10.2	47100	4.0	580	5.4	n.d.	22
1_WSL_9m	10.1	49500	3.5	625	4.9	n.d.	20
1_WSL_11m	10.1	49200	3.7	640	4.6	n.d.	23
1_WSL_11m	-	50000	4.2	620	5.4	n.d.	23
1_WSL_11m	-	50500	5.0	615	5.6	n.d.	23
	weight shale [g]	Conductivity [µS/cm]	pH	Eh [mV]	Oxygen [mg/L]	Alkalinity [meq/L]	Temperature [°C]
1_SL_1d	10.1	41500	7.5	490	4.1	-	23
1_SL_1w	10.2	41600	7.4	500	3.8	2.8	23
1_SL_2w	10.2	41800	7.4	509	3.5	2.5	23
1_SL_1m	10.2	42500	7.5	510	4.9	2.5	22
1_SL_1m	10.1	42400	7.4	550	4.3	2.4	22
1_SL_1m	10.1	42700	7.4	540	4.5	2.5	22
1_SL_2m	10.2	44100	7.5	525	5.2	3.2	24
1_SL_3m	10.2	45500	7.6	514	4.8	2.7	25
1_SL_4m	10.1	45500	7.4	500	4.4	2.4	24
1_SL_5m	10.1	45600	7.5	540	4.9	2.4	22
1_SL_6m	-	45700	7.4	580	5.0	2.8	24
1_SL_6m	-	46000	7.4	578	5.0	2.7	24
1_SL_6m	-	46200	7.3	565	5.2	2.8	24
1_SL_7m	10.1	45900	7.5	511	5.1	2.8	22
1_SL_9m	10.1	48700	7.5	530	5.2	n.d.	20
1_SL_11m	10.1	49100	7.5	487	4.5	2.7	23
1_SL_11m	-	49000	7.4	529	4.8	1.4	23
1_SL_11m	-	49500	7.4	526	4.4	2.4	23
	weight shale [g]	Conductivity [µS/cm]	pH	Eh [mV]	Oxygen [mg/L]	Alkalinity [meq/L]	Temperature [°C]
1_BSL_1d	0.00	41700	7.7	450	5.8	-	23
1_BSL_1w	0.00	41300	7.6	450	4.1	2.2	23
1_BSL_2w	0.00	41900	7.6	459	4.1	2.2	23
1_BSL_1m	0.00	42300	7.3	476	5.4	2.2	22
1_BSL_2m	0.00	44000	7.4	503	5.4	2.3	24
1_BSL_3m	0.00	45500	7.5	484	5.4	2.1	25
1_BSL_4m	0.00	45600	7.8	455	4.9	2.2	24
1_BSL_5m	0.00	43500	7.8	510	5.2	2.1	22
1_BSL_6m	0.00	45500	7.6	540	6.0	2.4	24
1_BSL_7m	0.00	46000	7.8	490	5.3	2.1	22
1_BSL_9m	0.00	48500	7.8	562	5.6	-	20
1_BSL_11m	0.00	48800	7.8	485	4.6	2.5	23

Table A 6: Results of field parameters and alkalinity in Experiment 2, where only unweathered shale was used. B: Blank, F: Freshwater, S: Seawater, O: Oxic, A: Anoxic.

	Conductivity [µS/cm]	pH	Eh [mV]	Oxygen [mg/L]	Alkalinity [meq/L]	Temperature [°C]
2_SO_1w	46200	7.8	493	7.5	2.5	22
2_SO_1m	45700	8.0	447	8.0	3.1	20
2_SO_2m	47900	8.0	541	8.8	-	20
2_SO_4m	46800	7.9	531	8.1	3.4	23
2_SO_4m	48800	7.9	529	7.9	1.6	23
2_SO_4m	48600	7.9	525	8.0	1.6	23
	Conductivity [µS/cm]	pH	Eh [mV]	Oxygen [mg/L]	Alkalinity [meq/L]	Temperature [°C]
2_BSO_1w	46300	8.0	488	8.5	2.1	22
2_BSO_1m	46600	8.1	421	8.8	2.3	20
2_BSO_2m	48500	8.1	523	8.9	5.3	20
2_BSO_4m	48700	8.1	513	8.2	2.3	23
	Conductivity [µS/cm]	pH	Eh [mV]	Oxygen [mg/L]	Alkalinity [meq/L]	Temperature [°C]
2_FO_1w	375	7.6	500	7.4	0.17	22
2_FO_1m	532	8.0	441	8.3	1.1	20
2_FO_2m	601	8.2	539	8.8	0.97	20
2_FO_4m	698	8.1	510	8.2	1.0	23
2_FO_4m	691	8.1	508	8.0	1.0	23
2_FO_4m	710	8.1	508	8.0	1.0	23
	Conductivity [µS/cm]	pH	Eh [mV]	Oxygen [mg/L]	Alkalinity [meq/L]	Temperature [°C]
2_BFO_1w	2.6	6.1	519	8.5	n.d.	22
2_BFO_1m	2.3	6.1	534	8.7	n.d.	20
2_BFO_2m	4.0	6.2	568	8.8	n.d.	20
2_BFO_4m	3.0	5.7	550	8.3	n.d.	23
	Conductivity [µS/cm]	pH	Eh [mV]	Oxygen [mg/L]	Alkalinity [meq/L]	Temperature [°C]
2_BSA_1w	45800	8.0	445	0.30	2.1	23
2_BSA_1m	46200	7.9	226	0.34	3.3	21
2_BSA_2m	48100	8.0	230	0.60	-	20
2_BSA_4m	48900	8.0	231	0.54	2.5	23
	Conductivity [µS/cm]	pH	Eh [mV]	Oxygen [mg/L]	Alkalinity [meq/L]	Temperature [°C]
2_SA_1w	44900	7.6	390	0.36	2.3	23
2_SA_1m	46000	7.4	232	0.36	6.5	21
2_SA_2m	48300	7.5	282	0.39	-	20
2_SA_4m	49300	7.4	210	0.48	3.0	23
2_SA_4m	49000	7.4	223	0.52	3.0	23
2_SA_4m	49200	7.4	222	0.63	3.1	23
	Conductivity [µS/cm]	pH	Eh [mV]	Oxygen [mg/L]	Alkalinity [meq/L]	Temperature [°C]
2_FA_1w	318	7.6	384	0.32	0.24	23
2_FA_1m	461	7.9	324	0.37	0.64	21
2_FA_2m	477	8.0	290	0.47	0.91	20
2_FA_4m	493	7.9	321	0.66	1.2	23
2_FA_4m	490	7.9	304	0.51	1.3	23
2_FA_4m	462	-	-	0.51	1.1	23
	Conductivity [µS/cm]	pH	Eh [mV]	Oxygen [mg/L]	Alkalinity [meq/L]	Temperature [°C]
2_BFA_1w	4.8	7.0	433	0.51	n.d.	23
2_BFA_1m	2.9	6.6	378	0.36	n.d.	21
2_BFA_2m	6.0	6.8	275	0.49	n.d.	20
2_BFA_4m	6.0	6.9	318	0.58	n.d.	23

Table A 7: Main cat- and anions measured in the ion chromatography (IC) analyses for Experiment 1. B: Blank, W: Weathered shale, F: Freshwater, S: Seawater, O: Oxic, L: Low-oxygen.

Sample	Na [ppm]	K [ppm]	Mg [ppm]	Ca [ppm]	F [ppm]	Cl [ppm]	SO4 [ppm]	Br[ppm]	NO3 [ppm]	PO4 [ppm]
1_WFO_1d	-	-	-	-	n.a.	n.a.	1189	n.a.	n.a.	n.a.
1_WFO_1w	-	-	-	-	0.46	n.a.	1541	n.a.	n.a.	n.a.
1_WFO_2w	-	-	-	-	0.77	6.2	1500	n.a.	n.a.	n.a.
1_WFO_1m	7.0	n.a.	84	446	n.a.	7.0	1817	n.a.	10	n.a.
1_WFO_1m	7.1	n.a.	83	450	n.a.	6.6	1830	n.a.	10	n.a.
1_WFO_1m	7.0	n.a.	89	434	n.a.	6.8	1816	n.a.	10	n.a.
1_WFO_2m	3.3	2.6	72	492	n.a.	n.a.	2045	5.5	n.a.	n.a.
1_WFO_3m	n.a.	n.a.	64	533	2.3	n.a.	2023	1.3	n.a.	n.a.
1_WFO_4m	n.a.	n.a.	86	550	2.9	n.a.	2032	1.2	n.a.	n.a.
1_WFO_5m	7.9	n.a.	92	564	n.a.	n.a.	2191	41	14	n.a.
1_WFO_6m	22	n.a.	86	608	n.a.	n.a.	2168	n.a.	n.a.	n.a.
1_WFO_6m	21	n.a.	77	598	n.a.	n.a.	2046	n.a.	n.a.	n.a.
1_WFO_6m	21	n.a.	82	599	n.a.	n.a.	2242	n.a.	n.a.	n.a.
1_WFO_7m	n.a.	n.a.	75	519	n.a.	n.a.	2113	n.a.	n.a.	n.a.
1_WFO_9m	n.a.	n.a.	72	497	n.a.	n.a.	2048	n.a.	6.9	n.a.
1_WFO_11m	2.1	n.a.	66	528	n.a.	n.a.	1933	n.a.	n.a.	n.a.
1_WFO_11m	n.a.	n.a.	81	550	n.a.	n.a.	2113	n.a.	n.a.	n.a.
1_WFO_11m	2.2	n.a.	82	529	n.a.	9	2022	n.a.	n.a.	n.a.
	Na [ppm]	K [ppm]	Mg [ppm]	Ca [ppm]	F [ppm]	Cl [ppm]	SO4 [ppm]	Br[ppm]	NO3 [ppm]	PO4 [ppm]
1_BFO_1d	-	-	-	-	n.a.	0.058	0.18	n.a.	0.18	n.a.
1_BFO_1w	-	-	-	-	n.a.	0.074	0.65	n.a.	0.25	n.a.
1_BFO_2w	-	-	-	-	n.a.	0.072	0.11	n.a.	0.20	n.a.
1_BFO_1m	0.10	0.087	n.a.	0.37	n.a.	0.077	0.077	0.14	0.079	n.a.
1_BFO_2m	0.037	0.054	n.a.	0.46	n.a.	0.17	n.a.	0.32	n.a.	n.a.
1_BFO_3m	0.13	0.085	n.a.	0.31	n.a.	0.062	0.0086	0.11	0.041	n.a.
1_BFO_4m	0.061	0.056	n.a.	0.25	n.a.	0.0015	n.a.	n.a.	n.a.	n.a.
1_BFO_5m	0.076	0.051	n.a.	0.32	n.a.	0.12	0.14	0.19	n.a.	n.a.
1_BFO_6m	0.067	0.052	n.a.	0.22	n.a.	0.063	0.048	0.042	n.a.	n.a.
1_BFO_7m	0.0026	n.a.	n.a.	n.a.	n.a.	0.044	n.a.	n.a.	n.a.	n.a.
1_BFO_9m	0.018	0.021	n.a.	n.a.	n.a.	0.10	0.052	n.a.	n.a.	n.a.
1_BFO_11m	1.1	0.079	0.22	n.a.	n.a.	2.0	0.56	0.20	n.a.	n.a.
	Na [ppm]	K [ppm]	Mg [ppm]	Ca [ppm]	F [ppm]	Cl [ppm]	SO4 [ppm]	Br[ppm]	NO3 [ppm]	PO4 [ppm]
1_FO_1d	-	-	-	-	n.a.	0.62	94	n.a.	n.a.	n.a.
1_FO_1w	-	-	-	-	n.a.	0.61	150	n.a.	n.a.	n.a.
1_FO_2w	-	-	-	-	n.a.	0.60	171	n.a.	n.a.	n.a.
1_FO_1m	7.5	11	7.0	125	n.a.	6.1	217	14	10	n.a.
1_FO_1m	7.3	11	8.5	152	n.a.	6.1	212	18	10	n.a.
1_FO_1m	7.4	11	6.4	122	n.a.	6.3	209	14	10	n.a.
1_FO_2m	1.2	5.0	13	125	n.a.	n.a.	246	4.8	n.a.	n.a.
1_FO_3m	n.a.	4.9	13	139	n.a.	n.a.	288	n.a.	n.a.	n.a.
1_FO_4m	n.a.	5.2	16	155	n.a.	n.a.	329	n.a.	n.a.	n.a.
1_FO_5m	1.2	5.7	12	167	n.a.	n.a.	380	24	13	n.a.
1_FO_6m	n.a.	6.2	12	183	n.a.	0.15	357	n.a.	n.a.	n.a.
1_FO_7m	1.2	4.9	12	163	n.a.	n.a.	397	n.a.	n.a.	n.a.
1_FO_9m	0.86	5.4	20	190	n.a.	n.a.	466	n.a.	n.a.	n.a.
1_FO_11m	1.0	6.1	16	214	n.a.	9.0	515	n.a.	n.a.	n.a.
1_FO_11m	0.9	6.4	21	226	n.a.	15.0	544	n.a.	n.a.	n.a.
1_FO_11m	1.1	6.2	16	216	n.a.	9.2	531	n.a.	n.a.	n.a.
	Na [ppm]	K [ppm]	Mg [ppm]	Ca [ppm]	F [ppm]	Cl [ppm]	SO4 [ppm]	Br[ppm]	NO3 [ppm]	PO4 [ppm]
1_WSO_1d	-	-	-	-	n.a.	19934	4849	286	n.a.	n.a.
1_WSO_1w	-	-	-	-	n.a.	20406	5356	342	n.a.	n.a.
1_WSO_2w	-	-	-	-	n.a.	20235	5455	348	n.a.	n.a.
1_WSO_1m	11740	354	1431	1019	n.a.	19922	5541	179	78	n.a.
1_WSO_1m	10785	339	1362	931	n.a.	18983	5132	204	77	n.a.
1_WSO_1m	11344	356	1434	946	n.a.	19890	5183	182	102	n.a.
1_WSO_2m	11040	363	1466	1212	n.a.	19717	5710	50	n.a.	n.a.
1_WSO_3m	12277	340	1468	1280	n.a.	19222	5805	121	n.a.	n.a.
1_WSO_4m	12402	358	1486	1307	n.a.	19408	5924	125	n.a.	n.a.
1_WSO_5m	11864	358	1511	1408	n.a.	20715	6267	220	n.a.	n.a.
1_WSO_6m	12035	332	1378	1210	n.a.	19072	6139	14	n.a.	n.a.
1_WSO_6m	11802	325	1388	1246	n.a.	18955	5968	6	n.a.	n.a.
1_WSO_6m	11954	327	1388	1251	n.a.	19128	6199	11	n.a.	n.a.
1_WSO_7m	9723	279	1259	1003	n.a.	17623	5658	149	n.a.	n.a.
1_WSO_9m	10120	320	1359	1050	n.a.	18458	6057	210	n.a.	n.a.
1_WSO_11m	10522	342	1352	1151	n.a.	18634	6177	278	n.a.	n.a.
1_WSO_11m	10203	335	1327	1147	n.a.	18222	6138	279	n.a.	n.a.
1_WSO_11m	9841	320	1262	1131	n.a.	17503	5980	273	n.a.	n.a.

	Na [ppm]	K [ppm]	Mg [ppm]	Ca [ppm]	F [ppm]	Cl [ppm]	SO4 [ppm]	Br[ppm]	NO3 [ppm]	PO4 [ppm]
1_BSO_1d	-	-	-	-	n.a.	20025	3119	360	n.a.	n.a.
1_BSO_1w	-	-	-	-	n.a.	20308	2965	396	n.a.	n.a.
1_BSO_2w	-	-	-	-	n.a.	20516	3190	416	n.a.	n.a.
1_BSO_1m	11447	446	1568	460	n.a.	20082	3157	168	75	n.a.
1_BSO_2m	11108	397	1566	486	n.a.	19821	3048	56	n.a.	n.a.
1_BSO_3m	12697	406	1593	477	n.a.	19847	3164	126	n.a.	n.a.
1_BSO_4m	12487	403	1582	549	n.a.	19482	3070	125	n.a.	n.a.
1_BSO_5m	12115	430	1616	557	n.a.	21074	3345	215	n.a.	n.a.
1_BSO_6m	12168	384	1474	441	n.a.	19457	3325	34	n.a.	n.a.
1_BSO_7m	9082	315	1314	326	n.a.	18831	3353	132	n.a.	n.a.
1_BSO_9m	10390	381	1317	405	n.a.	18130	3247	212	n.a.	n.a.
1_BSO_11m	10275	364	1379	264	n.a.	18098	3321	251	n.a.	n.a.
	Na [ppm]	K [ppm]	Mg [ppm]	Ca [ppm]	F [ppm]	Cl [ppm]	SO4 [ppm]	Br[ppm]	NO3 [ppm]	PO4 [ppm]
1_SO_1d	-	-	-	-	n.a.	20065	3253	231	n.a.	n.a.
1_SO_1w	-	-	-	-	n.a.	20448	3235	241	n.a.	n.a.
1_SO_2w	-	-	-	-	n.a.	20335	3265	241	n.a.	n.a.
1_SO_1m	11740	388	1368	522	n.a.	19781	3328	164	76	n.a.
1_SO_1m	11672	384	1359	526	n.a.	19822	3295	165	76	n.a.
1_SO_1m	11256	387	1366	531	n.a.	19809	3277	166	78	n.a.
1_SO_2m	11071	399	1550	670	n.a.	19792	3276	55	n.a.	n.a.
1_SO_3m	11934	364	1523	671	n.a.	19645	3274	n.a.	n.a.	n.a.
1_SO_4m	12624	401	1574	729	n.a.	19568	3304	126	n.a.	n.a.
1_SO_5m	12071	417	1603	766	n.a.	21034	3680	216	n.a.	n.a.
1_SO_6m	12132	360	1401	596	n.a.	19580	3814	n.a.	n.a.	n.a.
1_SO_6m	11798	352	1362	592	n.a.	19013	3679	n.a.	n.a.	n.a.
1_SO_7m	10032	340	1238	397	n.a.	18621	3487	127	n.a.	n.a.
1_SO_9m	10636	379	1317	588	n.a.	19231	3812	213	n.a.	n.a.
1_SO_11m	10635	378	1321	594	n.a.	18856	3839	268	n.a.	n.a.
1_SO_11m	10660	386	1376	605	n.a.	18908	3941	269	n.a.	n.a.
1_SO_11m	10814	384	1325	596	n.a.	19249	2993	271	n.a.	n.a.
	Na [ppm]	K [ppm]	Mg [ppm]	Ca [ppm]	F [ppm]	Cl [ppm]	SO4 [ppm]	Br[ppm]	NO3 [ppm]	PO4 [ppm]
1_WFL_1d	-	-	-	-	0	n.a.	1968	n.a.	n.a.	n.a.
1_WFL_1w	-	-	-	-	0	6.2	1574	n.a.	n.a.	n.a.
1_WFL_2w	-	-	-	-	0	6.5	1746	n.a.	n.a.	n.a.
1_WFL_1m	7.2	n.a.	83	482	n.a.	7.2	1890	n.a.	10	n.a.
1_WFL_1m	n.a.	n.a.	74	457	n.a.	6.9	1837	n.a.	10	n.a.
1_WFL_1m	7.6	n.a.	75	490	n.a.	7.2	1856	n.a.	10	n.a.
1_WFL_2m	n.a.	n.a.	79	511	n.a.	1.6	1940	13	n.a.	n.a.
1_WFL_3m	n.a.	n.a.	80	532	n.a.	n.a.	2112	n.a.	n.a.	n.a.
1_WFL_4m	n.a.	n.a.	78	558	n.a.	n.a.	1995	n.a.	n.a.	n.a.
1_WFL_5m	7.3	n.a.	87	567	0	n.a.	2257	n.a.	14	n.a.
1_WFL_6m	21	n.a.	76	612	n.a.	n.a.	2250	n.a.	n.a.	n.a.
1_WFL_6m	21	n.a.	83	615	n.a.	n.a.	2219	n.a.	n.a.	n.a.
1_WFL_6m	22	n.a.	78	610	n.a.	n.a.	2139	n.a.	n.a.	n.a.
1_WFL_7m	1.4	n.a.	85	520	n.a.	4.3	2085	n.a.	n.a.	n.a.
1_WFL_9m	n.a.	n.a.	81	529	n.a.	n.a.	2004	n.a.	n.a.	n.a.
1_WFL_11m	n.a.	n.a.	80	557	n.a.	9.0	2186	n.a.	9.0	n.a.
1_WFL_11m	n.a.	n.a.	90	556	n.a.	9.4	2276	n.a.	9.4	n.a.
	Na [ppm]	K [ppm]	Mg [ppm]	Ca [ppm]	F [ppm]	Cl [ppm]	SO4 [ppm]	Br[ppm]	NO3 [ppm]	PO4 [ppm]
1_BFL_1d	-	-	-	-	0.0075	0.10	0.13	n.a.	0.18	n.a.
1_BFL_1w	-	-	-	-	n.a.	0.092	0.40	n.a.	0.18	n.a.
1_BFL_2w	-	-	-	-	n.a.	0.068	0.31	n.a.	0.25	n.a.
1_BFL_1m	0.080	0.073	0.0092	0.45	n.a.	0.071	0.54	0.13	0.077	n.a.
1_BFL_2m	0.031	0.037	0.43	0.60	n.a.	0.14	n.a.	0.22	n.a.	n.a.
1_BFL_3m	0.035	0.062	n.a.	0.20	n.a.	0.011	n.a.	n.a.	n.a.	n.a.
1_BFL_4m	0.13	0.062	0.0095	0.47	n.a.	0.0015	n.a.	n.a.	n.a.	n.a.
1_BFL_5m	0.054	0.047	0.00022	0.23	n.a.	0.12	0.14	0.20	0.13	n.a.
1_BFL_6m	0.036	n.a.	n.a.	0.10	n.a.	0.044	0.26	0.029	n.a.	n.a.
1_BFL_7m	n.a.	n.a.	n.a.	n.a.	n.a.	0.045	n.a.	n.a.	n.a.	n.a.
1_BFL_9m	n.a.	n.a.	n.a.	n.a.	n.a.	0.096	0.14	n.a.	n.a.	n.a.
1_BFL_11m	0.073	n.a.	n.a.	n.a.	n.a.	0.18	0.18	n.a.	n.a.	n.a.

	Na [ppm]	K [ppm]	Mg [ppm]	Ca [ppm]	F [ppm]	Cl [ppm]	SO4 [ppm]	Br[ppm]	NO3 [ppm]	PO4 [ppm]
1_FL_1d	-	-	-	-	n.a.	0.64	106	n.a.	n.a.	n.a.
1_FL_1w	-	-	-	-	n.a.	0.73	159	n.a.	n.a.	n.a.
1_FL_2w	-	-	-	-	n.a.	0.72	161	n.a.	n.a.	n.a.
1_FL_1m	7.3	11	6.3	118	n.a.	6.2	199	14	10	n.a.
1_FL_1m	7.7	12	7.7	152	n.a.	6.3	201	14	10	n.a.
1_FL_1m	7.2	11	7.9	144	n.a.	6.4	199	14	11	n.a.
1_FL_2m	n.a.	5.1	8.4	125	n.a.	n.a.	237	4.9	n.a.	n.a.
1_FL_3m	n.a.	4.9	9.0	135	n.a.	n.a.	251	n.a.	n.a.	n.a.
1_FL_4m	n.a.	5.0	9.5	149	n.a.	n.a.	285	n.a.	n.a.	n.a.
1_FL_5m	1.4	5.6	16	169	n.a.	n.a.	356	23	13	n.a.
1_FL_6m	3.6	6.6	12	196	n.a.	0.35	345	n.a.	n.a.	n.a.
1_FL_6m	-	-	12	187	-	-	-	-	-	-
1_FL_6m	-	-	11	184	-	-	-	-	-	-
1_FL_7m	1.2	5.1	11	185	n.a.	n.a.	379	n.a.	n.a.	n.a.
1_FL_9m	0.84	5.8	17	193	n.a.	n.a.	439	n.a.	n.a.	n.a.
1_FL_11m	1.3	6.5	15	212	n.a.	9.7	491	23	n.a.	n.a.
1_FL_11m	1.1	6.6	17	223	n.a.	19	504	n.a.	n.a.	n.a.
1_FL_11m	1.3	6.6	16	219	n.a.	9.2	493	n.a.	n.a.	n.a.
	Na [ppm]	K [ppm]	Mg [ppm]	Ca [ppm]	F [ppm]	Cl [ppm]	SO4 [ppm]	Br[ppm]	NO3 [ppm]	PO4 [ppm]
1_WSL_1d	-	-	-	-	0.63	20072	5929	345	n.a.	n.a.
1_WSL_1w	-	-	-	-	0.71	19948	5540	334	n.a.	n.a.
1_WSL_2w	-	-	-	-	0.87	20188	5523	351	n.a.	n.a.
1_WSL_1m	10885	355	1393	1011	n.a.	19080	5248	184	106	n.a.
1_WSL_1m	11078	353	1381	972	n.a.	19543	5214	188	106	n.a.
1_WSL_1m	11069	350	1385	981	n.a.	19529	5400	192	105	n.a.
1_WSL_2m	10980	371	1443	1186	n.a.	19621	5711	56	n.a.	n.a.
1_WSL_3m	12535	377	1471	1258	n.a.	19635	5962	125	n.a.	n.a.
1_WSL_4m	12406	361	1506	1347	n.a.	19434	5762	122	39	n.a.
1_WSL_5m	12021	368	1520	1332	n.a.	21011	6465	222	n.a.	n.a.
1_WSL_6m	12205	326	1320	1091	n.a.	19852	6735	n.a.	n.a.	n.a.
1_WSL_6m	12237	322	1352	1118	n.a.	19978	6439	n.a.	n.a.	n.a.
1_WSL_7m	9977	297	1213	1025	n.a.	18143	5807	152	n.a.	n.a.
1_WSL_9m	10477	339	1345	1153	n.a.	17448	5909	209	n.a.	n.a.
1_WSL_11m	11010	362	1423	1213	n.a.	19514	6106	280	n.a.	n.a.
1_WSL_11m	10878	357	1417	1252	n.a.	19239	6149	282	n.a.	n.a.
1_WSL_11m	10880	363	1403	1231	n.a.	19378	6023	278	n.a.	n.a.
	Na [ppm]	K [ppm]	Mg [ppm]	Ca [ppm]	F [ppm]	Cl [ppm]	SO4 [ppm]	Br[ppm]	NO3 [ppm]	PO4 [ppm]
1_SL_1d	-	-	-	-	n.a.	20001	3236	228	n.a.	n.a.
1_SL_1w	-	-	-	-	n.a.	20758	3315	243	n.a.	n.a.
1_SL_2w	-	-	-	-	n.a.	20216	3334	238	n.a.	n.a.
1_SL_1m	11187	382	1351	520	n.a.	19705	3147	188	104	n.a.
1_SL_1m	11060	377	1338	510	n.a.	19485	3157	185	102	n.a.
1_SL_1m	11608	382	1355	521	n.a.	19723	3178	187	105	n.a.
1_SL_2m	10992	395	1548	694	n.a.	19659	3192	54	n.a.	n.a.
1_SL_3m	12572	403	1582	701	n.a.	19714	3322	126	n.a.	n.a.
1_SL_4m	12629	345	1553	711	n.a.	19705	3368	125	n.a.	n.a.
1_SL_5m	11985	397	1595	778	n.a.	20934	3623	216	n.a.	n.a.
1_SL_6m	12125	359	1405	637	n.a.	19571	3680	1.8	n.a.	n.a.
1_SL_6m	11635	351	1336	515	n.a.	19285	3657	n.a.	n.a.	n.a.
1_SL_6m	11506	348	1294	523	-	-	-	-	-	-
1_SL_7m	10156	342	1258	489	n.a.	19182	3722	127	n.a.	n.a.
1_SL_9m	10313	373	1320	581	n.a.	17542	3396	211	n.a.	n.a.
1_SL_11m	10775	395	1362	625	n.a.	19206	3862	270	n.a.	n.a.
1_SL_11m	10332	377	1308	606	n.a.	18401	3718	267	n.a.	n.a.
1_SL_11m	10815	396	1423	633	n.a.	19245	3852	268	n.a.	n.a.
	Na [ppm]	K [ppm]	Mg [ppm]	Ca [ppm]	F [ppm]	Cl [ppm]	SO4 [ppm]	Br[ppm]	NO3 [ppm]	PO4 [ppm]
1_BSL_1d	-	-	-	-	n.a.	20414	3189	225	n.a.	n.a.
1_BSL_1w	-	-	-	-	n.a.	19947	3036	225	n.a.	n.a.
1_BSL_2w	-	-	-	-	n.a.	19987	3093	227	n.a.	n.a.
1_BSL_1m	11115	429	1523	448	n.a.	19553	2925	186	102	n.a.
1_BSL_2m	11313	407	1601	507	n.a.	20187	3124	56	n.a.	n.a.
1_BSL_3m	12057	390	1535	468	n.a.	19780	3040	n.a.	n.a.	n.a.
1_BSL_4m	12680	440	1625	563	n.a.	19779	3067	127	n.a.	n.a.
1_BSL_5m	12082	435	1633	595	n.a.	20981	3213	217	125	n.a.
1_BSL_6m	12315	380	1487	447	n.a.	19744	3394	35	n.a.	n.a.
1_BSL_7m	10052	346	1234	326	n.a.	18380	3228	125	n.a.	n.a.
1_BSL_9m	10589	386	1349	412	n.a.	17622	3170	209	n.a.	n.a.
1_BSL_11m	10365	368	1412	295	n.a.	18414	3149	253	n.a.	n.a.

Table A 8: Main cat- and anions measured in the ion chromatography (IC) analyses for Experiment 2, where only unweathered shale was used. B: Blank, F: Freshwater, S: Seawater, O: Oxic, A: Anoxic.

Sample	Na [ppm]	K [ppm]	Mg [ppm]	Ca [ppm]	F [ppm]	Cl [ppm]	SO4 [ppm	Br [ppm]	NO3 [ppm	PO4 [ppm
2_SO_1w	9268	339	1255	431	n.a.	19240	3527	129	n.a.	n.a.
2_SO_1m	10438	369	1257	512	n.a.	18584	3569	192	n.a.	n.a.
2_SO_2m	10196	371	1319	524	n.a.	18436	3412	210	n.a.	n.a.
2_SO_4m	10091	353	242	515	n.a.	17904	3536	264	n.a.	n.a.
2_SO_4m	10709	378	1334	563	n.a.	19031	3689	269	n.a.	n.a.
2_SO_4m	10586	374	1309	557	n.a.	18736	3806	268	n.a.	n.a.
	Na [ppm]	K [ppm]	Mg [ppm]	Ca [ppm]	F [ppm]	Cl [ppm]	SO4 [ppm	Br [ppm]	NO3 [ppm	PO4 [ppm
2_BSO_1w	9073	350	1255	335	n.a.	18641	3291	125	n.a.	n.a.
2_BSO_1m	10885	390	1309	410	n.a.	19351	3457	195	n.a.	n.a.
2_BSO_2m	9361	375	1300	400	n.a.	17041	3105	207	n.a.	n.a.
2_BSO_4m	10000	361	1355	267	n.a.	17755	3175	251	n.a.	n.a.
	Na [ppm]	K [ppm]	Mg [ppm]	Ca [ppm]	F [ppm]	Cl [ppm]	SO4 [ppm	Br [ppm]	NO3 [ppm	PO4 [ppm
2_FO_1w	0.07	3.9	1.1	86	n.a.	n.a.	176	n.a.	n.a.	n.a.
2_FO_1m	0.20	4.4	7.1	102	n.a.	0	210	2	0.36	n.a.
2_FO_2m	0.95	4.2	7.9	114	n.a.	0.8	233	n.a.	0.72	n.a.
2_FO_4m	1.4	5.0	11	143	n.a.	10	332	n.a.	n.a.	n.a.
2_FO_4m	1.3	4.9	11	138	n.a.	9	329	n.a.	n.a.	n.a.
2_FO_4m	1.2	5.1	11	145	n.a.	n.a.	339	n.a.	n.a.	n.a.
	Na [ppm]	K [ppm]	Mg [ppm]	Ca [ppm]	F [ppm]	Cl [ppm]	SO4 [ppm	Br [ppm]	NO3 [ppm	PO4 [ppm
2_BFO_1w	n.a.	n.a.	n.a.	n.a.	n.a.	0	n.a.	n.a.	n.a.	n.a.
2_BFO_1m	n.a.	n.a.	n.a.	n.a.	n.a.	0	0.23	1.8	n.a.	n.a.
2_BFO_2m	0.076	0.038	n.a.	n.a.	16	9.5	4.5	n.a.	n.a.	n.a.
2_BFO_4m	0.12	0.027	n.a.	n.a.	n.a.	0	0	n.a.	n.a.	n.a.
	Na [ppm]	K [ppm]	Mg [ppm]	Ca [ppm]	F [ppm]	Cl [ppm]	SO4 [ppm	Br [ppm]	NO3 [ppm	PO4 [ppm
2_BSA_1w	9293	346	1234	326	n.a.	19187	3337	133	n.a.	n.a.
2_BSA_1m	10494	387	1289	403	n.a.	18642	3293	191	n.a.	n.a.
2_BSA_2m	9467	385	1334	411	n.a.	17185	3093	209	n.a.	n.a.
2_BSA_4m	10042	354	1361	267	n.a.	17762	3246	250	n.a.	n.a.
	Na [ppm]	K [ppm]	Mg [ppm]	Ca [ppm]	F [ppm]	Cl [ppm]	SO4 [ppm	Br [ppm]	NO3 [ppm	PO4 [ppm
2_SA_1w	8211	308	1151	381	n.a.	17197	3168	120	n.a.	n.a.
2_SA_1m	10525	377	1284	512	n.a.	18788	3501	199	n.a.	n.a.
2_SA_2m	9433	372	1340	528	n.a.	17242	3176	213	n.a.	n.a.
2_SA_4m	10621	373	1341	533	n.a.	18973	3519	267	n.a.	n.a.
2_SA_4m	11261	381	1384	547	n.a.	19405	3531	267	n.a.	n.a.
2_SA_4m	10981	384	1388	554	n.a.	19506	3614	268	n.a.	n.a.
	Na [ppm]	K [ppm]	Mg [ppm]	Ca [ppm]	F [ppm]	Cl [ppm]	SO4 [ppm	Br [ppm]	NO3 [ppm	PO4 [ppm
2_FA_1w	1.0	3.5	6.8	57	n.a.	0.73	123	n.a.	n.a.	n.a.
2_FA_1m	0.32	3.8	5.5	85	n.a.	0.54	169	2.2	0.33	n.a.
2_FA_2m	0.94	3.2	6.0	89	n.a.	0.97	162	n.a.	n.a.	n.a.
2_FA_4m	1.3	3.6	6.5	100	n.a.	1.2	171	n.a.	0.93	n.a.
2_FA_4m	1.7	3.1	8.5	92	n.a.	1.4	157	n.a.	0.90	n.a.
2_FA_4m	1.5	3.3	6.0	92	n.a.	1.3	163	n.a.	1.04	n.a.
	Na [ppm]	K [ppm]	Mg [ppm]	Ca [ppm]	F [ppm]	Cl [ppm]	SO4 [ppm	Br [ppm]	NO3 [ppm	PO4 [ppm
2_BFA_1w	n.a.	n.a.	n.a.	n.a.	n.a.	0.61	n.a.	n.a.	n.a.	n.a.
2_BFA_1m	n.a.	0.14	n.a.	n.a.	n.a.	0.35	0.56	1.9	0.35	n.a.
2_BFA_2m	0.29	0.10	n.a.	n.a.	n.a.	2.1	0.19	n.a.	0.1	n.a.
2_BFA_4m	0.42	0.19	n.a.	n.a.	0.0020	0.84	0.12	n.a.	n.a.	n.a.

Table A 9: Trace metal concentrations measured in the leachate of samples in Experiment 1, obtained from the inductively coupled plasma mass spectrometry (ICP-MS) analyses. B: Blank, W: Weathered shale, F: Freshwater, S: Seawater, O: Oxic, L: Low-oxygen.

	Al	As	Ba	Cd	Co	Cr	Cu	Fe	Mn	Mo	Ni	Pb	Sb	Se	Sn	Tl	U	V	Zn
Unit symbol	µg/L	µg/L	µg/L	µg/L	µg/L	µg/L	µg/L	µg/L	µg/L	µg/L	µg/L	µg/L	µg/L	µg/L	µg/L	µg/L	µg/L	µg/L	µg/L
1_WFO_1d	25200	1.3	17	31	276	26	833	12800	2520	<1	1840	0.5	<1	<6	<10	0.10	1750	<5	1010
1_WFO_2w	27900	<0.5	13	58	487	7.6	925	1780	5000	<1	3260	<0.2	<1	<6	<10	0.10	1550	<5	1800
1_WFO_2m	41200	<0.5	12	50	425	17	1500	5390	4100	<1	2880	<0.2	<1	<6	<10	0.10	2650	<5	1570
1_WFO_4m	25000	<0.5	12	65	486	<3	852	247	5310	<1	3340	<0.2	<1	<6	<10	0.30	1450	<5	1830
1_WFO_7m	36700	<0.5	6.8	54	436	5.4	1110	1310	4660	<1	2980	<0.2	<1	<6	<10	0.20	1950	<5	1640
1_WFO_11m	24200	<0.5	8.9	54	427	<3	871	363	4480	<1	2810	<0.2	<1	<6	<10	0.10	1390	<5	1570
1_WFO_11m	33100	<0.5	8.5	62	493	5.4	1140	1270	5270	<1	3200	<0.2	<1	<6	<10	0.20	2180	<5	1830
1_WFO_11m	26600	<0.5	8.3	56	437	<3	895	360	4730	<1	3000	<0.2	<1	<6	<10	0.30	1520	<5	1700
	Al	As	Ba	Cd	Co	Cr	Cu	Fe	Mn	Mo	Ni	Pb	Sb	Se	Sn	Tl	U	V	Zn
1_BFO_1d	<20	<0.5	<1	<0.1	<0.2	<3	<4	<2	<1	<1	<2	<0.2	<1	<6	<10	<0.1	0.10	<5	45
1_BFO_2w	<20	<0.5	<1	<0.1	<0.2	<3	<4	<2	<1	<1	<2	<0.2	<1	<6	<10	<0.1	0.10	<5	92
1_BFO_2m	<20	<0.5	<1	<0.1	<0.2	<3	<4	<2	<1	<1	<2	<0.2	<1	<6	<10	<0.1	0.10	<5	72
1_BFO_4m	<20	<0.5	<1	<0.1	<0.2	<3	<4	<2	<1	<1	<2	<0.2	<1	<6	<10	<0.1	0.10	<5	90
1_BFO_7m	<20	<0.5	<1	<0.1	<0.2	<3	<4	5	<1	<1	<2	<0.2	<1	<6	<10	<0.1	0.20	<5	60
1_BFO_11m	<20	<0.5	<1	<0.1	<0.2	<3	5.9	<2	<1	<1	<2	<0.2	<1	<6	<10	<0.1	0.10	<5	115
	Al	As	Ba	Cd	Co	Cr	Cu	Fe	Mn	Mo	Ni	Pb	Sb	Se	Sn	Tl	U	V	Zn
1_FO_1d	50	<0.5	123	0.50	0.70	<3	<4	184	98	244	37	0.2	3.1	<6	<10	0.10	11	<5	16
1_FO_2w	<20	<0.5	76	2.6	3.0	<3	<4	<2	313	740	142	<0.2	6.6	<6	<10	0.10	50	<5	55
1_FO_2m	<20	<0.5	30	4.3	3.9	<3	<4	<2	485	932	161	<0.2	9.8	<6	<10	0.10	110	<5	73
1_FO_4m	<20	<0.5	23	5.2	5.2	<3	<4	<2	670	988	196	<0.2	7.5	<6	<10	0.10	142	<5	148
1_FO_7m	<20	<0.5	20	6.0	7.7	<3	<4	2.4	910	1090	238	<0.2	5.9	7.6	<10	0.10	168	<5	162
1_FO_11m	<20	<0.5	19	8.5	9.4	<3	<4	<2	1100	1570	252	<0.2	5.2	9.2	<10	0.20	201	<5	233
1_FO_11m	<20	<0.5	17	8.6	4.3	<3	<4	<2	846	1360	255	<0.2	4.8	10	<10	0.10	207	<5	235
1_FO_11m	<20	<0.5	19	8.5	9.9	<3	<4	<2	1160	1380	249	<0.2	4.8	10	<10	0.20	195	<5	217
	Al	As	Ba	Cd	Co	Cr	Cu	Fe	Mn	Mo	Ni	Pb	Sb	Se	Sn	Tl	U	V	Zn
1_WSO_1d	16700	<0.5	20	27	223	<3	423	1900	2030	<1	1460	0.80	1.0	<6	<10	3.3	827	<5	765
1_WSO_2w	25500	<0.5	24	56	465	<3	435	396	4660	<1	3020	0.50	<1	<6	<10	11	1040	<5	1480
1_WSO_2m	21600	0.70	27	59	478	<3	300	166	4810	<1	3160	0.20	<1	<6	<10	6.7	951	<5	1490
1_WSO_4m	12700	0.70	33	67	520	<3	154	84.6	5420	<1	3480	0.20	<1	<6	<10	7.7	511	<5	1530
1_WSO_7m	6740	0.80	28	60	448	<3	80	46.9	4850	<1	3040	0.20	<1	<6	<10	6.3	271	<5	1250
1_WSO_11m	17000	0.50	23	64	519	<3	184	123	5340	<1	3370	0.20	<1	<6	<10	1.3	756	<5	1660
1_WSO_11m	23500	0.90	23	68	546	<3	282	270	5630	<1	3490	<0.2	<1	<6	<10	0.60	1130	<5	1760
1_WSO_11m	14700	0.70	23	62	488	<3	168	86.7	5170	<1	3160	<0.2	<1	<6	<10	1.7	626	<5	1520

	Al	As	Ba	Cd	Co	Cr	Cu	Fe	Mn	Mo	Ni	Pb	Sb	Se	Sn	Tl	U	V	Zn
Unit symbol	µg/L	µg/L	µg/L	µg/L	µg/L	µg/L	µg/L	µg/L	µg/L	µg/L	µg/L	µg/L	µg/L	µg/L	µg/L	µg/L	µg/L	µg/L	µg/L
1_BSO_1d	<20	1.6	7.6	<0.1	<0.2	<3	<4	<2	1	11	<2	0.2	1.1	<6	<10	<0.1	3.2	<5	4.5
1_BSO_2w	<20	1.5	6.9	<0.1	<0.2	<3	<4	<2	<1	11	<2	<0.2	<1	<6	<10	<0.1	3.1	<5	3.4
1_BSO_2m	<20	1.5	6.8	<0.1	<0.2	<3	<4	4.1	<1	10	<2	<0.2	<1	<6	<10	<0.1	3.2	<5	<3
1_BSO_4m	<20	1.6	7.0	<0.1	<0.2	<3	<4	2.2	<1	11	<2	<0.2	<1	<6	<10	<0.1	3.1	<5	<3
1_BSO_7m	<20	1.6	6.8	<0.1	<0.2	<3	<4	5.7	<1	10	<2	<0.2	<1	<6	<10	<0.1	3.0	<5	4.3
1_BSO_11m	<20	1.6	7.0	<0.1	<0.2	<3	<4	4.3	<1	12	<2	<0.2	<1	<6	<10	<0.1	3.3	<5	4.5
	Al	As	Ba	Cd	Co	Cr	Cu	Fe	Mn	Mo	Ni	Pb	Sb	Se	Sn	Tl	U	V	Zn
1_SO_1d	<20	0.90	49	31	9.7	<3	<4	<2	437	263	435	0.20	4.2	<6	<10	2.0	49	<5	251
1_SO_2w	<20	0.70	58	86	26	<3	5.4	49	1230	1120	1180	0.20	13	<6	<10	3.9	187	<5	698
1_SO_2m	<20	0.90	53	109	26	<3	<4	<2	1330	1510	980	<0.2	18	6.8	<10	3.8	319	<5	489
1_SO_4m	<20	1.2	48	127	29	<3	<4	4	1700	1730	920	<0.2	17	8.4	<10	3.8	355	<5	567
1_SO_7m	<20	0.50	39	174	34	<3	<4	3.8	1970	1950	898	<0.2	10	7.4	<10	4.4	336	<5	741
1_SO_11m	<20	1.3	43	180	36	<3	<4	2.9	2460	2710	905	<0.2	13	9.6	<10	4.9	491	<5	729
1_SO_11m	<20	0.60	43	194	36	<3	<4	2.5	2390	2770	851	<0.2	12	11	<10	4.7	474	<5	758
1_SO_11m	<20	0.90	44	173	29	<3	<4	<2	2060	2350	754	<0.2	11	11	<10	4.2	438	<5	628
	Al	As	Ba	Cd	Co	Cr	Cu	Fe	Mn	Mo	Ni	Pb	Sb	Se	Sn	Tl	U	V	Zn
1_WFL_1d	42000	5.3	20	45	417	61	1340	44200	3760	1.4	2790	0.40	<1	<6	<10	0.10	2620	<5	1530
1_WFL_2w	29800	<0.5	15	51	455	15	979	14800	4620	<1	3010	0.90	<1	<6	<10	0.10	1680	<5	1650
1_WFL_2m	30100	<0.5	13	53	434	6	1030	465	4670	<1	2920	<0.2	<1	<6	<10	0.20	1590	<5	1590
1_WFL_4m	20100	<0.5	10	55	443	<3	580	155	4860	<1	2980	<0.2	<1	<6	<10	0.30	1170	<5	1570
1_WFL_7m	30900	<0.5	8.1	59	451	<3	969	514	4930	<1	3110	<0.2	<1	<6	<10	0.40	1670	<5	1730
1_WFL_11m	45500	<0.5	10	66	515	18	1470	5270	5140	<1	3460	<0.2	<1	<6	<10	0.10	3030	<5	2000
1_WFL_11m	23600	<0.5	8.4	61	477	<3	804	350	5120	<1	3290	<0.2	<1	<6	<10	0.30	1440	<5	1730
1_WFL_11m	50700	<0.5	7.7	70	550	17	1590	5400	5640	<1	3630	<0.2	<1	<6	<10	0.30	3330	<5	2090
	Al	As	Ba	Cd	Co	Cr	Cu	Fe	Mn	Mo	Ni	Pb	Sb	Se	Sn	Tl	U	V	Zn
1_BFL_1d	<20	<0.5	<1	<0.1	<0.2	<3	<4	2.8	<1	<1	<2	<0.2	<1	<6	<10	<0.1	0.1	<5	<3
1_BFL_2w	<20	<0.5	<1	<0.1	<0.2	<3	<4	<2	<1	<1	<2	<0.2	<1	<6	<10	<0.1	0.1	<5	<3
1_BFL_2m	<20	<0.5	<1	<0.1	<0.2	<3	<4	2	<1	<1	<2	<0.2	<1	<6	<10	<0.1	0.1	<5	<3
1_BFL_4m	<20	<0.5	<1	<0.1	<0.2	<3	<4	5.7	<1	<1	<2	<0.2	<1	<6	<10	<0.1	0.1	<5	<3
1_BFL_7m	<20	<0.5	<1	<0.1	<0.2	<3	<4	7.8	<1	<1	<2	<0.2	<1	<6	<10	<0.1	0.2	<5	<3
1_BFL_11m	<20	<0.5	<1	<0.1	<0.2	<3	<4	<2	<1	<1	<2	<0.2	<1	<6	<10	<0.1	0.2	<5	<3

	Al	As	Ba	Cd	Co	Cr	Cu	Fe	Mn	Mo	Ni	Pb	Sb	Se	Sn	Tl	U	V	Zn
Unit symbol	µg/L	µg/L	µg/L	µg/L	µg/L	µg/L	µg/L	µg/L	µg/L	µg/L	µg/L	µg/L	µg/L	µg/L	µg/L	µg/L	µg/L	µg/L	µg/L
1_FL_1d	22	<0.5	54	0.80	0.90	<3	<4	<2	105	253	46.8	<0.2	3.4	<6	<10	0.10	9	<5	10
1_FL_2w	<20	<0.5	70	2.6	2.6	<3	<4	<2	278	709	123	<0.2	6.5	<6	<10	0.10	45	<5	60
1_FL_2m	<20	<0.5	35	4.8	4.6	<3	<4	<2	592	863	218	<0.2	9.0	<6	<10	0.10	106	<5	98
1_FL_4m	<20	<0.5	28	6.7	7.5	<3	<4	4.8	806	962	310	<0.2	8.4	6.9	<10	0.10	162	<5	179
1_FL_7m	<20	<0.5	22	8.5	8.9	<3	<4	4.0	1140	918	408	<0.2	6.5	<6	<10	0.20	204	<5	264
1_FL_11m	<20	<0.5	19	12	13	<3	<4	2.5	1460	1230	457	<0.2	5.3	11	<10	0.20	264	<5	375
1_FL_11m	<20	<0.5	18	12	15	<3	<4	2.4	1680	1150	453	<0.2	4.7	10	<10	0.20	236	<5	368
1_FL_11m	<20	<0.5	20	12	15	<3	4.2	<2	1620	1120	501	<0.2	5.0	11	<10	0.20	266	<5	372
	Al	As	Ba	Cd	Co	Cr	Cu	Fe	Mn	Mo	Ni	Pb	Sb	Se	Sn	Tl	U	V	Zn
1_WSL_1d	48600	1.8	33	47	424	39	1220	15200	3840	<1	2770	2.5	<1	<6	<10	5.7	2520	<5	1460
1_WSL_2w	34700	0.50	23	52	472	12	709	2290	4590	<1	3110	1.0	<1	<6	<10	11	1700	<5	1550
1_WSL_2m	22600	0.50	22	56	444	4	425	94	4570	<1	2960	0.3	<1	<6	<10	8.7	1110	<5	1370
1_WSL_4m	8570	0.50	31	59	451	<3	145	23	4820	<1	2970	<0.2	<1	<6	<10	11	386	<5	1220
1_WSL_7m	8630	<0.5	27	58	447	<3	102	50	4840	<1	3030	0.2	<1	<6	<10	6.8	326	<5	1260
1_WSL_11m	21200	0.50	24	68	528	<3	231	141	5340	<1	3340	<0.2	<1	<6	<10	0.90	917	<5	1660
1_WSL_11m	4980	0.60	27	63	492	<3	66	20	5020	<1	3230	<0.2	<1	<6	<10	9.0	218	<5	1390
	Al	As	Ba	Cd	Co	Cr	Cu	Fe	Mn	Mo	Ni	Pb	Sb	Se	Sn	Tl	U	V	Zn
1_SL_1d	<20	0.7	71	42	13	<3	<4	<2	562	391	606	<0.2	6.5	<6	<10	3.5	69	<5	480
1_SL_2w	<20	0.6	63	81	26	<3	<4	<2	1270	1110	1170	<0.2	12	<6	<10	3.9	196	<5	700
1_SL_2m	<20	0.5	55	147	39	<3	<4	<2	1630	1350	1680	<0.2	18	6.8	<10	4.1	342	<5	1140
1_SL_4m	<20	0.7	51	187	50	<3	<4	<2	2100	1820	1830	<0.2	16	7.8	<10	4.9	462	<5	1510
1_SL_7m	<20	0.6	43	183	49	<3	<4	2710	2220	1700	1680	0.2	13	8.6	<10	4.5	484	<5	1520
1_SL_11m	<20	0.9	42	249	67	<3	<4	2.8	3200	2100	1990	<0.2	12	12	<10	5.0	642	<5	1880
1_SL_11m	<20	0.6	44	247	63	<3	<4	<2	3020	2400	1700	<0.2	11	10	<10	5.9	670	<5	1840
1_SL_11m	<20	<0.5	45	236	58	<3	<4	<2	2880	2300	1730	<0.2	11	11	<10	6.0	597	<5	1610
	Al	As	Ba	Cd	Co	Cr	Cu	Fe	Mn	Mo	Ni	Pb	Sb	Se	Sn	Tl	U	V	Zn
1_BSL_1d	<20	1.4	7.5	<0.1	<0.2	<3	9.0	<2	<1	11	<2	<0.2	<1	<6	<10	<0.1	3.0	<5	6.9
1_BSL_2w	<20	1.8	7.2	<0.1	<0.2	<3	<4	<2	<1	11	<2	<0.2	<1	<6	<10	<0.1	3.2	<5	5.4
1_BSL_2m	<20	1.5	6.9	<0.1	<0.2	<3	<4	4.1	<1	11	<2	<0.2	<1	<6	<10	<0.1	3.0	<5	8.2
1_BSL_4m	<20	1.7	6.9	<0.1	<0.2	<3	<4	<2	<1	10	<2	<0.2	<1	<6	<10	<0.1	3.0	<5	4.3
1_BSL_7m	<20	1.3	6.5	<0.1	<0.2	<3	<4	2.8	<1	10	<2	<0.2	<1	<6	<10	<0.1	3.0	<5	4.6
1_BSL_11m	<20	1.5	6.9	0.10	<0.2	<3	<4	2.6	<1	13	11	<0.2	<1	<6	<10	<0.1	3.3	<5	11

Table A 10: Trace metal concentrations measured in the leachate of samples in Experiment 2, obtained from the inductively coupled plasma mass spectrometry (ICP-MS) analyses. B: Blank, F: Freshwater, S: Seawater, O: Oxic, A: Anoxic.

Sample	Al	As	Ba	Cd	Co	Cr	Cu	Fe	Mn	Mo	Ni	Pb	Sb	Se	Sn	Tl	U	V	Zn
Unit symbol	µg/L	µg/L	µg/L	µg/L	µg/L	µg/L	µg/L	µg/L	µg/L	µg/L	µg/L	µg/L	µg/L	µg/L	µg/L	µg/L	µg/L	µg/L	µg/L
2_SO_1w	<20	1.2	59	79	29	<3	<4	<2	1240	774	1160	<0.2	8.6	<6	<10	3.6	149	<5	622
2_SO_1m	<20	1.0	57	78	26	<3	<4	5	1320	1310	982	0.20	19	6.1	<10	2.8	282	<5	290
2_SO_2m	<20	1.0	52	81	22	<3	<4	<2	804	1500	865	<0.2	20	6.4	<10	2.6	324	<5	271
2_SO_4m	<20	0.80	54	95	17	<3	<4	2.8	455	1640	661	<0.2	18	7.9	<10	2.9	320	<5	289
2_SO_4m	<20	<0.5	48	111	25	<3	<4	<2	1080	1760	830	<0.2	16	6.7	<10	2.5	329	<5	476
2_SO_4m	<20	0.60	49	88	21	<3	<4	<2	973	1740	641	<0.2	18	8.1	<10	2.8	343	<5	304
	Al	As	Ba	Cd	Co	Cr	Cu	Fe	Mn	Mo	Ni	Pb	Sb	Se	Sn	Tl	U	V	Zn
2_BSO_1w	<20	1.7	13	<0.1	<0.2	<3	<4	<2	17	11	<2	<0.2	<1	<6	<10	<0.1	3.3	<5	<3
2_BSO_1m	21	1.6	18	<0.1	<0.2	<3	<4	3.5	28	12	<2	0.3	<1	<6	<10	<0.1	3.3	<5	6.0
2_BSO_2m	23	1.7	21	<0.1	<0.2	<3	<4	<2	14	11	<2	<0.2	<1	<6	<10	<0.1	3.0	<5	5.0
2_BSO_4m	<20	<0.5	12	<0.1	<0.2	<3	<4	<2	<1	5.5	<2	<0.2	<1	<6	<10	<0.1	1.4	<5	<3
	Al	As	Ba	Cd	Co	Cr	Cu	Fe	Mn	Mo	Ni	Pb	Sb	Se	Sn	Tl	U	V	Zn
2_FO_1w	<20	<0.5	94	2.6	4.9	<3	<4	<2	358	439	220	<0.2	4.2	<6	<10	0.20	38	<5	84
2_FO_1m	<20	<0.5	34	3.0	3.4	<3	<4	2.4	407	991	143	<0.2	10	<6	<10	0.10	81	<5	47
2_FO_2m	<20	<0.5	29	2.4	2.8	<3	<4	<2	372	991	91	<0.2	10	6.0	<10	0.10	107	<5	35
2_FO_4m	<20	<0.5	27	3.3	3.7	<3	<4	2.6	475	1200	116	<0.2	9.3	8.0	<10	0.10	131	<5	52
2_FO_4m	<20	<0.5	26	3.0	3.2	<3	<4	<2	464	1120	99.3	<0.2	8.8	7.2	<10	0.10	120	<5	42
2_FO_4m	<20	<0.5	25	2.9	2.8	<3	<4	<2	449	1140	88	<0.2	9.0	6.9	<10	0.10	121	<5	40
	Al	As	Ba	Cd	Co	Cr	Cu	Fe	Mn	Mo	Ni	Pb	Sb	Se	Sn	Tl	U	V	Zn
2_BFO_1w	<20	<0.5	<1	<0.1	<0.2	<3	<4	<2	<1	<1	<2	<0.2	<1	<6	<10	<0.1	<0.04	<5	<3
2_BFO_1m	<20	<0.5	<1	<0.1	<0.2	<3	<4	2.3	3.3	<1	<2	<0.2	<1	<6	<10	<0.1	<0.04	<5	<3
2_BFO_2m	<20	<0.5	1.3	<0.1	<0.2	<3	<4	2.0	6.6	<1	<2	<0.2	<1	<6	<10	<0.1	<0.04	<5	<3
2_BFO_4m	<20	<0.5	<1	<0.1	<0.2	<3	<4	<2	<1	<1	<2	<0.2	<1	<6	<10	<0.1	<0.04	<5	<3
	Al	As	Ba	Cd	Co	Cr	Cu	Fe	Mn	Mo	Ni	Pb	Sb	Se	Sn	Tl	U	V	Zn
2_BSA_1w	<20	<0.5	<1	<0.1	<0.2	<3	<4	<2	<1	<1	<2	<0.2	<1	<6	<10	<0.1	<0.04	<5	<3
2_BSA_1m	349	1.5	21	<0.1	<0.2	<3	<4	3.4	37	11	<2	<0.2	<1	<6	<10	<0.1	2.5	<5	3.9
2_BSA_2m	78	1.6	24	<0.1	<0.2	<3	<4	5.6	49	11	<2	<0.2	<1	<6	<10	<0.1	3.2	<5	12
2_BSA_4m	71	1.4	29	<0.1	<0.2	<3	<4	3.9	62	11	<2	<0.2	<1	<6	<10	<0.1	3.0	<5	21
	Al	As	Ba	Cd	Co	Cr	Cu	Fe	Mn	Mo	Ni	Pb	Sb	Se	Sn	Tl	U	V	Zn
2_SA_1w	<20	1.2	56	62	24	<3	<4	<2	1190	845	1070	<0.2	9.5	<6	<10	2.3	148	<5	513
2_SA_1m	48	1.0	59	43	25	<3	<4	17	1530	1230	1210	<0.2	22	<6	<10	1.0	242	<5	563
2_SA_2m	<20	0.90	53	2.1	13	<3	<4	143	1710	1450	1140	<0.2	45	<6	<10	0.10	329	<5	486
2_SA_4m	<20	0.50	53	1.6	0.20	<3	<4	1980	2050	1560	90.6	<0.2	45	<6	<10	<0.1	360	<5	12
2_SA_4m	<20	<0.5	52	1.4	0.20	<3	<4	1380	2010	1430	142	<0.2	41	<6	<10	<0.1	367	<5	52
2_SA_4m	<20	0.60	52	1.6	0.70	<3	<4	720	1900	1570	497	<0.2	47	<6	<10	<0.1	411	<5	216
	Al	As	Ba	Cd	Co	Cr	Cu	Fe	Mn	Mo	Ni	Pb	Sb	Se	Sn	Tl	U	V	Zn
2_FA_1w	1980	<0.5	95	0.80	1.7	<3	<4	9.2	229	375	84	<0.2	3.6	<6	<10	0.1	19	<5	28
2_FA_1m	<20	<0.5	47	1.0	1.3	<3	<4	18	327	1020	79	<0.2	13	<6	<10	<0.1	63	<5	<3
2_FA_2m	<20	<0.5	35	1.2	<0.2	<3	<4	61	329	1140	6.2	<0.2	23	<6	<10	<0.1	47	<5	<3
2_FA_4m	<20	<0.5	36	1.2	<0.2	<3	<4	19	326	1320	2.1	<0.2	29	<6	<10	<0.1	20	<5	3.8
2_FA_4m	<20	<0.5	36	1.3	<0.2	<3	<4	17	257	1330	<2	<0.2	34	<6	<10	<0.1	13	<5	<3
2_FA_4m	<20	<0.5	36	1.1	<0.2	<3	<4	17	326	1200	<2	<0.2	27	<6	<10	<0.1	44	<5	<3
	Al	As	Ba	Cd	Co	Cr	Cu	Fe	Mn	Mo	Ni	Pb	Sb	Se	Sn	Tl	U	V	Zn
2_BFA_1w	<20	<0.5	2.3	<0.1	<0.2	<3	<4	<2	15	<1	<2	<0.2	<1	<6	<10	<0.1	<0.04	<5	13
2_BFA_1m	<20	<0.5	2.1	<0.1	<0.2	<3	<4	42	10	<1	<2	<0.2	<1	<6	<10	<0.1	0.10	<5	8.1
2_BFA_2m	3320	<0.5	3.8	<0.1	<0.2	<3	<4	5.2	23	<1	<2	<0.2	<1	<6	<10	<0.1	0.10	<5	53
2_BFA_4m	<20	<0.5	<1	<0.1	<0.2	<3	<4	<2	<1	<1	<2	<0.2	<1	<6	<10	<0.1	<0.04	<5	<3

Table A 11: Quality standards for metals in freshwater (Norwegian Environment Agency, 2016).

Freshwater	Class I	Class II	Class III	Class IV	Class V
As	0 - 0.15	0.15-0.5	0.5-8.5	8.5-85	>85
Pb	0 - 0.02	0.02-1.2	1.2-14	14-57	>57
Cd	0-0.003	0.003-0.25	0.25-1.5	1.5-15	>15
Cu	0-0.3	0.3-7.8		7.8-15.6	>15.6
Cr	0 - 0.1	0.1-3.4			>3.4
Ni	0-0.5	0.5-4	4 -34	34-67	>67
Zn	0 - 1.5	1.5 - 11		11-60	>60

Table A 12: Quality standards for metals in costal water (Norwegian Environment Agency, 2016).

Costal water	Class I	Class II	Class III	Class IV	Class V
As	0 - 0.15	0.15-0.6	0.6-8.5	8.5-85	>85
Pb	0 - 0.02	0.02-1.3	1.3-14	14-57	>57
Cd	0-0.003	0.003-0.2	0.2-1.5	1.5-15	>15
Cu	0-0.3	0.3-2.6		2.6-5.2	>5.2
Cr	0 - 0.1	0.1-3.4	3.4-35.8	35.8-358	>358
Ni	0-0.5	0.5-8.6	8.6 -34	34-67	>67
Zn	0 - 1.5	1.5 - 3.4	3.4-6	6-60	>60

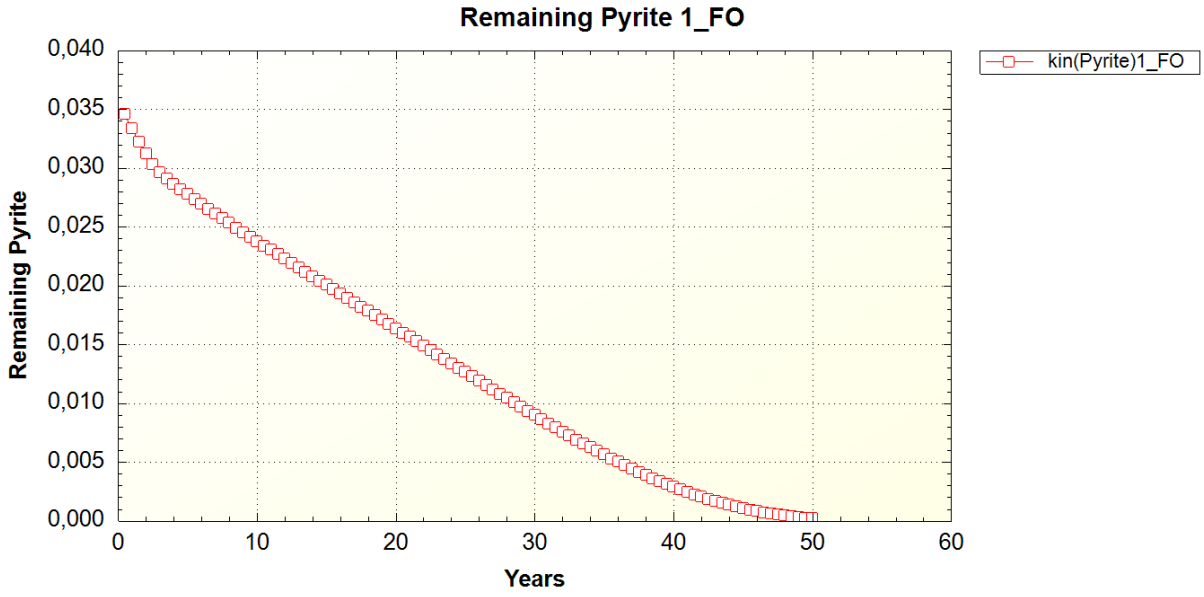

Figure A 2: Dissolution of pyrite in the calibration model when extrapolated to 50 years.

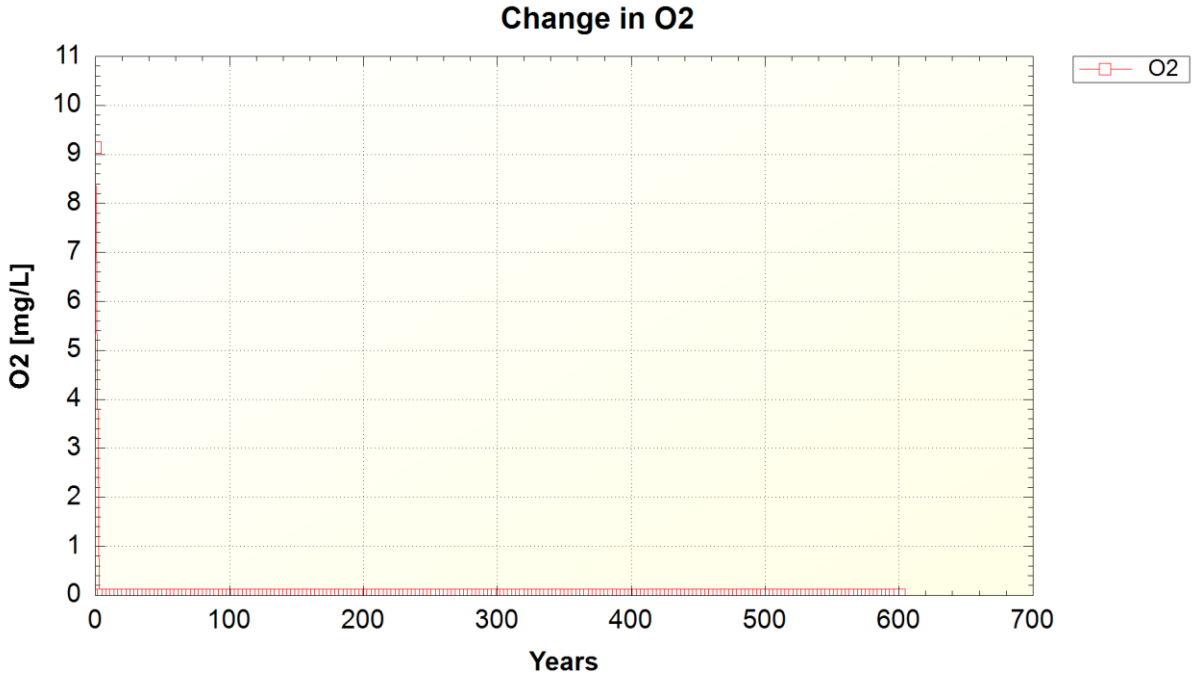

Figure A 3: Dissolved oxygen concentrations in the transport model simulating the conditions in the Drammensfjord when water was exchanged every three years.

Code A 1:PHREEQC script used to calculate SI of gypsum in the batch with unweathered shale treated with seawater for 5 months stored under oxic conditions.

```
#Composition of 1_SO_5m (Unweathered shale treated with seawater for 5 m)
SOLUTION 1
    temp      22
    pH        7.8
    pe        8.2
    redox     pe
    units     ppm
    density   1
    Br        216
    C(4)      84 as HCO3-
    Ca        766
    Cl        21034
    K         417
    Mg        16603
    Na        12071
    S(6)      3680
    O(0)      8.4
    -water    1 # kg

EQUILIBRIUM_PHASES 1
    O2(g)     -0.7 10
    CO2(g)    -3.39 10
```

Code A 2: PHREEQC script used to calculate SI of gypsum in the batch with unweathered shale treated with seawater for 7 months stored under oxic conditions.

```
#Composition of 1_SO_7m (Unweathered shale treated with seawater for 7 m)
SOLUTION 1
    temp      22
    pH        7.8
    pe        8.8
    redox     pe
    units     ppm
    density   1
    Br        127
    C(4)      110 as HCO3-
    Ca        397
    Cl        18621
    K         340
    Mg        1238
    Na        10032
    O(0)      8.5
    S(6)      3487
    -water    1 # kg

EQUILIBRIUM_PHASES 1
    O2(g)     -0.7 10
    CO2(g)    -3.39 10
```